SUPERSONIC WAVE DRAG OF THIN AIRFOILS

Thesis by

Allen E. Puckett

In Partial Fulfillment of the Requirements

for the Degree of Doctor of Philosophy

California Institute of Technology

Pasadena, California

1949

ABSTRACT

The linearization of the equations of motion for the supersonic flow of a perfect fluid is discussed, and methods of solution using elementary source sink solutions are developed. These methods are applied to the calculation of the performance of several types of three-dimensional supersonic airfoils; in particular, the drag at zero lift of a family of almost triangular, symmetrical wings is calculated. The significance of the results is discussed.

ACKNOWLEDGEMENTS

The author wishes to express his appreciation to Prof. Th. von Karman for his suggestions and assistance in the initial formulation of the problem, and for the inspiration furnished by his methods and solutions in approaching other problems in this field. Sincere thanks are also due Prof. H. J. Stewart for his constant help and guidance during the course of the work, and to Miss Shirley Woodbury for her assistance in the preparation of the manuscript.

TABLE OF CONTENTS

LIST OF FIGURES

PART I

INTRODUCTION AND SUMMARY

The flow of an incompressible, non-viscous fluid around a three dimensional non-lifting body can, in principle, be calculated for rather general shapes, and reasonably simple closed solutions exist for a few special shapes. These possibilities exist, of course, because the incompressible equations of motion are linear. These solutions, however, do not answer directly one of the fundamental aeronautical problems - the calculation of the drag - since in an incompressible fluid this arises essentially from viscous effects.

On the other hand, in a compressible fluid, at supersonic speeds, an important part of the drag does arise from the non-viscous flow, and is known as wave or pressure drag. Unfortunately, however, the complete compressible flow equations are non-linear, and at present can be solved only in two-dimensional and axially symmetric cases, and then only by an approximate numerical procedure. However the importance of the perfect fluid solutions in drag calculations (aside from their obvious importance in lift calculations) has emphasized the usefulness of approximate solutions for engineering purposes, and perhaps stimulated the carrying out of such calculations to an even greater degree than existed in the low-speed case.

The most practical approach to an approximate solution is the "small perturbation" assumption - that is, the assumption that the important features of the flow are represented by velocity fields in which the velocities do not differ much from the free stream velocity.

It can be shown that this amounts to requiring that the slopes of elements of the surface of the body are almost parallel to the direction of the free stream velocity. This is most likely to be true for thin airfoils, or thin bodies of revolution. Even in these cases, there may be regions in which the local (approximately) calculated velocities clearly do not satisfy the small perturbation assumption. In these regions, at worst we must recognize that the approximate calculation is locally in serious error, while at best we may hope that the general behaviour of the solution, as to the extent and order of magnitude of "pressure peaks", for instance, may still be predicted correctly, and that in the integrals of the solutions, representing total forces or total drag, the error may be small.

Comparison with analogous situations in approximate incompressible flow calculations allow some optimism regarding the latter possibility, while at the same time careful examination of the approximations made to the complete equations permit more quantitative specification of the probable limits within which the errors of the solution lie below certain tolerances. In the last analysis, from an engineering point of view, the justification for any approximate method of solution, and the determination of its range of usefulness, lies in comparison with experimental results.

In the following chapters a brief summary will be given of the methods of linearizing the general equations of motion for a compressible fluid, and of obtaining solutions to these equations for supersonic flows. An extended account will be given of the application of one

method, the "source solutions" to the calculation of the flow around thin three-dimensional airfoils at zero lift. In particular, calculations are carried out and results presented in detail for one simple but especially interesting family of airfoil planforms, the "delta wings", which have an essentially triangular planform, but are also allowed to have various trailing edge angles. This family is particularly interesting because it is characterized by only a few geometrical parameters, but at the same time exhibits most of the peculiarities, also possesed by more complicated airfoils, in the behaviour of the drag coefficient as the leading edge angle or position of maximum thickness line are varied. Local behaviour of the pressure coefficient is also typical of local conditions in more complicated cases. In this way, the calculations allow the development of some engineering feeling for the relation of airfoil drag performance to the critical geometrical parameters.

The most important results of the calculations are presented in the curves of drag coefficient vs. Mach number for airfoils of this family, in Figs. 20 to 32 . It is seen there that the most important geometrical parameters are the ratios of the angles defining position of leading edge and trailing edge, and maximum thickness line, to the Mach angle, and that certain singularities occur in the solution when any one of these ratios is 1.0. In general, for an airfoil of given thickness, the drag of the airfoil is decreased considerably when both the leading edge and the line of maximum thickness are swept well behind the angle of the Mach waves.

It is also found that in certain cases the drag coefficients approach finite values when the Mach number approaches 1, in contrast

to the results in two-dimensional cases, and in spite of the usual suspicion that the linearized approximation fails completely in this neighborhood. It seems likely that some of the details of the flow in this limiting case do fall outside the scope of the linearized theory, but it also seems quite possible that this evidence of great improvement in undesirable drag characteristics near Mach number 1 by using swept leading and trailing edges is evidence of a real phenomenon. This is borne out to a considerable extent by existing experimental data.

PART II

LINEARIZATION OF EQUATIONS AND METHOD OF SOLUTION

A. Basic Equations

The following symbols will be used:

U, V, W, = velocities in direction of x, y, and z (or x_i) or U_i axis respectively

U_o = undisturbed or free stream velocity, in direction of x-axis

u, v, w, = perturbation velocities in direction of x, y, and z (or x_i) axis respectively or u_i

ϕ = perturbation velocity potential

M = Mach number, U/a

a = speed of sound

p = pressure

ρ = density

γ = ratio of specific heats, c_p/c_v

$\beta^2 = M^2 - 1$

λ_x = slope of airfoil surface in x-direction

Subscript $(\ )_o$ will denote conditions in the free stream (i.e., at infinity).

Certain additional symbols will be introduced later in the discussion of properties of particular airfoils.

Although the technique of linearizing the equations of motion is well known, it will be exhibited here in somewhat complete form in order to demonstrate clearly the order of magnitude of the terms neglected. The fundamental equations governing the steady motion of a compressible,

inviscid fluid are the Euler equation,

$$v_j \frac{\partial v_i}{\partial x_j} = -\frac{1}{\rho} \frac{\partial p}{\partial x_i} \tag{1}$$

and the continuity equation,

$$\frac{\partial}{\partial x_i} (\rho u_i) = 0 \tag{2}$$

It can also be shown from the equation for conservation of energy that, in the absence of viscosity, and heat transfer, the density will be a unique function of pressure, given by the isentropic law

$$p = \text{const.}\ \rho^{\gamma} \ . \tag{3}$$

In this case it can also be shown that a flow initially irrotation will, in the absence of discontinuities (shock waves) remain always irrotational, and that equation (1) can be reduced to the Bernoulli equation

$$\frac{v_i v_i}{2} + \frac{\gamma}{\gamma - 1} \frac{p}{\rho} = \text{Const.} \tag{4}$$

$$\frac{v_i v_i}{2} + \frac{1}{\gamma - 1} a^2 = \text{Const.} \tag{4a}$$

where a is the local speed of sound, $\sqrt{\gamma p/\rho}$. The continuity equation can then be written as

$$\frac{\partial v_i}{\partial x_i} = -\frac{v_i}{\rho} \frac{dp}{d\rho} \frac{\partial \rho}{\partial x_i} = + \frac{v_i v_j}{a^2} \frac{\partial v_i}{\partial x_j} \tag{5}$$

or, in expanded form, as

$$\frac{\partial U}{\partial x}\left(1-\frac{U^2}{a^2}\right)+\frac{\partial V}{\partial y}\left(1-\frac{V^2}{a^2}\right)+\frac{\partial W}{\partial z}\left(1-\frac{W^2}{a^2}\right)$$

$$-2\frac{UV}{a^2}\frac{\partial V}{\partial x}-2\frac{UW}{a^2}\frac{\partial W}{\partial x}-2\frac{VW}{a^2}\frac{\partial W}{\partial y}=0 \qquad (5a)$$

We now suppose the net velocity to consist of small disturbances to the free stream velocity, U_o, so that

$$U = U_o + u$$
$$V = v$$
$$W = w \qquad (6)$$

where u/U_o, v/U_o, w/U_o are all small compared to one. The speed of sound, a, can be expressed in terms of these perturbations, using equation (4a), as

$$a^2 - a_o^2 = \frac{\gamma-1}{2}\left(U_o^2 - U^2 - V^2 - W^2\right)$$

$$= -\frac{\gamma-1}{2}U_o^2\left\{2\frac{u}{U_o}+\left(\frac{u}{U_o}\right)^2+\left(\frac{v}{U_o}\right)^2+\left(\frac{w}{U_o}\right)^2\right\} \qquad (7)$$

So that $$\frac{1}{a^2} = \frac{1}{a_o^2}\left\{1+(\gamma-1)M_o^2\left(\frac{u}{U_o}\right)+O\left[\left(\frac{u}{U_o}\right)^2\right]\right\} \qquad (8)$$

where $M_o = U_o/a_o$. Using this expression in equation (5a), we obtain

$$\frac{\partial u}{\partial x}(1-M_o^2)+\frac{\partial v}{\partial y}+\frac{\partial w}{\partial z}=\frac{\partial u}{\partial x}M_o^2\left\{2+(\gamma-1)M_o^2\right\}\left(\frac{u}{U_o}\right)$$

$$+\frac{\partial v}{\partial x}\cdot 2M_o^2\frac{v}{U_o}+\frac{\partial w}{\partial x}2M_o^2\frac{w}{U_o}$$

$$+O\left[\frac{\partial u}{\partial x}\left(\frac{u}{U_o}\right)^2\right] \qquad (9)$$

The following assumptions are now made:

(1) $M^2(u/U_o)$ is small compared to $(1-M_o)^2$ at low supersonic Mach numbers. This implies that either u/U_o must be extremely small, or the Mach number cannot be allowed to approach too closely to 1.

(2) $M_o^2(u/U_o)$ is small compared to 1 for high Mach numbers, M_o. Since it will be found from the first approximate solutions that (u/U_o) is of the order $(v/U_o)/M_o$, or α/M_o, where α is the local angle between a surface element and the flow direction, this assumption implies that αM is small compared to 1. Since M is of the order $1/\mu$, where μ is the Mach angle, we thus have

$$\alpha/\mu << 1.$$

Thus at very high Mach numbers, with small values of μ, the second order effects become increasingly important.

If these assumptions are made, (9) becomes the basic equation of the linearized theory:

$$\frac{\partial u}{\partial x}(1-M_o^2)+\frac{\partial v}{\partial y}+\frac{\partial w}{\partial z}=0 \qquad (10)$$

The solution to this can be regarded as the first step in a series of successive approximations. Substituting the values of u, v, w found from (10) into the right hand side of (9) a new linear equation is obtained which might be solved for the second approximation. This is essentially the procedure used by Hentsche and Wendt, (Ref. 7) in the subsonic two-dimensional case; it can also be carried out explicitly in the supersonic two-dimensional case, but has not as yet been worked out in the general three-dimensional case. However there is some question about the convergence of this process even in the two-dimensional case.

Since the flow is irrotational, the velocities can be given as:

$$u = \partial\phi/\partial x \equiv \phi_x$$

$$v = \partial\phi/\partial y \equiv \phi_y$$

$$w = \partial\phi/\partial z \equiv \phi_z$$

and equation (10) becomes:

$$\phi_{xx}(M_0^2 - 1) - \phi_{yy} - \phi_{zz} = 0 \qquad (11)$$

This is the three-dimensional form of the perturbation equation first introduced by Ackeret (Ref. 1) and Glauert (Ref. 3).

The boundary condition, that the velocity component normal to the surface be zero, may be expressed completely as:

$$U\ell + Vm + Wn = 0 \qquad (12)$$

where ℓ, m, n are the direction cosines of the normal to the surface.

If we describe the surface of a thin airfoil as t = t(x,y), then:

$$\ell : m : n = -\frac{\partial t}{\partial x} : -\frac{\partial t}{\partial y} : 1$$

so that equation (12) becomes

$$(U_0 + u)\frac{\partial t}{\partial x} + v\frac{\partial t}{\partial y} - w = 0 \qquad (13)$$

If $\partial t/\partial x$ and $\partial t/\partial y$ are both small, even though possibly of the same order of magnitude, we have

$$\frac{w}{U_0} = \frac{\partial t}{\partial x} + O\left[\frac{u}{U_0}\frac{\partial t}{\partial x}\right] \qquad (14)$$

Thus in this first approximation, the boundary conditions relates only the downwash, w, to the x-slope of the surface.

A corresponding linearized calculation of the pressure changes in the flow is necessary. If the Bernoulli equation for the pressure in terms of the velocities (equation (4)) is expanded in a Taylor series about the free stream velocity, we find that

$$p - p_0 = -\rho_0 U_0^2\left\{\frac{u}{U_0} + \frac{v^2 + w^2}{2U_0^2}\right\} + \frac{\rho_0 U_0^2}{2}(M_0^2 - 1)\left(\frac{u}{U_0}\right)^2 + O\left[\left(\frac{u}{U_0}\right)^3\right]$$

We may define the pressure coefficient, C_p, by:

$$C_p = \frac{p - p_0}{\rho_0 U_0^2/2} = -2\frac{u}{U_0} + (M_0^2 - 1)\left(\frac{u}{U_0}\right)^2 - \frac{v^2 + w^2}{U_0^2} + O\left[\left(\frac{u}{U_0}\right)^3\right] \qquad (15)$$

In the first order approximation, we then have

$$C_p = - 2u/U_o \tag{16}$$

B. Methods of Solution

There are two general methods of arriving at solutions to equation (11). One is to investigate immediately the existence of certain typical "conical" solutions, that is, a solution with u, v, w constant along each ray through a point. This form of solution was discussed by Busemann (Ref. 6). As shown by Stewart (Ref. 8) such solutions can be represented as functions of a complex variable in a distorted plane perpendicular to U. More general solutions can then be produced by combinations of special conical solutions.

The other method of attack is to represent the solution as an integral of certain elementary solutions which can be interpreted as supersonic sources or doublets. Such elementary solutions were used by Karman and Moore in calculating the flow around slender bodies of revolution (Ref. 2), and were discussed by Prandtl, and used by Schlichting, in connection with lifting-wing problems (Ref. 4 and 9). This type of solution is particularly adaptable to calculation of flow around thin wings at zero lift, as will be seen.

C. The Source Solution

If we let

$$\phi(x,y,z) = \frac{q(\xi,\eta)}{\sqrt{(x-\xi)^2 - \beta^2\{(y-\eta)^2 + z^2\}}} \tag{17}$$

where $\beta^2 = M_o^2 - 1$, this potential will be a solution to equation (11).

If M_o goes to zero, it does, in fact, become the potential for a subsonic source located at (ξ, η) in the x, y plane. However for $\beta^2 > 0$, the expression under the radical vanishes for certain values of x, y, and z, namely, at those values representing the surface of the cone defined by

$$(x-\xi)^2 = \beta^2\{(y-\eta)^2 + z^2\} \tag{18}$$

This cone is, of course, the Mach cone, with central half-angle of

$$\mu = \cot^{-1}\beta$$

which is the Mach angle, and vertex at $(\xi, \eta, 0)$. This cone is shown in Fig. 1. Equation (18) defines two cones, one estending upstream, which may be called the "forecone", and one extending downstream, which may be called the "aftercone". Apparently ϕ is defined for x, y, z lying within either of these cones. However from physical considerations we shall suppose that the disturbance q at (ξ, η) can affect only conditions downstream, that is, in the aftercone of q. The cone is the stationary wave front produced by a disturbance at (ξ, η) in a flow at Mach number M_o.

If the point $P \equiv (x, y, z)$ lies in the aftercone of (ξ, η), then (ξ, η) also lies in the Mach cone extending upstream with vertex at P, i.e., the forecone of P. Apparently ϕ at P is affected only by points whose aftercones include P, and therefore by disturbances at points lying within the forecone of P. This cone intersects the ξ, η plane in a hyperbola, given essentially by equation (18), and shown in Fig. 2.

A general solution can now be constructed by superpositions of elementary solutions of the type in equation (17), with $q(\xi, \eta)$ interpreted as a source strength per unit area. It can be noted that these solutions will produce $w = \partial\phi/\partial z$ antisymmetric in z, but u and v symmetric. The general solution can be represented by

$$\phi(x, y, z) = \int_0^{\xi_1} d\xi \int_{\eta_1}^{\eta_2} \frac{q(\xi, \eta)\, d\eta}{\sqrt{(x-\xi)^2 - \beta^2\{(y-\eta)^2 + z^2\}}} \tag{19}$$

where it is assumed that no disturbances exist ahead of $\xi = 0$. The curves η_1, and η_2 are defined by

$$\eta_1 = y - \sqrt{(x-\xi)^2/\beta^2 - z^2}$$

$$\eta_2 = y + \sqrt{(x-\xi)^2/\beta^2 - z^2}$$

$$\xi_1 = x - \beta z$$

that is, the two branches of the hyperbola of Fig. 2.

The downwash, or w-velocity, in the xy-plane, associated with the potential of equation (19) has a very simple expression. However the calculation of $w = \partial\phi/\partial z$ directly from equation (19) is somewhat awkward, since the limits of integration involve z, and the integrand becomes infinite at these limits. Therefore certain transformations are necessary. Integrating the second integral of (19) by parts, with

$$u = g(\xi, \eta) \qquad dv = d\eta \Big/ \sqrt{(x-\xi)^2 - \beta^2\{(y-\eta)^2 + z^2\}}$$

$$du = \frac{\partial g}{\partial \eta} d\eta \qquad v = -\frac{1}{\beta} \sin^{-1} \frac{\beta(y-\eta)}{\sqrt{(x-\xi)^2 - \beta^2 z^2}}$$

and noting that

$$q(\xi,\eta)\,\sin^{-1}\frac{\beta(y-\eta)}{\sqrt{(x-\xi)^2-\beta^2z^2}}\Bigg|_{\eta_1}^{\eta_2} = -\frac{\pi}{2}\left\{q(\xi,\eta_2)-q(\xi,\eta_1)\right\}$$

we obtain:

$$\phi = \frac{\pi}{2\beta}\int_0^{x-\beta z}\left\{q(\xi,\eta_2)-q(\xi,\eta_1)\right\}d\xi + \frac{1}{\beta}\int_0^{x-\beta z}d\xi\int_{\eta_1}^{\eta_2}\frac{\partial q}{\partial\eta}\sin^{-1}\frac{\beta(y-\eta)}{\sqrt{(x-\xi)^2-\beta^2z^2}}\,d\eta$$

The w-velocity may now be calculated;

$$\frac{\partial\phi}{\partial z} = -\pi\,q(x-\beta z,\,y) + T_1 + T_2 \qquad (20)$$

where

$$T_1 = \frac{\pi}{2\beta}\int_0^{x-\beta z}\frac{\partial}{\partial z}\left\{q(\xi,\eta_2)-q(\xi,\eta_1)\right\}d\xi \qquad (21)$$

$$= \frac{\pi}{2\beta}\int_0^{x-\beta z}\frac{\beta z}{\sqrt{(x-\xi)^2-\beta^2z^2}}\left\{\left(\frac{\partial q}{\partial\eta}\right)_1-\left(\frac{\partial q}{\partial\eta}\right)_2\right\}d\xi$$

and

$$T_2 = \frac{1}{\beta}\frac{\partial}{\partial z}\int_0^{x-\beta z}d\xi\int_{\eta_1}^{\eta_2}\frac{\partial q}{\partial\eta}\sin^{-1}\frac{\beta(y-\eta)}{\sqrt{(x-\xi)^2-\beta^2z^2}}\,d\eta$$

$$= -\lim_{\xi\to x-\beta z}\int_{\eta_1}^{\eta_2}\frac{\partial q}{\partial\eta}\sin^{-1}\frac{\beta(y-\eta)}{\sqrt{(x-\xi)^2-\beta^2z^2}}\,d\eta$$

$$+\frac{1}{\beta}\int_0^{x-\beta z}d\xi\,\frac{\partial}{\partial z}\int_{\eta_1}^{\eta_2}\frac{\partial q}{\partial\eta}\sin^{-1}\frac{\beta(y-\eta)}{\sqrt{(x-\xi)^2-\beta^2z^2}}\,d\eta \qquad (22)$$

Denoting the first of the two integrals in the last expression for T_2 by I, and I_2 respectively, it is clear that

$$|I_1| \leq \left(\frac{\partial q}{\partial \eta}\right)_{max.} \cdot \frac{\pi}{2} \cdot \lim_{\xi \to x-\beta z} (\eta_2 - \eta_1) = 0$$

if $(\partial q / \partial \eta)$ is finite.

We also note that, in I_2,

$$\frac{\partial}{\partial z}\int_{\eta_1}^{\eta_2} \frac{\partial q}{\partial \eta} \sin^{-1}\frac{\beta(y-\eta)}{\sqrt{(x-\xi)^2-\beta^2z^2}}\,d\eta = \frac{\partial \eta_2}{\partial z}\lim_{\eta\to\eta_2}\left(\frac{\partial q}{\partial \eta}\right)\sin^{-1}\frac{\beta(y-\eta)}{\sqrt{(x-\xi)^2-\beta^2z^2}}$$

$$- \frac{\partial \eta_1}{\partial z}\lim_{\eta\to\eta_1}\left(\frac{\partial q}{\partial \eta}\right)\sin^{-1}\frac{\beta(y-\eta)}{\sqrt{(x-\xi)^2-\beta^2z^2}}$$

$$+ \int_{\eta_1}^{\eta_2} \frac{\partial q}{\partial \eta}\,\frac{\beta^3 z(y-\eta)\,d\eta}{\{(x-\xi)^2-\beta^2z^2\}\sqrt{(x-\xi)^2-\beta^2\{(y-\eta)^2+z^2\}}} \qquad (23)$$

We are interested in the value of w at z = 0. The integral in the last term of equation (21) is obviously convergent, and therefore approaches zero as z → 0. The first two terms are

$$\frac{\beta z}{\sqrt{(x-\xi)^2-\beta^2z^2}}\,\frac{\pi}{2}\left\{\left(\frac{\partial q}{\partial \eta}\right)_2 - \left(\frac{\partial q}{\partial \eta}\right)_1\right\}$$

which also approaches zero as z → 0. As seen from equation (22), it

is actually necessary to prove that the integral of this expression with respect to ξ vanishes, which is easily shown as follows. If

$$I = \int_0^{x-\beta z} \frac{z\, d\xi}{\sqrt{(x-\xi)^2 - \beta^2 z^2}} \left\{ \left(\frac{\partial q}{\partial \eta}\right)_2 - \left(\frac{\partial q}{\partial \eta}\right)_1 \right\}$$

then

$$|I| \leq K \int_0^{x-\beta z} \frac{z\, d\xi}{\sqrt{(x-\xi)^2 - \beta^2 z^2}}$$

where

$$K \geq \left| \left(\frac{\partial q}{\partial \eta}\right)_2 - \left(\frac{\partial q}{\partial \eta}\right)_1 \right|$$

So that

$$|I| \leq K\, z \log \left\{ (x-\xi) + \sqrt{(x-\xi)^2 - \beta^2 z^2} \right\} \Bigg|_0^{\xi = x-\beta z}$$

$$\leq K \left| z \log \frac{\beta z}{x + \sqrt{x^2 - \beta^2 z^2}} \right|$$

and

$$\lim_{z \to 0} |I| = \lim_{z \to 0} z \log z = 0$$

Thus T_2 becomes zero, and in a similar manner, T_1 approaches zero as $z \to 0$. Therefore

$$w_{z=0} = \lim_{z \to 0} \left(\frac{\partial \phi}{\partial z}\right) = -\pi q(x, y) \tag{24}$$

This extremely simple result indicates that the velocity potential may be written immediately in terms of a known downwash distribution in the xy-plane, with

$$q = -\frac{w}{\pi} \tag{24a}$$

The same result was demonstrated previously (Ref. 10) in a somewhat simpler manner, relying to some extent on a physical argument, but which unfortunately was not rigorous mathematically. As noted previously this solution will produce a distribution of $\underline{w}$ which is antisymmetric about the xy-plane, which, from the boundary condition, (equation 14) corresponds to a symmetric body at zero lift. A potential of this type will thus be useful mainly for calculations of drag of thin airfoils.

In this case, the local slope of the airfoil surface in the x-direction, λ_x, gives the source distribution immediately, for, from equation (14),

$$w = U_o \lambda_x \tag{25}$$

In certain special cases, this solution can also be used to calculate the lift distribution on an airfoil. Consider the airfoil of Fig. 3, in which the angle between the tangent to any part of the leading edge or trailing edge and the x-axis, θ, is always greater than the Mach angle, μ. In this case there is no disturbance in the field ahead of the wing. Suppose that the angle of attack distribution over the surface of the wing is α; then in the upper half-space ($z > 0$) we may represent the potential in the form of equation (19), with $q = -\alpha(\xi, \eta)/\pi$. In the lower half-space we may define the solution as the negative of this, thus obtaining a total solution for which w is symmetric, and u antisymmetric about (x, y), i.e., a solution for a lifting wing of zero thickness. Since ϕ is zero everywhere ahead of the airfoil, and the Mach waves from the tips, the two solutions agree here, and since conditions behind the airfoil cannot influence conditions of the surface,

it is unnecessary to calculate conditions here. The type of solution cannot, of course, be used to calculate directly the flow in the wake of the airfoil, when the solution must again be symmetric in w. Leading and trailing edges of this type are called "supersonic" since the component of the free stream Mach number normal to the leading edge is greater than 1:

$$M_n = M \sin \theta > M \sin \mu = 1 . \qquad (26)$$

Thus the "source distribution" technique can be used to calculate the lift as well as drag of any airfoil with entirely supersonic leading and trailing edges.

For airfoils with "tips" which are essentially subsonic leading or trailing edges, as in Fig. 4, the source solution can be applied to calculate lift on all parts of the airfoil except the regions, A, affected by the tips (the shaded zones). In principal, the same technique can be used even here, if a source distribution can be found for both regions A and B which results in the proper upwash over A, and a zero u-velocity over B, for in this case the two potentials for the upper and lower half-spaces would match in the free stream areas B. In general, this would appear to lead to an integral equation for the source distribution; however Evaard (Ref. 11) has shown that a solution can be written immediately in terms of the angle of attack distribution in region A. Thus even in this case the solution can be represented immediately by simple integrals of the type of equation (19). This method fails if the influence zone from one of the tip regions B, or from the area ahead of a subsonic part of the leading edge, falls on part of the opposite region A.

In the general case of airfoils with subsonic leading edges, the lift problem may be solved by superpositions of special conical flow solutions of the type described in the first part of this chapter. Another technique is also suggested by the special properties of the solution in equation (19). We observe first that not only the potential, ϕ, but also the perturbation velocity components, u, v, and w must satisfy the basic equation (11). Thus if

$$\bar{u}(x,y,z) = -\frac{1}{\pi}\frac{\partial}{\partial z}\int_0^{\xi_1} d\xi \int_{\eta_1}^{\eta_2} \frac{u(\xi,\eta)\, d\xi\, d\eta}{\sqrt{(x-\xi)^2 - \beta^2\{(y-\eta)^2 + z^2\}}} \tag{27}$$

we see from the properties of (19) as indicated in (24) that

$$\bar{u}(x, y, 0) = u(x, y).$$

This distribution of u will be antisymmetric in the xy-plane - i.e., it represents a lifting surface. A potential which will produce this u-field is:

$$\phi = \int \bar{u}(x,y,z)\, dx$$

If the integration with respect to x and the differentiation with respect to z are carried out, we find that

$$\phi = -\frac{1}{\pi}\int_0^{\xi_1}\int_{\eta_1}^{\eta_2} \frac{u(\xi,\eta)\, z\cdot(x-\xi)\, d\xi\, d\eta}{\{(y-\eta)^2 + z^2\}\sqrt{(x-\xi)^2 - \beta^2\{(y-\eta)^2+z^2\}}} \tag{28}$$

From equation (16), the velocity u is essentially the lift per unit area, L', for

$$\frac{L'}{\rho U^2/2} = -2C_p = +4\frac{u}{U_o} \tag{29}$$

Thus the potential for a wing of given lift distribution may be written down immediately, but the angle of attack distribution must, in general, be calculated from equation (28). In the inverse problem, that of given shape, the lift distribution will, according to this method, be the solution of an integral equation.

The above results may be arrived at in another (rather similar) manner, but which brings out more clearly its physical interpretation. Imagine a row of supersonic "sources" of constant strength q starting at the origin and extending back along the x-axis to ∞ . According to equation (19), the potential for this row of sources will be

$$\phi_1(x, y, z) = \int_0^{\xi_1} \frac{q_1 \, d\xi}{\sqrt{(x-\xi)^2 - \beta^2(y^2+z^2)}} \tag{30}$$

where

$$\xi_1 = x - \beta\sqrt{y^2+z^2}$$

Thus

$$\phi_1(x, y, z) = +q_1 \cosh^{-1}\frac{x}{\beta\sqrt{y^2+z^2}}$$

A row of "doublets", obtained by bringing another source row up from below, will be represented by

$$\phi_2(x, y, z) = \frac{\partial \phi_1}{\partial z} = -\frac{q_1 \cdot x \cdot z}{(y^2+z^2)\sqrt{x^2-\beta^2(y^2+z^2)}} \tag{31}$$

Now by analogy with the subsonic interpretation of such a doublet line, this should represent an infinitesimal horseshoe vortex, commencing at the origin, as in Fig. 5, with finite product of circulation Γ and width $d\eta$, but, in this limiting case, infinite circulation. The flow field associated with the potential ϕ_2 might be considered a distorted version of the subsonic horseshoe vortex, and is therefore not recognizable as such - but if we proceed to the Treftz plane ($x \to \infty$), and restrict ourselves to the neighborhood of the x-axis, the flow field is immediately recognizable as identical to the subsonic doublet. For

$$\lim_{x \to \infty} \phi_2 = - \frac{q_1 z}{(y^2 + z^2)} \tag{32}$$

which is the potential for a horseshoe vortex of width a, and circulation Γ, for $a \to 0$, with $q_1 = - \Gamma a/2\pi$, and with circulation in the sense shown in Fig. 5. Since the vortex laws and the Kutta-Joukowski law still hold in the supersonic flow, we know that the total lift on the bound part of this vortex system (i.e., at the origin) is

$$L = \rho U \Gamma a = - \rho U \cdot 2\pi q \,. \tag{33}$$

Thus

$$q_1 = - \frac{U}{4\pi} \cdot \frac{L}{\rho U^2/2} \tag{34}$$

If we now suppose q_1 to be a doublet strength per unit area, introduce this in equation (31) and integrate over an area in the ξ, η plane the result agrees with equations (28) and (29) exactly.

This approach has incidentally indicated a method for calculating the downwash behind a supersonic wing of known lift distribution in a plane very far behind the wing, and in a region well inside the Mach cone. In this plane, the chordwise distribution of lift on the wing is obviously unimportant. If the total lift per unit span is L', than the potential in the Treftz plane is approximately, from equations (32) and (34),

$$\phi = \frac{U}{4\pi} \frac{1}{\rho U^2/2} \int_{-b/2}^{b/2} \frac{L'(\eta)\, z\, d\eta}{(y-\eta)^2 + z^2} \tag{35}$$

where the wing span runs from -b/2 to b/2. Or, alternatively, this field can be calculated using any of the standard techniques for obtaining the flow field far behind a subsonic wing of known lift distribution. The above calculation will not, of course, give the field correctly near the Mach cone from the wing.

In the remainder of this presentation, attention will be centered on the calculations which can be made using the potential of the type in equation (19), with particular attention to drag calculations.

In Ref. 13, R. T. Jones makes use of a source distribution similar to the solution of equation (19), actually an integral of a uniform distribution over certain basic areas, to calculate the drag of certain swept back wings. Again, in Ref. 14, Jones makes use of the solutions of the type in equation (28) to calculate the characteristics of wings with given lift distribution. Further application of an extended form of the solution in equation (19) was used by Evvard in Refs. (15), (16) and (17) to calculate lift near subsonic wing tips, downwash fields,

and performance of yawed wings. The doublet distributions of equation (28) are used again by Heaslet and Lomax in Ref. 18 for the calculation of downwash fields.

Extensive calculations of airfoil drag for vaious specific planforms were made using the source distribution method by Margolis in Refs. (19), (20) and (21). The source solutions were also presented by Th. von Karman in terms of Fourier integrals in Ref. 22.

PART III

SPECIAL APPLICATIONS TO INFINITE WINGS

As a first illustration of the application of the source type of potential, a calculation will be made of the pressure distribution and drag on an infinite two-dimensional wing of small but finite thickness and at zero angle of attack which is swept back or yawed. Two cases are of interest: (1) the angle θ between wing leading edge and x-axis is greater than the Mach angle, μ, or (2) θ is less than μ. The first case is shown in Fig. 6. In this case, the "sweepback angle", σ, is such that $\tan \sigma > \beta$.

The pressure coefficient at a point P, which we may take to be on the x axis, and in the plane of the airfoil, will be determined by the source distribution within the forecone of P, the region A in Fig. 6. This forecone is bounded by the Mach lines

$$\eta = \pm (x - \xi)/\beta$$

and by the leading edge

$$\xi = k\eta$$

where $k = \tan \sigma$.

From equations (19) and (24), the potential at P is given by

$$\phi(x) = -\frac{1}{\pi} \iint_A \frac{w \, d\xi \, d\eta}{\sqrt{(x-\xi)^2 - \beta^2 \eta^2}} \qquad (36)$$

where w is the (known) downwash in the ξ, η plane. Let λ be the slope of a surface element of the airfoil measured in the x-direction. Then λ is constant along lines parallel to the leading edge of the

airfoil. If we introduce

$$s = \xi - k\eta \tag{37}$$

then s is constant along lines parallel to the leading edge, and

$$w = \lambda(s) \cdot U \tag{38}$$

Equation (36) now becomes:

$$\phi = -\frac{1}{\pi}\int_0^x w\,ds \int_{\eta_1}^{\eta_2} \frac{d\eta}{\sqrt{(x-s-k\eta)^2-\beta^2\eta^2}} \tag{39}$$

while the limits of integration are:

$$\eta_1 = -(x-\xi)/\beta = -\frac{x-s}{\beta-k}$$
$$\eta_2 = +(x-\xi)/\beta = +\frac{x-s}{\beta+k} \tag{40}$$

Equation (39) may be rewritten as:

$$\phi = -\frac{1}{\pi}\int_0^x w(s)\,ds \int_{\eta_1}^{\eta_2} \frac{d\eta}{\sqrt{\frac{\beta^2(x-s)^2}{\beta^2-k^2} - \left\{\frac{(x-s)k}{\sqrt{\beta^2-k^2}} + \eta\sqrt{\beta^2-k^2}\right\}^2}} \tag{41}$$

This is immediately integrated to

$$\phi = -\frac{1}{\pi}\int_0^x \frac{w(s)\,ds}{\sqrt{\beta^2-k^2}} \sin^{-1}\left\{\frac{k}{\beta} + \frac{(\beta^2-k^2)}{\beta(x-s)}\eta\right\}\Bigg|_{\eta_1}^{\eta_2}$$

or,

$$\phi = -\int_0^x \frac{w(s)\,ds}{\sqrt{\beta^2 - k^2}} \tag{42}$$

The x-velocity increment is

$$u = \frac{\partial \phi}{\partial x} = -\frac{w(x)}{\sqrt{\beta^2 - k^2}} = -\frac{U\lambda}{\sqrt{\beta^2 - k^2}} \tag{43}$$

The pressure coefficient can, of course, be calculated immediately from equation (16). It will, however, be more convenient to express the pressure coefficient in terms of the component of velocity normal to the airfoil leading edge. We may let

$$U_n = U \cos \sigma$$

$$M_n = M \cos \sigma$$

and

$$C_{P_n} = \frac{\Delta p}{\rho U_n^2/2} \tag{44}$$

where Δp is the pressure disturbance on the airfoil surface. We may further note that

$$\cos \sigma = 1/\sqrt{1 + k^2}$$

and we may define a new "β" for the normal Mach number by

$$(\beta')^2 = M_n^2 - 1 = \frac{M^2}{1+k^2} - 1 = \frac{\beta^2 - k^2}{1+k^2} \tag{45}$$

The slope of the airfoil measured normal to the leading edge is

$$\lambda_n = \frac{\lambda}{\cos\sigma} = \lambda\sqrt{1+k^2} \tag{46}$$

Combining equations (43), (44), (45), and (46), we obtain finally

$$C_{p_n} = + \frac{2\lambda_n}{\beta'} = + \frac{2\lambda_n}{\sqrt{M_n^2 - 1}} \tag{47}$$

This is identical with the result obtained by Ackeret (Ref. 1) for the pressure coefficient on a two-dimensional airfoil, referred here to the velocity and Mach number of the flow normal to the leading edge. The initial requirement that $\beta > k$ ensures that M_n is greater than 1. This result is easily obtained also by the direct physical argument that the pressures in this case must be determined only by the component flow normal to the leading edge, as was pointed out in 1935 by Busemann (Ref. 5). In other words, the true free stream velocity can be supposed to consist of one component parallel to the wing leading edge, which cannot affect the pressure distribution, and a normal component. The pressure coefficient referred to the true free stream dynamic pressure is

$$C_p = - \frac{2\lambda_n \cos^2\sigma}{\sqrt{M_n^2 - 1}} \tag{48}$$

For this two-dimensional airfoil, the normal to each surface element is also normal to the airfoil leading edge, and therefore the horizontal component of the net force on each element is normal to the leading edge. The component of this force, ΔF, parallel to the x-axis will give its contribution to the airfoil drag, ΔD, as

$$\Delta D = \Delta F \cos \sigma \tag{49}$$

Thus the elementary drag coefficient will be

$$\Delta C_D = - \frac{2 \lambda_n^2 \cos^3 \sigma}{\sqrt{M_n^2 - 1}}$$

or

$$\Delta C_D = - \frac{2 \lambda^2 \cos \sigma}{\sqrt{M_n^2 - 1}} \tag{50}$$

where the x-direction slope, λ , has again been introduced.

If we consider an airfoil with fixed profile in the xz-plane, but variable sweepback, and thus consider only the variation in $\cos \sigma / \sqrt{M_n^2 - 1}$ with σ , we see that the drag is actually increased with increasing σ , and approaches the usual two-dimensional sigularity at $M_n = 1$. Even in this very simplified case it thus appears likely that primary drag advantage from sweepback must come from sweeping the wing back so far that $M_n < 1$, or else taking advantage of the new geometry to decrease the slopes, λ , measured parallel to the free stream flow.

A similar calculation may now be made for the second case mentioned at the beginning of this section - the infinite wing swept at an angle such that the leading edge is behind the Mach waves, i.e., tan $\sigma > \beta$. this case is illustrated in Fig. 7. The forecone of P will now intersect both leading and trailing edges of the wing, so the limits of integration must be revised somewhat. It is convenient to carry out the integration in two parts, one over the area ahead of the line L, and bounded by the

upper Mach wave, and the other over the region behind L. Using again

$$s = \xi - k\eta$$

we have the complete potential

$$\phi = -\frac{1}{\pi}\iint_A \frac{w\, ds\, d\eta}{\sqrt{(x-s)^2 - 2(x-s)k\eta + (k^2-\beta^2)\eta^2}} \tag{51}$$

where A is the forecone of P. If we divide the integral as above, with

$$\phi = I_1 + I_2$$

then

$$I_1 = -\frac{1}{\pi}\int_0^x w\, ds \int_a^{\eta_2} \frac{d\eta}{\sqrt{\left\{\frac{(x-s)k}{\sqrt{k^2-\beta^2}} - \eta\sqrt{k^2-\beta^2}\right\}^2 - \frac{\beta^2(x-s)^2}{k^2-\beta^2}}} \tag{52}$$

and

$$I_2 = -\frac{1}{\pi}\int_x^c w\, ds \int_a^{\eta_1} \frac{d\eta}{\sqrt{\left\{\frac{(x-s)k}{\sqrt{k^2-\beta^2}} - \eta\sqrt{k^2-\beta^2}\right\}^2 - \frac{\beta^2(x-s)^2}{k^2-\beta^2}}} \tag{53}$$

where η_1 and η_2 are still given as in equation (40), and the lower limit a will be allowed to approach minus infinity. In order to obtain the principal value of these integrals, the squared quantities under the square root must be taken in such sense that they are positive in the range considered. The expression in brackets under the square root is positive in both cases. In I_1, (x-s) is greater than zero, so

$$I_1 = \frac{1}{\pi\sqrt{k^2-\beta^2}}\int_0^x w\, ds\, \cosh^{-1}\left\{\frac{k}{\beta} - \frac{(k^2-\beta^2)\eta}{\beta(x-s)}\right\}\Bigg|_a^{\eta_1}$$

At $\eta = \eta_1$, the expression in brackets becomes unity, so that

$$I_1 = -\frac{1}{\pi\sqrt{k^2-\beta^2}} \int_0^x w\,ds\, \cosh^{-1}\left\{\frac{k}{\beta} - \frac{(k^2-\beta^2)a}{\beta(x-s)}\right\} \tag{54}$$

The second integral is similar except that (s-x) is now greater than zero. Thus

$$I_2 = \frac{1}{\pi\sqrt{k^2-\beta^2}} \int_x^c w\,ds\, \cosh^{-1}\left\{-\frac{k}{\beta} - \frac{(k^2-\beta^2)\eta}{\beta(s-x)}\right\}\Bigg|_a^{\eta_2}$$

or

$$I_2 = -\frac{1}{\pi\sqrt{k^2-\beta^2}} \int_x^c w\,ds\, \cosh^{-1}\left\{-\frac{k}{\beta} - \frac{(k^2-\beta^2)a}{\beta(s-x)}\right\} \tag{55}$$

These two integrals may be combined to:

$$\phi = -\frac{1}{\pi\sqrt{k^2-\beta^2}} \int_0^c w\,ds\, \cosh^{-1}\left|\frac{k}{\beta} - \frac{(k^2-\beta^2)a}{\beta(x-s)}\right| \tag{56}$$

since the expression in brackets in both equations (54) and (55) is positive in the range of s considered. The incremental u-velocity is then:

$$\frac{\partial\phi}{\partial x} = -\frac{\sqrt{k^2-\beta^2}}{\pi} \int_0^c \frac{a\,w(s)\,ds}{(s-x)\sqrt{\{k(x-s)-(k^2-\beta^2)a\}^2-\beta^2(x-s)^2}}$$

If a is now allowed to approach minus infinity, we find

$$u = \frac{\partial \phi}{\partial x} = -\frac{1}{\pi\sqrt{k^2-\beta^2}} \int_0^c \frac{w(s)\, ds}{(s-x)} \tag{57}$$

This disturbance velocity is of the same form as that obtained in the two-dimensional thin wing theory for the representation of the pressures over a symmetrical airfoil of finite thickness at zero lift. In fact, for an airfoil at zero Mach number, with a chordwise slope distribution $\lambda_o(s)$, in a flow at velocity U_o, the perturbation velocity over the surface would be

$$\frac{\partial \phi}{\partial x} = -\frac{U_o}{\pi} \int_0^c \frac{\lambda_o(s)\, ds}{(s-x)} \tag{58}$$

The pressure coefficient corresponding to the supersonic case will be, from equations (38) and (57),

$$C_p = +\frac{2}{\pi\sqrt{k^2-\beta^2}} \int_0^c \frac{\lambda(s)\, ds}{(s-x)} \tag{59}$$

where $\lambda(s)$ is still the slope in the x-direction. In the incompressible case, from equation (58), the pressure coefficient is

$$C_{p_o} = +\frac{2}{\pi} \int_0^c \frac{\lambda_o(s)\, ds}{(s-x)} \tag{60}$$

In our supersonic case, we may now rewrite equation (59) in terms of the velocity, Mach number and slope normal to the leading edge, using equations (38), (44), and (46), and referring the pressure coefficient to the dynamic pressure of the normal flow as before. We note that

$$1 - M_n^2 = 1 - \frac{M^2}{1 + k^2} = \frac{k^2 - \beta^2}{1 + k^2} \tag{61}$$

The new supersonic pressure coefficient, C_{p_n}, becomes

$$C_{p_n} = \frac{2}{\pi\sqrt{1 - M_n^2}} \int_0^c \frac{\lambda_n(s)\, ds}{(s - x)}$$

$$= \frac{1}{\sqrt{1 - M_n^2}}\, C_{p_o} \tag{62}$$

Thus, as again might be expected from very simple physical considerations, the pressure distribution over the airfoil is determined only by the component of flow normal to the leading edge. In this case, the normal Mach number is less than 1, and the pressure distribution is subsonic in character, being exactly equal to that computed for the two dimensional normal profile with a Prandtl-Glauert correction based on the normal Mach number. The drag in this case is obviously zero, according to the D'Alembert paradox, or as may be easily shown by integrating the pressure distribution of equation (59) multiplied by the local slope over the chord of the airfoil.

It must be noted that the integrals of equations (54) and (55), and particularly of (56) and (57) are all singular at $s = x$. In equation (57) it is necessary to take the Cauchy principle value. In (54), (55) and (56) the singularity is essentially logarithmic, and causes no trouble.

The above calculation suggests strongly that appreciable drag reductions may be obtained with wings swept back behind the Mach angle. However, in the form presented it cannot give any quantatative indication of this

in a practical case, since any real wing must be finite in span, and therefore no part of it will be free from the influence of the center section. If a real wing consists of two two-dimensional wings both swept back from a center plane of symmetry then the conditions infinitely far from the center must approach the results of the previous calculation. The real problem is the calculation of the flow resulting from the geometry of the center section.

PART IV

APPLICATION TO DELTA WINGS; SCHEME OF CALCULATIONS

As a particularly simple case of a finite three-dimensional wing, we shall consider the wing with planform shown in Fig. 8, called a delta wing. For simplicity the profile is taken to be a double wedge, with variable location of the vertex, B. The three essential geometrical parameters are the three sweepback angles of the leading edge, maximum thickness line, and trailing edge; σ_1, σ_2, and σ_3, respectively, or their tangents,

$$\begin{aligned} k_1 &= \tan \sigma_1 \\ k_2 &= \tan \sigma_2 \\ k_3 &= \tan \sigma_3 \end{aligned} \tag{63}$$

It will also be convenient to define

$$\begin{aligned} r &= k_2/k_1 \\ a &= k_3/k_1 \end{aligned} \tag{64}$$

The area, S, and aspect ratio, $\mathcal{R}$, are respectively

$$S = \frac{b^2}{4}(k_1 - k_3) \quad , \quad \mathcal{R} = \frac{4}{k_1 - k_3} \tag{65}$$

$$= \frac{b^2}{4}(1-a)k_1$$

The thickness is τ times the true root chord, $\ell = (1 - a)C$. The slopes (in the x-direction) in regions I and II respectively will thus be

$$\lambda_1 = \frac{(1-a)}{2(1-r)} \quad , \quad \lambda_2 = \frac{(1-a)}{2(r-a)} \tag{66}$$

It is desired to compute the drag of this wing at zero lift, using the source solutions of the type of equation (19) to describe the flow field. The computation scheme thus becomes quite simple in principle; since the slope in region I is a constant, λ_1, its contribution to the solution is represented by a constant source distribution in region I, and similarly in region II. In order to simplify still further the classification of the basic integrals required, the wing planform can be composed in a somewhat different way. The slope distribution can be supposed to result from the superposition of three triangles, with vertices at A, B and C, respectively, each extending indefinitely in the positive x-direction. The slopes of the surfaces of these triangles will then be

$$\lambda_A = \lambda_1$$

$$\lambda_B = \lambda_2 - \lambda_1$$

$$\lambda_C = -\lambda_2 \qquad (67)$$

which, upon superposition will give the correct actual slopes in regions I and II, and zero slope in the wake. The basic pressure distribution required will therefore be that associated with a single such triangle of constant slope. For the sake of order, the scheme of superposition and calculation of mutual influences will be set up fairly completely in this section, before any of the calculations are carried out.

In the calculation of the drag of the complete wing, four cases must be considered, determined by the direction of the Mach wave relative to the three lines AT, BT, and CT on the wing. These cases are characterised by

(1) $\beta > k_1$

(2) $k_1 > \beta > k_2$

(3) $k_2 > \beta > k_3$

(4) $k_3 > \beta$

and are illustrated in Fig. 1. We notice that in cases (1) and (2), the pressures associated with the source distribution in the triangle A, will act upon both regions I and II, while the source distribution in B will act only upon region II. In case (3), the pressures due to B can also act on region I, while in case (4), the pressures due to both B and C can act on both regions I and II.

Let C_{p_j} be the pressure coefficient for the field associated with a uniform source distribution in a triangle with vertex at j and a (positive) unit slope in the x-direction. Then let D_{ij} be the drag in region i due to the source distribution in triangle with vertex j. In general, the total drag for both sides of the delta wing will then consist of the following six terms:

$$(1)\quad \frac{D_{IA}}{q} = 2\lambda_1\lambda_A \int_I C_{p_A}\, dA$$

$$(2)\quad \frac{D_{IB}}{q} = 2\lambda_1\lambda_B \int_I C_{p_B}\, dA$$

$$(3)\quad \frac{D_{IC}}{q} = 2\lambda_1\lambda_C \int_I C_{p_C}\, dA$$

$$(4)\quad \frac{D_{IIA}}{q} = 2\lambda_2\lambda_A \int_{II} C_{p_A}\, dA$$

$$(5)\quad \frac{D_{IIB}}{q} = 2\lambda_2\lambda_B \int_{II} C_{p_B}\, dA$$

$$(6)\quad \frac{D_{IIC}}{q} = 2\lambda_2\lambda_C \int_{II} C_{p_C}\, dA$$

Introducing the values of the slopes from equations (66) and (67), and dividing by the actual area of the wing, we have the individual contributions to the drag coefficient as:

$$(1) \quad C_{D_{IA}} = \frac{\tau^2}{2} \frac{(1-a)^2}{(1-r)^2} \frac{1}{S} \int_I C_{P_A} \, dA \qquad (69a)$$

$$(2) \quad C_{D_{IB}} = -\frac{\tau^2}{2} \frac{(1-a)^3}{(1-r)^2(r-a)} \frac{1}{S} \int_I C_{P_B} \, dA \qquad (69b)$$

$$(3) \quad C_{D_{IC}} = \frac{\tau^2}{2} \frac{(1-a)^2}{(1-r)(r-a)} \frac{1}{S} \int_I C_{P_C} \, dA \qquad (69c)$$

$$(4) \quad C_{D_{IIA}} = -\frac{\tau^2}{2} \frac{(1-a)^2}{(1-r)(r-a)} \frac{1}{S} \int_{II} C_{P_A} \, dA \qquad (69d)$$

$$(5) \quad C_{D_{IIB}} = \frac{\tau^2}{2} \frac{(1-a)^3}{(r-a)^2(1-r)} \frac{1}{S} \int_{II} C_{P_B} \, dA \qquad (69e)$$

$$(6) \quad C_{D_{IIC}} = -\frac{\tau^2}{2} \frac{(1-a)^2}{(r-a)^2} \frac{1}{S} \int_{II} C_{P_C} \, dA \qquad (69f)$$

The total drag coefficient for both sides of the airfoil will be the sum of these terms.

In the first and second cases of Fig. 9, terms (2), (3) and (6) are zero. In case three, terms (3) and (6) are zero. Term (1) and (4) will have a singularity when $k_1 = \beta$, and term (5) will have a singularity when $k_2 = \beta$, or $k_1 r = \beta$. This essentially completes the cataloging of the necessary calculations. The only problem remaining is the calculation of the various pressure distributions and the special integrals of these pressure distributions as required by equations (69).

PART V

BASIC PRESSURE DISTRIBUTIONS AND SURFACE INTEGRALS

A. Pressures over unit-slope triangle.

As concluded in the last section, the initial problem is the calculation of the pressure field associated with one of the basic triangles. This pressure field will have a different representation depending on whether k is greater or less than β, i.e., whether the leading edge is ahead of or behind the Mach wave from its vertex. The first case is illustrated in Fig. 10, for a point within the triangle.

The potential on the airfoil surface at point $P = (x, y)$ will be the integral over the region between the leading edges and the Mach lines going forward from P of the uniform source distribution. This integration is most conveniently carried out in three parts, corresponding to the regions (1), (2) and (3) in Fig. 10. Since the pressure field is to be calculated for a triangle with unit slope, the potential is:

$$\phi(x, y) = I_1 + I_2 + I_3, \text{ say,}$$

where

$$I_1 = -\frac{U}{\pi} \int_{y_1}^{0} d\eta \int_{-k\eta}^{\xi_1} f(\xi, \eta)\, d\xi$$

$$I_2 = -\frac{U}{\pi} \int_{0}^{y} d\eta \int_{+k\eta}^{\xi_1} f(\xi, \eta)\, d\xi$$

$$I_3 = -\frac{\sigma}{\pi}\int_{y}^{y_2} d\eta \int_{k\eta}^{\xi_2} f(\xi,\eta)\, d\xi \tag{70}$$

with

$$f(\xi,\eta) = \left\{(x-\xi)^2 - \beta^2(y-\eta)^2\right\}^{-1/2}$$

and

$$\xi_1 = x - \beta(y-\eta)$$

$$\xi_2 = x + \beta(y-\eta)$$

The points y_1 and y_2 are given by

$$ky_2 = x + \beta(y - y_2)$$

and

$$-ky_1 = x - \beta(y - y_1)$$

or

$$y_2 = \frac{x+\beta y}{k+\beta}, \quad y_1 = -\frac{x+\beta y}{k+\beta} \tag{71}$$

Integrating these expressions once, one obtains:

$$I_1 = +\frac{\sigma}{\pi}\int_{y_1}^{0} d\eta \cosh^{-1}\frac{x-\xi}{\beta(y-\eta)}\Bigg|_{-k\eta}^{\xi_1}$$

$$= -\frac{\sigma}{\pi}\int_{y_1}^{0} d\eta \cosh^{-1}\frac{x+k\eta}{\beta(y-\eta)}$$

$$I_2 = +\frac{\sigma}{\pi}\int_{0}^{y} d\eta \cosh^{-1}\frac{x-\xi}{\beta(y-\eta)}\Bigg|_{+k\eta}^{\xi_1}$$

$$= -\frac{\sigma}{\pi}\int_{0}^{y} d\eta \cosh^{-1}\frac{x-k\eta}{\beta(y-\eta)}$$

$$I_3 = + \frac{\sigma}{\pi} \int_y^{y_2} d\eta \cosh^{-1} \frac{x-\xi}{\beta(y-\eta)} \Big|_{k\eta}^{\xi_2}$$

$$= - \frac{\sigma}{\pi} \int_y^{y_2} d\eta \cosh^{-1} \frac{x-k\eta}{\beta(y-\eta)} \tag{72}$$

These integrals may immediately be differentiated to find the u-velocity. Since the integrands vanish at $= y_1$ or y_2, we obtain:

$$u = \frac{\partial \phi}{\partial x} = - \frac{\sigma}{\pi} \int_{y_1}^{0} \frac{d\eta}{\sqrt{(x+k\eta)^2 - \beta^2(y-\eta)^2}}$$

$$- \frac{\sigma}{\pi} \int_0^{y_2} \frac{d\eta}{\sqrt{(x-k\eta)^2 - \beta^2(y-\eta)^2}} \tag{73}$$

These integrations can be carried out easily if one notes that

$$(x+k\eta)^2 - \beta^2(y-\eta)^2 = \left(\frac{kx+\beta^2 y}{\sqrt{k^2-\beta^2}} + \eta\sqrt{k^2-\beta^2} \right)^2 - \frac{\beta^2(x+ky)^2}{k^2-\beta^2}$$

$$(x-k\eta)^2 - \beta^2(y-\eta)^2 = \left(\frac{kx-\beta^2 y}{\sqrt{k^2-\beta^2}} - \eta\sqrt{k^2-\beta^2} \right)^2 - \frac{\beta^2(x-ky)^2}{k^2-\beta^2} \tag{74}$$

Denoting the integrals of equation (73) by I_1 and I_2 respectively, these become:

$$I_1 = -\frac{U}{\pi\sqrt{k^2-\beta^2}} \cosh^{-1} \frac{kx+\beta^2 y + \eta\sqrt{k^2-\beta^2}}{\beta(x+ky)} \Bigg|_{y_1}^{0}$$

$$I_2 = +\frac{U}{\pi\sqrt{k^2-\beta^2}} \cosh^{-1} \frac{kx-\beta^2 y - \eta\sqrt{k^2-\beta^2}}{\beta(x-ky)} \Bigg|_{0}^{y_2}$$

At the limits y_1 and y_2, the inverse hyperbolic cosine terms vanish, so that one finally obtains:

$$u = \frac{\partial\phi}{\partial x} = -\frac{U}{\pi\sqrt{k^2-\beta^2}} \left[\cosh^{-1}\left\{\frac{kx+\beta^2 y}{\beta(x+ky)}\right\} + \cosh^{-1}\left\{\frac{kx-\beta^2 y}{\beta(x-ky)}\right\}\right] \qquad (75)$$

It is clear, of course, that this solution must be essentially conical, that is, the velocities and pressures must be constant on rays through the vertex of the triangle. Therefore let

$$t = ky/x$$

so that $t = 1$ on the leading edge. It is also clear that the solution must depend essentially on the ratio k/β, so we shall let

$$n = k/\beta .$$

Thus $t = n$ on the Mach wave from the vertex of the triangle. This factor, n, might be called the "relative sweepback", since it is essentially the

ratio of leading edge sweepback to the "sweepback" of the Mach waves. The present calculation has required n > 1. Then

$$u = \frac{\partial \phi}{\partial x} = -\frac{v}{\pi\beta}\frac{1}{\sqrt{n^2-1}}\left[\cosh^{-1}\frac{n^2+t}{n(1+t)} + \cosh^{-1}\frac{n^2-t}{n(1-t)}\right] \qquad (76)$$

Now if

$$\cosh a = \frac{n^2+t}{n(1+t)}, \quad \cosh\beta = \frac{n^2-t}{n(1-t)}$$

then it can be easily proved by elementary identities that

$$\cosh\frac{\alpha+\beta}{2} = n\sqrt{\frac{1-(t/n)^2}{1-t^2}}$$

The final expression for u may therefore be written:

$$u = -\frac{2v}{\pi\beta\sqrt{n^2-1}}\cosh^{-1}\sqrt{\frac{n^2-t^2}{1-t^2}} \qquad (77)$$

As t approaches 1, that is, the leading edge of the triangle, the disturbance velocity has a logarithmic singularity. Since in this case, with n > 1, the leading edge of the triangle is "subsonic", this behaviour might well be expected. The expression also becomes complex for 1 < t < n, that is, for points between the leading edge and the Mach wave from the vertex. However for the case n > 1, there is also a disturbance in this region which is required in the airfoil drag calculation. In order to verify the form of the pressure distribution in this region, it is necessary to make a calculation similar to the preceding for a point off of the

triangle, but behind the Mach wave. This situation is illustrated in Fig. 11. The integration of the source influence at P may be carried out in two parts. Again, for the triangle of unit slope in the x direction,

$$\phi = -\frac{v}{\pi}\int_{y_1}^{0} d\eta \int_{-k\eta}^{x-\beta(y-\eta)} \frac{d\xi}{\sqrt{(x-\xi)^2-\beta^2(y-\eta)^2}}$$

$$-\frac{v}{\pi}\int_{0}^{y_2} d\eta \int_{+k\eta}^{x-\beta(y-\eta)} \frac{d\xi}{\sqrt{(x-\xi)^2-\beta^2(y-\eta)^2}} \qquad (78)$$

where

$$y_1 = \frac{x-\beta y}{k-\beta}, \quad y_2 = -\frac{x-\beta y}{k+\beta}$$

Integrating, one obtains:

$$\phi = -\frac{v}{\pi}\int_{y_1}^{0} d\eta \cosh^{-1}\frac{x+k\eta}{\beta(y-\eta)} - \frac{v}{\pi}\int_{0}^{y_2} d\eta \cosh^{-1}\frac{x-k\eta}{\beta(y-\eta)}$$

Since the integrands again vanish at y_1 and y_2, the derivative with respect to x becomes:

$$u = \frac{\partial\phi}{\partial x} = -\frac{v}{\pi}\int_{y_1}^{0} \frac{d\eta}{\sqrt{(x+k\eta)^2-\beta^2(y-\eta)^2}}$$

$$-\frac{v}{\pi}\int_{0}^{y_2} \frac{d\eta}{\sqrt{(x-k\eta)^2-\beta^2(y-\eta)^2}} \qquad (79)$$

A transformation essentially the same as that in equation (74) may now be made. In order to obtain the proper value of the integral, it must be remembered that now $x < ky$, and $kx > \beta^2 y$, so that the sign of the last term in parenthesis in the second of equation (74) must be reversed. The result is then obtained that:

$$u = -\frac{v}{\pi}\frac{1}{\sqrt{k^2-\beta^2}}\left\{\cosh^{-1}\frac{kx+\beta^2 y}{\beta(x+ky)} + \cosh^{-1}\frac{kx-\beta^2 y}{\beta(ky-x)}\right\}$$

or

$$u = -\frac{v}{\pi\beta}\frac{1}{\sqrt{n^2-1}}\left\{\cosh^{-1}\frac{n^2+t}{n(1+t)} + \cosh^{-1}\frac{n^2-t}{n(t-1)}\right\} \qquad (80)$$

As before this expression may be transformed to:

$$u = -\frac{2v}{\pi\beta\sqrt{n^2-1}}\cosh^{-1}\sqrt{\frac{n^2-1}{t^2-1}} \qquad (81)$$

in which form it is real for $1 < t < n$.

This expression again has a logarithmic singularity as t approaches 1, which matches the singularity of equation (77), but it approaches zero as t approaches n, that is, as the point P approaches the Mach wave. Equations (77) and (81) complete the description of the pressure field for $n > 1$, that is, sweepback behind the Mach line, or subsonic leading edge.

It is now necessary to calculate the disturbance field associated with the triangle having $k < \beta$, or $n < 1$, i.e., a supersonic leading

edge. This situation is illustrated in Fig. 12. For $k < \beta$, there is no disturbance ahead of the leading edge of the triangle, so the calculations are concerned only with points on the wing. However here, again, two types of points must be distinguished. Points such as P_1, Fig. 12, lying between the leading edge and the Mach wave M, $(1 > t > n)$ have a potential determined only by the sources lying within the cross-hatched region (1). But this potential apparently must be the same as that for a point on an infinite wing, since the vertex does not lie in this region. The disturbance velocity at P_1 must thus be equal to that calculated for the infinite wing in Part III, and from equation (43) one observes immediately:

$$u(P_1) = -\frac{U}{\sqrt{\beta^2 - k^2}} = -\frac{U}{\beta\sqrt{1-n^2}} \tag{82}$$

At point P_2 the influence of the vertex is felt. However the potential at P_2 must be equal to the potential at P_1 decreased by the influence of a uniform source distribution in the cross-hatched region (2), or, for positive unit slope,

$$\phi(P_2) = \phi(P_1) - \Delta\phi \tag{83}$$

where

$$\Delta\phi = -\frac{U}{\pi}\iint_{(2)} \frac{d\xi\, d\eta}{\sqrt{(x-\xi)^2 - \beta^2(y-\eta)^2}}$$

Writing this integral in two parts, we have:

$$\Delta\phi = -\frac{U}{\pi}\int_{y_1}^{y_2} d\eta \int_{k\eta}^{x-\beta(y-\eta)} f(\xi,\eta)\, d\xi - \frac{U}{\pi}\int_{y_2}^{0} d\eta \int_{k\eta}^{-k\eta} f(\xi,\eta)\, d\xi \qquad (84)$$

where

$$y_1 = -\frac{x-\beta y}{\beta - k}, \qquad y_2 = -\frac{x-\beta y}{\beta + k}$$

Carrying out these integrations, there results:

$$\Delta\phi = -\frac{U}{\pi}\int_{y_1}^{y_2} d\eta \, \cosh^{-1}\frac{x-k\eta}{\beta(y-\eta)} - \frac{U}{\pi}\int_{y_2}^{0} d\eta \left\{ \cosh^{-1}\frac{x-k\eta}{\beta(y-\eta)} - \cosh^{-1}\frac{x+k\eta}{\beta(y-\eta)} \right\}$$

$$\Delta\phi = -\frac{U}{\pi}\int_{y_1}^{0} d\eta \, \cosh^{-1}\frac{x-k\eta}{\beta(y-\eta)} + \frac{U}{\pi}\int_{y_2}^{0} d\eta \, \cosh^{-1}\frac{x+k\eta}{\beta(y-\eta)} \qquad (85)$$

The u-velocity associated with this potential may now be computed. The integrands vanish for $\eta = y_1$ or y_2, and the u-velocity is therefore

$$\Delta u = \frac{\partial}{\partial x}(\Delta\phi) = -\frac{U}{\pi}\int_{y_1}^{0} \frac{d\eta}{\sqrt{(x-k\eta)^2 - \beta^2(y-\eta)^2}} - \frac{U}{\pi}\int_{y_2}^{0} \frac{d\eta}{\sqrt{(x+k\eta)^2 - \beta^2(y-\eta)^2}} \qquad (86)$$

These become elementary integrals if it is noted that

$$(x-k\eta)^2-\beta^2(y-\eta)^2 = \frac{\beta^2(x-ky)^2}{\beta^2-k^2} - \left\{\frac{kx-\beta^2y}{\sqrt{\beta^2-k^2}} + \eta\sqrt{\beta^2-k^2}\right\}^2$$

$$(x+k\eta)^2-\beta^2(y-\eta)^2 = \frac{\beta^2(x+k\eta)^2}{\beta^2-k^2} - \left\{\eta\sqrt{\beta^2-k^2} - \frac{kx+\beta^2y}{\sqrt{\beta^2-k^2}}\right\}^2 \qquad (87)$$

These expressions are essentially the same as those of equations (74), except that the signs of the terms have been chosen so as to keep the quantities in brackets positive through the range of integration, in order to obtain the principal value of the integral. Introducing equations (87) into (86) and integrating, we obtain

$$\Delta u = -\frac{v}{\pi\sqrt{\beta^2-k^2}}\left\{\sin^{-1}\frac{kx-\beta^2y}{\beta(x-ky)} + \sin^{-1}\frac{kx+\beta^2y}{\beta(x+ky)}\right\} \qquad (88)$$

If the variable $t = ky/x$ is introduced, and this equation is reduced by means of elementary trigonometric identities, it can be shown that

$$\Delta u = -\frac{2v}{\pi\beta\sqrt{1-n^2}}\sin^{-1}\sqrt{\frac{n^2-t^2}{1-t^2}} \qquad (89)$$

According to equation (83), the total u-velocity at point P_2, Fig. 12, will consist of the expression in equation (82) minus the increment in equation (89). Thus

$$u(P_2) = -\frac{v}{\beta\sqrt{1-n^2}}\left\{1 - \frac{2}{\pi}\sin^{-1}\sqrt{\frac{n^2-t^2}{1-t^2}}\right\} \qquad (90)$$

As t approaches n, equation (90) will, of course, approach equation (82).

We have now calculated the x-component of the perturbation velocities for both the case of $n > 1$ and $n < 1$, and for points both ahead of and behind the Mach wave. The pressure coefficients are obtained immediately from equation (16),

$$C_p = -2u/U$$

These pressure coefficients, all calculated for unit slope of the basic triangle, may be summarized as follows:

Case 1: $n > 1$

a) $0 < t < 1$ (Fig. 10)

$$C_p = \frac{4}{\pi\beta\sqrt{n^2-1}} \cosh^{-1}\sqrt{\frac{n^2-t^2}{1-t^2}} \qquad (91a)$$

b) $1 < t < n$ (Fig. 11)

$$C_p = \frac{4}{\pi\beta\sqrt{n^2-1}} \cosh^{-1}\sqrt{\frac{n^2-1}{t^2-1}} \qquad (91b)$$

Case 2: $n < 1$

a) $n < t < 1$ (P_1, Fig. 12)

$$C_p = \frac{2}{\beta\sqrt{1-n^2}} \qquad (91c)$$

b) $0 < t < n$

$$C_p = \frac{2}{\beta\sqrt{1-n^2}}\left\{1 - \frac{2}{\pi}\sin^{-1}\sqrt{\frac{n^2-t^2}{1-t^2}}\right\} \qquad (91d)$$

The pressure coefficient for a triangle of slope λ is, of course, obtained by multiplying the right hand side of equations (91) by λ.

For these triangles of slope λ, it is seen from equations (91) that the pressure coefficient in the form $C_p\beta/\lambda$, or $C_p\sqrt{M^2-1}/\lambda$, is a function only of t (position on the airfoil) and n (relative sweepback). Curves of the pressure coefficients in this form are plotted in Fig. 13. The case n = 0 will correspond to the case of the two-dimensional wing with no sweepback, for which it is well known that $C_p\beta/\lambda = 2$. Values of $t > 1$ correspond to points ahead of the triangle.

It can be shown that all of the expressions for pressure coefficient in equations (91) are equivalent to the real part of a single expression, identical to (91a):

$$C_p = Rl\,\frac{4}{\pi\beta\sqrt{n^2-1}}\cosh^{-1}\sqrt{\frac{n^2-t^2}{1-t^2}} \qquad (92)$$

For purposes of the surface integrals to be carried out later, however, and certainly for ordinary calculations, it is more convenient to have the real expressions of equations (91).

B. Surface Integrals of Pressure.

In order to carry out the drag calculations, it is now necessary to calculate the surface integrals required in equation (68) or (69).

The two basic types of integrations required correspond to parts (1) and (2) of equations (68); all the other integrals may be expressed in terms of integrals of these types.

Consider first the integral over the region shown in Fig. 14 of the pressures due to sources in this region - i.e., of pressure coefficient as given by equations (91a, c, or d). This integral will be required in the calculation of parts (1), (4) and (5) of equations (69). Since the pressure distributions are all conical in form, the integrations can be carried out over triangular strips, as shown in Fig. 14. In terms of the spanwise variable t, and the geometrical parameters shown in Fig. 14, the elementary area dA becomes:

$$dA = A_1 \frac{(1-s)^2}{(1-st)^2}\, dt \tag{93}$$

where $A_1 = c^2/2k = c^2/2\beta n$

Now let

$$S_1(n,s) = \int_A C_{p_A}\, dA = \frac{4(1-s)^2 A_1}{\pi\beta\sqrt{n^2-1}} \int_0^1 \frac{1}{(1-st)^2} \cosh^{-1}\sqrt{\frac{n^2-t^2}{1-t^2}}\, dt \tag{94}$$

where A is the area of figure 14, and C_{p_a} is the pressure distribution of equation (91a), and $n = k/\beta$. The integral in equation (94),

$$T = \int_0^1 \frac{1}{(1-st)^2} \cosh^{-1}\sqrt{\frac{n^2-t^2}{1-t^2}}\, dt \tag{95}$$

may be evaluated by an integration by parts. Let

$$u = \cosh^{-1}\sqrt{\frac{n^2-t^2}{1-t^2}} \qquad dv = \frac{dt}{(1-st)^2}$$

and

$$du = \frac{\sqrt{n^2-1}\;\, t\,dt}{(1-t^2)\sqrt{n^2-t^2}}, \qquad v = \frac{1}{s}\left\{\frac{1}{(1-st)} - \frac{1}{(1-s)}\right\}$$

$$= -\frac{(1-t)}{(1-st)(1-s)}$$

This particular form of v is used in order to avoid an infinity at one of the limits of integration. Since

$$\lim_{t\to 1}\,(1-t)\cosh^{-1}\sqrt{\frac{n^2-t^2}{1-t^2}} = \lim_{t\to 1}\,(1-t)\log(1-t) = 0$$

we have

$$T = \frac{1}{1-s}\cosh^{-1}n + \frac{\sqrt{n^2-1}}{1-s}\int_0^1 \frac{t\,dt}{(1-st)(1+t)\sqrt{n^2-t^2}} \qquad (96)$$

Since

$$\frac{t}{(1-st)(1+t)} = \frac{1}{1+s}\left\{\frac{1}{1-st} - \frac{1}{1+t}\right\}$$

the integral in equation (96) can be written as $I = I_1 + I_2$, with

$$I_1 = \frac{1}{1+s}\int_0^1 \frac{dt}{(1-st)\sqrt{n^2-t^2}}$$

$$I_2 = \frac{-1}{1+s}\int_0^1 \frac{dt}{(1+t)\sqrt{n^2-t^2}}$$

Upon substituting $t = n \sin\theta$, these integrals reduce to elementary forms,

$$I_1 = \frac{1}{1+s}\int_0^{\theta_1} \frac{d\theta}{1 - sn\sin\theta} = \frac{1}{(1+s)\sqrt{s^2n^2-1}} \log \frac{\sin\frac{\theta-\theta_2}{2}}{\cos\frac{\theta+\theta_2}{2}} \Bigg|_0^{\theta_1}$$

$$I_2 = \frac{-1}{1+s}\int_0^{\theta_1} \frac{d\theta}{1 + n\sin\theta} = \frac{-1}{(1+s)\sqrt{n^2-1}} \log \frac{\sin\frac{\theta+\theta_1}{2}}{\cos\frac{\theta-\theta_1}{2}} \Bigg|_0^{\theta_1} \qquad (97)$$

where

$$\theta_1 = \sin^{-1}\frac{1}{n}, \qquad \theta_2 = \sin^{-1}\frac{1}{sn}$$

The second of these two integrals is simply

$$I_2 = \frac{-1}{(1+s)\sqrt{n^2-1}} \log\left\{1 + \sqrt{1-(1/n)^2}\right\} \qquad (98)$$

The appropriate form for the evaluation of the second integral in (97) will apparently depend on whether $sn = sk/\beta$ is greater or less than 1, i.e., whether the trailing edge of this region is ahead of or behind its Mach wave. In the case that $sn > 1$, it can be written

$$I_1 = \frac{1}{(1+s)\sqrt{s^2n^2-1}} \log\left\{\frac{n+\sqrt{n^2-1} - sn + \sqrt{s^2n^2-1}}{n+\sqrt{n^2-1} - sn - \sqrt{s^2n^2-1}}\right\}$$

$$= \frac{1}{(1+s)\sqrt{s^2n^2-1}} \log\left\{1 + \frac{2\sqrt{s^2n^2-1}}{n+\sqrt{n^2-1} - sn - \sqrt{s^2n^2-1}}\right\} \qquad (99)$$

while in the case that sn < 1, it can be written

$$I_1 = \frac{2}{\sqrt{1-s^2n^2}} \left\{ \tan^{-1}\left(\frac{\frac{1}{n+\sqrt{n^2-1}} - sn}{\sqrt{1-s^2n^2}} \right) + \tan^{-1} \frac{sn}{\sqrt{1-s^2n^2}} \right\}$$

$$= \frac{2}{\sqrt{1-s^2n^2}} \tan^{-1}\left(\frac{\sqrt{1-s^2n^2}}{n+\sqrt{n^2-1}-sn} \right) \qquad (100)$$

When introducing I_2 into equation (96), one may observe that

$$\cosh^{-1} n - \frac{1}{1+s} \log \left(1 + \sqrt{1-(1/n)^2} \right)$$

$$= \frac{s}{1+s} \cosh^{-1} n + \frac{1}{1+s} \log n$$

Finally, using equations (98) and (99) or (100) in (96) and (94), the surface integral S_1 may be evaluated as

$$S_1(n,s) = \frac{4A_1}{\pi\beta} G_1(n,s) \qquad (101)$$

where, for ns > 1

$$G_1(n,s) = \frac{1-s}{1+s} \left[\frac{s \cosh^{-1} n}{\sqrt{n^2-1}} + \frac{\log n}{\sqrt{n^2-1}} \right. \qquad (102)$$

$$\left. + \frac{1}{\sqrt{s^2n^2-1}} \log \left\{ 1 + \frac{2\sqrt{s^2n^2-1}}{n+\sqrt{n^2-1}-sn-\sqrt{s^2n^2-1}} \right\} \right]$$

or, for sn < 1

$$G_1'(n,s) = \frac{1-s}{1+s}\left[\frac{s\cosh^{-1}n}{\sqrt{n^2-1}} + \frac{\log n}{\sqrt{n^2-1}} + \frac{2}{\sqrt{1-n^2s^2}}\tan^{-1}\left(\frac{\sqrt{1-n^2s^2}}{n+\sqrt{n^2-1}-ns}\right)\right] \tag{103}$$

The same type of surface integral must also be calculated for the case that n < 1, i.e., for the pressure distributions of equations (91c) and (91d). Since these pressure distributions are actually the real part of the expression in equation (91a), as mentioned previously, it is clear that the desired integral could be obtained by finding the real part of equation (102) or (103) for n < 1. It is, however, easier to calculate the integral directly. If

$$S_1'(n,s) = \int_A C_{p_d}\, dA$$

$$S_1'(n,s) = \frac{4(1-s)^2 A_1}{\pi\beta\sqrt{1-n^2}}\, Rl\int_0^1 \frac{1}{(1-st)^2}\left\{\frac{\pi}{2} - \sin^{-1}\sqrt{\frac{n^2-t^2}{1-t^2}}\right\}dt \tag{104}$$

then the integral will be

$$T = \frac{\pi}{2}\int_0^1 \frac{dt}{(1-st)^2} - \int_0^n \frac{1}{(1-st)^2}\sin^{-1}\sqrt{\frac{n^2-t^2}{1-t^2}}\, dt \tag{105}$$

The first integral is immediately:

$$I_1 = \frac{\pi}{2}\frac{1}{(1-s)}$$

The second integral can be evaluated by the same technique as that used in equation (95), with

$$u = \sin^{-1}\sqrt{\frac{n^2-t^2}{1-t^2}}, \qquad dv = \frac{dt}{(1-st)^2}$$

from which

$$I_2 = \frac{1}{1-s}\sin^{-1}\frac{1}{n} - \frac{\sqrt{1-n^2}}{1-s}\int_0^n \frac{t\,dt}{(1-st)(1+t)\sqrt{n^2-t^2}}$$

The integration of this last expressions proceeds in much the same way as the preceding computations, except that the principal values for n $<$ 1 must be computed. Carrying out this integration and combining terms, one finds that

$$I_2 = \frac{1}{1-s^2}\left[s\cdot\sin^{-1}n + \frac{\pi}{2} - \frac{\sqrt{1-n^2}}{\sqrt{1-s^2n^2}}\left(\sin^{-1}sn + \frac{\pi}{2}\right)\right]$$

Combining the above expressions for I_1 and I_2 in equation (105), the value of T becomes:

$$T = \frac{s}{1-s^2}\cos^{-1}n + \frac{1}{1-s^2}\frac{\sqrt{1-n^2}}{\sqrt{1-s^2n^2}}\left(\sin^{-1}sn + \frac{\pi}{2}\right) \qquad (106)$$

If the surface integral for n $<$ 1 is written in the same form as equation (101), with

$$S_1'(n,s) = \frac{4A_1}{\pi\beta}G_2(n,s) \qquad (107)$$

we find, using equation (104), that

$$G_2(n,s) = \frac{1-s}{1+s}\left[\frac{s}{\sqrt{1-n^2}}\cos^{-1}n + \frac{1}{\sqrt{1-s^2n^2}}\left(\frac{\pi}{2} + \sin^{-1}sn\right)\right] \qquad (108)$$

The first basic surface integral, as given by equation (94), has thus been expressed in three forms,

$$S_1(n,s) = \frac{4A_1}{\pi\beta} G_1(n,s), \quad \text{for } n > 1, \quad ns > 1$$

$$= \frac{4A_1}{\pi\beta} G_1'(n,s), \quad \text{for } n > 1, \quad ns < 1$$

$$= \frac{4A_1}{\pi\beta} G_2(n,s), \quad \text{for } n < 1, \quad ns < 1 \qquad (109)$$

with G_1, G_1', and G_2 given by equations (102), (103) and (108) respectively. The three expressions are, of course, completely equivalent, and can be derived directly from each other. Their equivalence at the various limits is seen immediately, for at $ns = 1$,

$$G(n,\tfrac{1}{n}) = G'(n,\tfrac{1}{n}) = \frac{n-1}{n+1}\left\{\frac{\cosh^{-1}n}{n\sqrt{n^2-1}} + \frac{\log n}{\sqrt{n^2-1}} + \frac{2}{n-1+\sqrt{n^2-1}}\right\} \qquad (110)$$

As n approaches 1, the expressions in general become indeterminate, but it is observed that

$$\lim_{n\to 1} \frac{\cosh^{-1} n}{\sqrt{n^2-1}} = 1, \qquad \lim_{n\to 1} \frac{\log n}{\sqrt{n^2-1}} = 0$$

and that

$$2\tan^{-1}\sqrt{\frac{1+s}{1-s}} = \pi - \sin^{-1}\sqrt{1-s^2}$$

$$= \pi - \cos^{-1} s$$

$$= \frac{\pi}{2} + \sin^{-1} s$$

The values of G as n approaches 1 then become

$$\lim_{n\to 1} G_1'(n,s) = \lim_{n\to 1} G_2(n,s) = \frac{1-s}{1+s}\left\{ s + \frac{1}{\sqrt{1-s^2}}\left(\frac{\pi}{2} + \sin^{-1} s\right)\right\} \qquad (111)$$

A particularly important limit occurs as s approaches 0 for n $<$ 1. From equation (108),

$$\lim_{s\to 0} G_2(n,s) = \frac{\pi}{2}$$

that is, the surface integral becomes independent of the sweepback, n.

The other necessary type of surface integral is that corresponding to part (2), (3) and (6) of equations (69). Consider the area B shown in Fig. 15, bounded at the front by a Mach wave from P. The integral B of the pressure due to a uniform source distribution in the triangle with vertex at P must be calculated. In terms of t = sky/x, the elementary area will be

$$dA = A_2 \frac{(1-s)^2}{(t-s)^2} dt$$

where

$$A_2 = sc^2/2k = sc^2/2\beta n$$

The pressure distribution is given by equation (91b), but with n replaced by sn. Then we may write

$$S_2(\eta, s) = \int_B C_{p_B} dA$$

$$= \frac{4(1-s)^2}{\pi\beta\sqrt{s^2n^2-1}} A_2 \int_1^{sn} \frac{1}{(t-s)^2} \cosh^{-1}\sqrt{\frac{s^2n^2-1}{t^2-1}}\, dt \qquad (113)$$

If one designates the integral in this expression by T, and integrate by parts, as in the previous calculations, with

$$u = \cosh^{-1}\sqrt{\frac{s^2n^2-1}{t^2-1}}, \qquad dv = \frac{dt}{(t-s)^2}$$

$$du = -\frac{t\sqrt{s^2n^2-1}}{(t^2-1)\sqrt{s^2n^2-t^2}} dt, \qquad v = \frac{(t-1)}{(1-s)(t-s)}$$

then

$$T = \frac{\sqrt{s^2n^2-1}}{1-s} \int_1^{sn} \frac{t\, dt}{(t+1)(t-s)\sqrt{s^2n^2-t^2}} \qquad (114)$$

This integral is again separated by partial fractions into I_1 and I_2, with

$$I_1 = \frac{1}{1+s} \int_1^{sn} \frac{dt}{(1+t)\sqrt{s^2n^2 - t^2}}$$

$$I_2 = \frac{s}{1+s} \int_1^{sn} \frac{dt}{(t-s)\sqrt{s^2n^2 - t^2}} \tag{115}$$

These integrals are, as previously, elementary forms, and are evaluated as:

$$I_1 = \frac{1}{1+s} \frac{\log sn}{\sqrt{s^2n^2 - 1}}$$

$$I_2 = \frac{1}{(1+s)\sqrt{n^2-1}} \log \frac{sn^2 - 1 + \sqrt{(n^2-1)(s^2n^2-1)}}{n(1-s)} \tag{116}$$

Writing equation (113) as

$$S_2(n,s) = \frac{4}{\pi\beta} A_2 F(n,s) \tag{117}$$

one then finds that

$$F(n,s) = \frac{1-s}{1+s} \left\{ \frac{\log sn}{\sqrt{s^2n^2-1}} + \frac{1}{\sqrt{n^2-1}} \log \frac{sn^2 - 1 + \sqrt{(n^2-1)(s^2n^2-1)}}{n(1-s)} \right\} \tag{118}$$

This expression has physical significance only when both $n > 1$ and $sn > 1$. It goes to zero, of course, for $sn = 1$.

This completes the calculation of the fundamental pressure distributions and integrals of the pressure distributions required for the calculation of the drag of a delta wing. To summarize, the various expressions for the pressure distributions are given in equations (91a) through (91d); the two types of surfaces integrals, illustrated in Figs. 14 and 15, are given in equations (109) and (117), together with the expressions for the related functions F and G.

Plots of $F(n, s)$ and $G(n, s)$ are given in Figs. 17 and 18. The G function is continuous in derivative across the line $sn = 1$, even though the real expression changes form. However the real part of $F(n, s)$ vanishes abruptly, with infinite slope, at $sn = 1$. This is to be expected, of course, since the pressure distribution acting ahead of the triangle in this case has an infinite pressure peak. This singularity will be seen later to have an essential effect on the character of the drag curves for $sn = 1$.

The curves of Figs. 17 and 18 can be used for approximate calculation of the drag coefficient components of equations described in the next section as long as none of the parameters are near any "critical" values, - i.e., n, sn, are not near 0 or 1. As any of the discontinuities are approached, the drag expressions involve small differences between large quantities, and more accurate calculations must be used.

PART VI

DRAG COEFFICIENTS AND PRESSURE DISTRIBUTIONS FOR THE DELTA WING

A. Calculation of Drag Coefficients, Double Wedge Profile.

The scheme of calculations set up in Part IV, as summarized in equations (68) and (69), contained surface pressure integrals which we can now express in terms of the basic integrals $S_1(n, s)$ and $S_2(n, s)$ calculated in the last section. It is necessary only to relate the geometrical parameters of the basic wing, as shown in Fig. 8, and equations (63) and (64), to the parameters defined for S_1 and S_2, as illustrated in Figs. 14 and 15. It must be noted that we will use a single relative sweepback parameter, referred to the leading edge,

$$n = k_1/\beta .$$

We then have, by inspection, for the integrals required in equations (68) or (69),

$$\int_I C_{P_A}\, dA = S_1(n, r)$$

$$\int_I C_{P_B}\, dA = S_2(n, r)$$

$$\int_I C_{P_C}\, dA = S_2(n, a) - S_2\left(rn, \frac{a}{r}\right)$$

$$\int_{II} C_{P_A}\, dA = S_1(n, a) - S_1(n, r)$$

$$\int_{II} C_{P_B}\, dA = S_1\left(rn, \frac{a}{r}\right)$$

$$\int_{II} C_{P_C}\, dA = S_2\left(rn, \frac{a}{r}\right) \tag{119}$$

The expressions for S_1 and S_2 as given in equations (109) and (117) may now be introduced, and the result substituted in equations (69) to obtain the final expressions for the drag coefficient. It must be noted that the integrations for S_1 and S_2 were, in effect, carried out over only one half of the airfoil, so the area S appearing in equations (69) must be interpreted as one-half the total area. Thus in (69a);

$$A_1/S = r/(1 - a)$$

In (69b); $$A_2/S = r/(1 - a)$$

and similarly for the other terms.

The complete expressions for the components of the drag coefficient of the two-slope or double wedge delta wing then become:

$$C_{D_{IA}} = \frac{2\tau^2}{\pi\beta^2} \frac{(1-a)}{(1-r)^2} G(n, r) \tag{120a}$$

$$C_{D_{IB}} = -\frac{2\tau^2}{\beta\pi}\frac{r(1-a)^2}{(1-r)^2(r-a)}F(n,r) \qquad (120b)$$

$$C_{D_{IC}} = \frac{2\tau^2}{\beta\pi}\frac{a(1-a)}{(1-r)(r-a)}\left\{F(n,a) - F(rn,\frac{a}{r})\right\} \qquad (120c)$$

$$C_{D_{IIA}} = -\frac{2\tau^2}{\beta\pi}\frac{(1-a)}{(1-r)(r-a)}\left\{G(n,a) - G(n,r)\right\} \qquad (120d)$$

$$C_{D_{IIB}} = \frac{2\tau^2}{\beta\pi}\frac{r(1-a)^2}{(1-r)(r-a)^2}G(rn,\frac{a}{r}) \qquad (120e)$$

$$C_{D_{IIC}} = -\frac{2\tau^2}{\beta\pi}\frac{a(1-a)}{(r-a)^2}F(rn,\frac{a}{r}) \qquad (120f)$$

The total wave drag coefficient, based on the actual airfoil plan area, is the sum of these six contributions. The expressions for G(n, s) are given in equations (102), (103) or (108) depending on the values of n and s, while F(n, s) is defined by equation (118). We may recall again the significance of the parameters appearing in these

equations: n is the basic "relative sweepback" parameter - since $n = k_1/\beta$, n gives the sweepback of the airfoil leading edge relative to a Mach wave from its vertex. The parameters a and r give the relative geometry of the planform; r defines the maximum thickness location, as a fraction of total chord, from apex to wing tips. It will also be convenient to express the location of the maximum thickness point as a fraction of the actual root chord, say b, in which case, from Fig. 8,

$$b = \frac{1 - r}{1 - a} \tag{121}$$

The number a gives the sweepback of the trailing edge relative to the sweepback of the leading edge; as $a \longrightarrow 1$ one obtains essentially a two-dimensional swept wing or arrow wing.

It is noticed first that the total drag coefficient resulting from equations (120) may be represented in the form $C_D\beta/\tau^2$, in which case it is a function only of n, a, r. Thus the drag for all Mach numbers and geometries may be represented in a reasonably simple family of plots. If, for instance, $C_D\beta/\tau^2$ is plotted against 1/n, this parameter, for a given sweepback, becomes proportional to $\sqrt{M^2 - 1}$, and the plot will immediately show relative variation of drag with Mach number.

Before proceeding with discussions of the final calculations of drag coefficient, it will be desirable to calculate one simple limiting case. As $n \longrightarrow 0$, we have either a swept wing at an indefinitely high Mach number, or a wing with zero sweepback - i.e., an essentially two dimensional wing. In this case, the contribution from the terms in

(120b), (120c), and (120f) is zero. Furthermore, as n 0, we have from equation (105),

$$G(o, s) = \frac{\pi}{2}(1 - s)$$

Substituting this in (120a), (120d) and (120e), there results:

$$\lim_{n \to 0} \frac{C_D \beta}{\tau^2} = \frac{(1-a)}{(1-r)^2}(1-r) - \frac{(1-a)}{(1-r)(r-a)}\left\{(1-a)-(1-r)\right\}$$

$$+ \frac{r(1-a)^2}{(1-r)(r-a)^2}\left(1 - \frac{a}{r}\right)$$

$$= \frac{(1-a)^2}{(1-r)(r-a)}$$

Using equation (121) to express r in terms of b, the location of maximum thickness, this becomes:

$$\lim_{n \to 0} \frac{C_D \beta}{\tau^2} = \frac{1}{b(1-b)} \qquad (122)$$

But this is exactly the expression for the drag coefficient of a two-dimensional double-wedge airfoil, with cross-section as shown in Fig. 19. The optimum location of maximum thickness for this airfoil, as is well known, occurs with the peak at the 50% chord point - i.e., b = 0.5, and then

$$\frac{C_D \beta}{\tau^2} = 4 \qquad (123)$$

Thus the equations (120) reduce to the correct value for the case of zero sweepback. Moreover, we have learned also that at extremely high Mach numbers, such that the Machwaves are swept well behind the leading edge, the drag coefficient again approaches the value pertaining to a two-dimensional wing with the same location of maximum thickness, independently of the sweep of the delta wing trailing edge - a rather remarkable result.

This also suggests that a result of essential interest in the case of the delta wing will be the location of the maximum thickness point which will result in least drag for various Mach number ranges. From the above calculation, it appears that b = 0.5 will be optimum for very high Mach numbers; it is certainly unlikely that this will be true at all Mach numbers.

In order to examine this, in Fig. 20 is plotted $C_D\beta/\tau^2$ vs. b, with n as parameter, for the case of zero trailing edge sweepback (a = 0). It is noticed first that with $0 < n < 1$, for all values of b, the drag of the delta wing is greater than that of a two-dimensional wing; this case corresponds to case (1) in Fig. 9a. As the sweepback is increased (n increased), the drag begins to drop, and one observes the large discontinuity in drag curve slope at the point $r = (1 - b) = 1/n$, i.e., when the Mach waves are parallel to the maximum thickness line. This situation forms the dividing line between cases (2) and (3) in Figs. (9b) and (9c). It is only with the maximum thickness point forward of this position, i.e., $b < 1 - 1/n$, that the drag finally drops below the value for a two-dimensional wing.

A remarkable and apparently fortuitous result now appears; for values of n greater than approximately 1.3, the minimum drag occurs with the maximum thickness line somewhere between the 10% chord and 20% chord positions, practically independently of the sweepback n. This means that the maximum thickness line is swept back approximately 80% as much as the leading edge. With this location of maximum thickness, the drag drops rapidly with increasing n; for n = 1.4, the drag has decreased to the minimum two-dimensional value, and for n = 2.0, it is approximately one-half of the minimum two-dimensional value. With increasing n, (greater sweepback or decreasing Mach number) the location of maximum thickness point becomes less and less critical.

The corresponding variation of $C_D\beta/\tau^2$ with b for the wing with trailing edge swept 50% as much as the leading edge, i.e., a = 0.5, is plotted in Fig. 21. The results are again qualitatively very similar to the case of a = 0. The important drag break now occurs, of course, at somewhat more rearward locations of the maximum thickness, since rn = 1 corresponds to b = (n - 1)/n(1 - a). However the minimum drag again occurs with maximum thickness located between the 10 and 20% chord points. It is significant that the drag drops much more abruptly with increasing n in this case; at n = 1.3 it is appreciably below the minimum two-dimensional drag, while at n = 2 it is almost 1/4 of the two-dimensional value.

Similar plots have been made for a = 0.25 and a = 0.75; in both these cases, a similar result concerning optimum location of maximum thickness point for high n's is observed - the minimum drag is achieved with b in the range from 10 to 20% of root chord. As the trailing edge

sweepback approaches that of the leading edge, i.e., as a approaches 1, it is hardly to be expected that this result would still be true. The wing in this case is approaching a two-dimensional swept wing, and the optimum location of maximum thickness should be more nearly at the 50% chord point.

B. Effects of Sweepback on Drag.

The effect of variation in sweepback on drag is seen more easily in plots of $C_D\beta/\tau^2$ vs. $1/n$; in Figs. 22, 23, 24, and 25, these plots are given for a = 0, 0.25, 0.50 and 0.75 respectively, with b as parameter for each. The real character of the peaks occurring at the critical values of n and rn can now be seen.

Consider first Fig. 22, for a = 0. At low values of $1/n$ (high sweepback or low M) the superiority of the small value of b is evident. It might also be remembered here that the minimum drag for a two-dimensional double wedge, with maximum thickness at 50% chord, gives

$$C_D\beta/\tau^2 = 4 ,$$

which furnishes an indication of the significance of the levels of the curves.

As $1/n$ is increased, the drag curves approach a first peak at rn (in this case $(1 - b)n = 1$, at which point the Mach waves are parallel to the maximum thickness line. Sometime before this point, the delta wing loses its superiority over the two-dimensional wing. Another essential effect becomes evident here; the smaller values of b will, of course, delay the occurrence of this peak to a higher Mach

number, but the height of the peak itself increases. Thus the forward location of maximum thickness is clearly an advantage only if the design operating condition for the wing is to the left of the peak; if for any reason the design condition must lie to the right of the peak, then a value of b near 0.5 would be advantageous, in that the peak itself is reduced.

A second peak occurs at $n = 1$ with all values of b, i.e., Mach waves parallel to the leading edge. Again, the height of this peak is increased by forward location of maximum thickness point. The drag decreases for greater values of $1/n$, and as $1/n$ approaches infinity (large M) the curves approach asymptotically the value given in equation (122) for a two-dimensional wing with the same maximum thickness location.

In Fig. 23 are shown the corresponding results for small sweepback of the trailing edge, $\underline{a} = 0.25$. The general character of the curves, and the relative drags for various values of b are much the same. An additional discontinuity has entered at $\underline{an} = 1$, i.e., when the Mach waves are parallel to the trailing edge. The drag rise occurring at this discontinuity is, however, very small, and not particularly important. The next peak has been delayed, but also increased in magnitude by the trailing edge sweepback. The "leading edge peak" ($n = 1$) is particularly increased in magnitude over the case with $\underline{a} = 0$. For large values of $1/n$, the curves approach the same asymtotic values as in the $\underline{a} = 0$ case.

The trends already exhibited in Figs. 22 and 23 are continued with the larger values of trailing edge sweep shown in Figs. 24 and 25, for $\underline{a} = 0.50$ and 0.75. In these cases, the value of the drag coefficient

for low (1/n) has become so small compared to the two-dimensional wing that the location of maximum thickness point actually becomes relatively unimportant. In fact, in practical cases, for the thickness ratios, τ, of practical importance, the value of the wave drag coefficient in this range of sweepback will be of the same order as or smaller than the drag due to skin friction. On the other hand, the drag peaks, at a = 0.75, for instance, now become so violent that the design condition for the airfoil must clearly lie at low values of 1/n. As shown by von Karman in Ref. 22, the corresponding drag peak for an infinite two-dimensional swept wing is infinite in magnitude.

To clarify further the effect of trailing edge sweep for constant location of maximum thickness point, in Figs. 26 and 27 are plotted $C_D\beta/\tau^2$ vs. 1/n with b = 0.2 and 0.5 respectively, and with a as parameter. With forward position of maximum thickness (Fig. 26), the amount of trailing edge sweep has an important influence on drag for all values of n, decreasing it strongly to the left of the peak, and increasing it through the peak. With the 50% chord location of maximum thickness point (Fig. 27), this effect becomes even more pronounced.

The important conclusions from these two sets of curves are easily summarized:

a) Moving maximum thickness forward decreases drag for small values of 1/n, although at very small values of 1/n, and particularly with large trailing edge sweep, it is not so important. On the other hand, the drag peak, although delayed, is greatly increased

in severity.

b) Increasing trailing edge sweep has a similar effect, but somewhat more pronounced.

The above representations of the drag variation, while quite general, do not allow immediate visualization of the variation of actual drag coefficient with Mach number, since this is partly included in the factor $\beta = M^2 - 1$. In order to present a clearer physical picture of the behaviour of the drag coefficient in typical cases, the function C_D/τ^2 is plotted vs. M in Fig. 28 for a family of airfoils with no trailing edge sweep, with maximum thickness at a constant 15% chord, but with varying leading edge angle. The sweep angle is there replaced by the apex half-angle, ω_o. These are, of course, obtained from a single curve in Fig. 22. The shift in pressure peak location and height, and the change in low Mach number drag coefficient with increasing sweep is clearly seen.

The behaviour of the curves near M = 1 should be particularly noted. In Fig. 22, the curve of $C_D\beta/\tau^2$ is seen to approach 0 as 1/n approaches 0, so that C_D/τ^2 is in this order indeterminate. The calculation of this limiting case is outlined in the next section, and it is shown there that C_D/τ^2 has a logarithmic approach to infinity at M = 1 for a = 0. This is, of course, much less severe than the one half power approach to infinity for the infinite two-dimensional wing.

The effect of peak location is also interesting when C_D/τ^2 is plotted directly. In Fig. 29 the drag coefficient is plotted against M for a family of airfoils with constant leading and trailing edge sweep, ($\omega_o = 30^\circ$ and a = 0), but with varying location of maximum

thickness. The shift of the pressure peak to higher Mach numbers, and its increase in height with decreasing b are easily seen.

In Fig. 30 are drag coefficient curves corresponding to the airfoil family of Fig. 28, but with trailing edge sweep of a = 0.5, and b = 0.2. The general behaviour for low Mach numbers is the same as in Fig. 28, with the important difference that the drag coefficient approaches a finite limit as M approaches 1. This limit is again indeterminate to the order of the curves of Fig. 24, but it is obvious that the limit is finite, as the curves in Fig. 24 approach $1/n = 0$ with finite slope. The evaluation of this limit is somewhat lengthy, and is carried out in the next section.

In Fig. 31 the effect of maximum thickness location on C_D/τ^2 is exhibited for the family of airfoils with 30° apex half-angle, and a = 0.5. The characteristics are much the same as Fig. 29.

In order to compare more clearly the effect of trailing edge sweep, Fig. 32 presents curves of C_D/τ^2 for wings with 30° and 15° apex half-angles, and values of a = 0 and 0.5. The similarity between the effects of sweeping maximum thickness line and sweeping trailing edge is again evident.

The character of the above curves, and in particular of Figs. 29 and 31, suggests that there are two ways in which advantage may be taken of the delta-wing drag properties. At reasonably low Mach numbers, the leading edge may be swept far enough so that the drag peak lies at a Mach number considerably higher than the design point, and with proper forward maximum thickness location, a substantial reduction in design point drag is possible. On the other hand, the

design Mach number may be so high that it is impractical to sweep the wing back far enough for this. In this case, the maximum thickness point may be located near the 50% chord point, and the primary effect of the delta wing will be to cause a very small drag rise through the low Mach number region, as compared to the two-dimensional wing, and to approach finally the two-dimensional value. The drag peak is then very small. This application may be the more important of the two for very high Mach numbers.

Another rather obvious consideration must be pointed out, which in an engineering problem may have decisive influence on the choice of optimum configuration. The representations so far have been of C_D/τ^2, where τ is the thickness-chord ratio. In a specific design problem, the actual wing root thickness will be determined by structural considerations, and presumably will not vary greatly within a reasonable range of configurations. However the change in configuration for a wing of given area, or given $dC_L/d\alpha$, may involve considerable changes in wing root chord and therefore in τ. It is actually in this way that the low aspect ratio (large sweepback) delta wings often achieve their greatest advantage. For the low aspect ratio generally implies much larger root chord (and often smaller absolute thickness) and therefore decreases τ materially. Since the drag coefficient varies with τ^2, the effects may be very large. The comparisons of drag coefficient discussed above then becomes essentially relative in character, and it is clear that the real choice of optimum configuration must depend largely on the special design parameters or conditions in a particular engineering problem.

C. Drag Coefficients and Drag-Strength Ratio for Modified Double-Wedge.

A further extension of the above drag calculations which has particular engineering importance now suggests itself. In the case of an infinite two-dimensional wing, the profile with least drag for a given thickness is the familiar double-wedge section, with maximum thickness at the 50% chord point, as previously described. However this is not, in general, the optimum profile in a practical problem; the usual design problem is to find a profile of minimum drag with some other section property given - either stiffness (moment of inertia) or strength (section modulus). The variation in profile may then include variation in thickness ratio. The section property must even depend, then, upon the type of structure chosen - whether, for instance, it is solid, or essentially monocoque, or a combination.

It was shown by the present author that for a two-dimensional solid airfoil, the least drag for given stiffness is obtained with an airfoil having a profile defined by an elliptic function - actually very close to a circular arc. For a monocoque structure, of given stiffness, the optimum section actually is a bi-convex circular arc profile. Optimum profiles for given section modulus varied only slightly from this. Only if the structure is concentrated primarily in a single spar at the maximum thickness point will the double-wedge section be optimum.

These calculations suggest that a) the double-wedge delta wing very probably may be the optimum profile for given thickness ratio, but that b) the optimum delta wing profile from the standpoint of a likely engineering requirement will probably have a continuous

curvature and more distributed thickness. The complete variational problem can be set up, much as was done for the two-dimensional wing. However, in order to avoid this generality and still establish the trend of the desired change in thickness distribution, a simple family of profiles will be considered which has one more parameter added. This profile, called a "three slope" profile, is shown in Fig. 33. The slope of the central part of the airfoil will be held zero, and the location of the forward and aft limits of this zone, i.e., b and a, allowed to vary. Only the case of zero trailing edge sweep will be considered.

The scheme of the calculation is essentially the same as for the two slope delta wing, and will be indicated briefly. Referring to Fig. 33, we will superimpose three triangles with vertices at A, B, and C, having slopes

$$\lambda_A = \lambda_1 , \quad \lambda_B = -\lambda_1 , \quad \lambda_C = \lambda_2$$

Furthermore,

$$\lambda_1 = \frac{\tau}{2}\,\frac{1}{1-r} , \quad \lambda_2 = -\frac{\tau}{2}\,\frac{1}{a}$$

Using the surface integral designations of equations (94) and (113), Part V, and the drag component notation introduced in equations (68), Part IV, we can immediately write

$$\frac{D_{IA}}{q} = 2\lambda_1 \lambda_A S_1(n, r)$$

$$\frac{D_{IB}}{q} = 2\lambda_1 \lambda_B S_2(n, r)$$

$$\frac{D_{IC}}{\mathcal{F}} = 2\lambda_1\lambda_C\left\{S_2(n,a) - S_2\left(rn,\frac{a}{r}\right)\right.$$

$$\frac{D_{IIIA}}{\mathcal{F}} = 2\lambda_3\lambda_A\left\{S_1(n,0) - S_1(n,a)\right\}$$

$$\frac{D_{IIIB}}{\mathcal{F}} = 2\lambda_3\lambda_B\left\{S_1(rn,0) - S_1\left(rn,\frac{a}{r}\right)\right\}$$

$$\frac{D_{IIIC}}{\mathcal{F}} = 2\lambda_3\lambda_C\ S_1(an,0) \qquad (124)$$

Substituting for the slopes, λ , as given above, and expressing S_1 and S_2 in terms of F and G according to equations (109) and (118), we have finally:

$$C_{D_{IA}} = \frac{2\tau^2}{\beta\pi}\frac{1}{(1-r)^2}G(n,r)$$

$$C_{D_{IB}} = -\frac{2\tau^2}{\beta\pi}\frac{r}{(1-r)^2}F(n,r)$$

$$C_{D_{IC}} = -\frac{2\tau^2}{\beta\pi}\frac{1}{(1-r)}\left\{F(n,a) - F\left(rn,\frac{a}{r}\right)\right\}$$

$$C_{D_{IIIA}} = -\frac{2\tau^2}{\beta\pi}\frac{1}{a(1-r)}\left\{G(n,0) - G(n,a)\right\}$$

$$C_{D_{IIIB}} = \frac{2\tau^2}{\beta\pi}\frac{r}{a(1-r)}\left\{G(rn,0) - G\left(rn,\frac{a}{r}\right)\right\}$$

$$C_{D_{IIIC}} = \frac{2\tau^2}{\beta\pi}\frac{1}{a}G(an,0) \qquad (125)$$

Calculations of the drag coefficient have been carried out for one particular value of relative sweepback, n = 2.5, and for various values of a and r. The variation of drag coefficient with position of this two maximum thickness points is shown in Fig. 34, where $C_D\beta/\tau^2$ is plotted against (1 - a), with b = 1 - r as the parameter. As (1 - a) approaches b, the airfoil is identical to the two slope delta wing with zero trailing edge sweep considered previously, so that the end points of the curves for various b's will produce the drag curve for n = 2.5 in Fig. 20.

It is immediately clear from Fig. 34 that for any location of P_1, the minimum $C_D\beta/\tau^2$ will occur when P_2 is identical with P_1. that is, the double-wedge airfoil does have the least drag for given thickness for this airfoil family. However, rearward motion of P_2 causes only a small increase in drag - for instance, with P_1 at 10% chord (b = 0.1), P_2 can be moved aft to the 30% chord point with only a 30% increase in drag. At the same time, it is clear that the strength of the section must be increased greatly by this change.

The section modulus, S, for this profile, assuming it to be solid, is given by

$$S = \frac{2I}{\tau c} = c^3 \frac{\tau^3}{24}(1 + 3r - 3a) \tag{126}$$

In order to find the airfoil of least drag for given section modulus, we may plot the ratio

$$\frac{C_D\beta/\tau^3}{S/c^3\tau^3} = \frac{C_D\beta}{S/c^3}$$

which does not involve the thickness ratio.

In Fig. 35, this ratio is plotted as a function of 1 - a for b = 0.05, 0.10 and 0.15. For each of these curves, the improvement in drag is very significant as P_2 is moved aft, with an optimum for P_2 at approximately 40% chord. The best drag-strength ratio is obtained for the value b = 0.10 and approximately (1 - a) = 0.4. At this point the drag-strength ratio has decreased approximately 19% below the value for the two slope wing with b = 0.1 or 0.2.

Thus for a solid three-slope or modified double-wedge wing of this family, the optimum profile will have a maximum thickness region distributed between approximately the 10% chord and the 40% chord stations. The resulting design is certainly more attractive from a structural standpoint in any case. Consideration of a more general family of shapes would undoubtedly lead to better profiles, but this first step clearly indicates the trend, namely, that the thickness must increase very rapidly near the leading edge, but then may continue without much decrease to the neighborhood of the 40 or 50% chord point. The location of this second point will, of course, depend on n, the leading edge sweepback, and will be higher for larger values of n.

D. Pressure Distributions Over Double-Wedge Wings.

The pressure distributions over the delta wings are of some interest, and shed some light on their possible behaviour in a real fluid. These distributions are easily calculated, of course, by proper superposition of the basic pressure fields of equations (91), using the source strengths defined by equations (66) and (67). The two important types occur when (a) $n < 1$, and (b) n and $rn > 1$ (cases (a) and (c), Fig. 9).

An example of the first type is shown in Fig. 36, where the chordwise pressure coefficient is plotted in the form $C_p\beta/\tau$ for several spanwise stations, with n = 0.8, and b = 0.5, i.e., maximum thickness at 50% chord, and no trailing edge sweep. The pressure remains constant for a short distance behind the leading edge, with the typical "supersonic leading edge" characteristic, and then drops rather rapidly. When the maximum thickness line is reached, a large drop occurs, with no pressure rise until the Mach wave from the maximum thickness line is crossed. Thus all pressure gradients are favorable up to this Mach wave, which lies well aft on the wing.

In Fig. 37 are plotted similar chordwise pressure distributions for the case n = 2.5 and b = 0.2, with no trailing edge sweep. The leading edge now has the subsonic (logarithmic) positive pressure peak, but the pressure begins to drop very rapidly as the maximum thickness line is approached. At this line a negative peak occurs, followed by a very rapid rise. This behaviour is expected, by analogy with the subsonic flow over such a two-dimensional corner, in which case it is first accelerated and then decelerated very rapidly. The important point in the present case is that the maximum thickness line for the two-slope airfoil will always introduce a large adverse pressure gradient, in cases when this line is swept behind the Mach waves. This gradient may have undesirable effects on the boundary layer. A profile with continuous curvature would certainly be more desirable in this respect.

E. Lift for Delta Wings With Supersonic Leading Edges.

One further application can be made of the calculations presented previously. In Part II it was pointed out that the source solutions can be used to calculate the lift on airfoils with "supersonic" leading

edges, since the flow in the upper half-space and lower half-space may be calculated separately. Imagine a flat-plate delta wing with n 1, of zero thickness, at angle of attack α. In the upper half-space the potential will be essentially that given by equation (83), which produces a constant downwash over the entire triangle, and the pressure distribution will be

$$C_p = -\frac{2\alpha}{\beta\sqrt{1-n^2}} Rl\left\{1 - \frac{2}{\pi}\sin^{-1}\sqrt{\frac{n^2-t^2}{1-t^2}}\right\} \qquad (127)$$

This distribution is shown in Fig. 13.

In the lower half-space, the potential is represented by the negative of that in the upper half-space, which reverses the sign of all perturbation velocities, and therefore gives a solution with downwash symmetric in z. The lift will then be twice the integral of the pressure distribution of equation (127) over the surface. But this is exactly the integral $S_1(n, s)$, carried out for a triangle with unit slope, and given by equations (109) and (108). Rewriting equation (108) slightly, and using equation (109), the lift coefficient becomes:

$$C_L = \frac{8\alpha}{\pi\beta}\frac{(1-a)}{(1+a)}\left\{\frac{a}{\sqrt{1-n^2}}\cos^{-1}n + \frac{1}{\sqrt{1-a^2n^2}}\cos^{-1}(-an)\right\} \qquad (128)$$

where a is the trailing edge sweepback parameter, as in Fig. 8, and n is less than 1.

For the case of no trailing edge sweepback, (a = 0), it is observed (as shown in equation (112)) that for any n,

$$C_L = \frac{4\alpha}{\beta} \tag{129}$$

This is exactly the lift coefficient on an infinite two-dimensional unswept wing. Thus we have the remarkable result that for a delta wing with leading edges ahead of the Mach waves, and no trailing edge sweep, the lift coefficient is independent of sweepback, and has the same value as the two-dimensional wing. By sweeping the trailing edge, the lift coefficient can be made much greater than the two-dimensional value. Curves of this lift coefficient were presented in Ref. 23, together with the lift coefficient curves for $n > 1$ which were calculated with the conical flow technique.

PART VII

LIMITING CASES

The behaviour of the drag coefficients previously calculated is of interest in several limiting cases. In particular, its behaviour as the Mach number approaches 1 can be calculated. The case of the wing with no trailing edge sweepback will be considered first, since this does not form a simple special case of the more general problem for a not equal to zero.

The drag is given by equations (120), with $C_{D_{IC}} = C_{D_{IIC}} = 0$, and a = 0 in the other drag components. As M approaches 1, with finite sweepback factor k, then $\beta = \sqrt{M^2 - 1}$ approaches 0, and the parameter $n = k/\beta$ approaches infinity. Therefore the limiting forms of G(n, s) and F(n, s) for large n must be computed. Noting that for large x,

$$\cosh^{-1} x \approx \log 2x \approx \log x,$$

one finds from equation (102) that G(n, s) approaches the value

$$G(n,s) \rightarrow \frac{1-s}{1+s}\left[\frac{s \log n}{n} + \frac{\log n}{n} + \frac{1}{ns}\log\frac{1}{1-s}\right]$$

$$\rightarrow (1-s)\frac{\log n}{n} \qquad (130)$$

where only terms of the order $(\log n)/n$ have been retained.

From equation (118) one also finds that as $n \rightarrow \infty$,

$$F(n,s) \rightarrow \frac{1-s}{1+s}\left\{\frac{\log n}{sn} + \frac{1}{n}\log\frac{sn^2-1+sn^2}{n(1-s)}\right\}$$

$$\rightarrow \frac{1-s}{s}\frac{\log n}{n} \tag{131}$$

to the same order of $(\log n)/n$. Substituting these in equations 120a, b, d, and e, with $a = 0$, one obtains:

$$\frac{C_D\beta}{\tau^2}\cdot\frac{\pi}{2} \rightarrow \frac{\log n}{n}\left\{\frac{1-r}{(1-r)^2} - \frac{(1-r)}{r(1-r)^2} - \frac{r}{r(1-r)} + \frac{1}{r^2(1-r)}\right\}$$

$$\rightarrow \frac{1}{r^2}\frac{\log n}{n} \tag{132}$$

Now substituting $n = k/\beta$,

$$\frac{C_D}{\tau^2} \rightarrow \frac{2}{\pi}\frac{1}{kr^2}\log\frac{1}{\beta} \tag{133}$$

As M approaches 1, therefore, the drag coefficient for the delta wing with no trailing edge sweepback approaches a logarithmic infinity. The character of this weak peak is shown in the previously discussed plots.

For the wing with trailing edge sweepback the situation is slightly more complicated. The terms in G and F may be arranged in the following decreasing orders of magnitude in n:

$$\frac{\log n}{n}, \quad \frac{1}{n}, \quad \frac{\log n}{n^2}, \quad \text{etc.}$$

Terms of the first two orders of magnitude will be needed. It will be most convenient, however, to calculate them separately. Denoting the contributions of terms of the largest order by $C_D^{(1)}$, one finds, upon introducing equations (130) and (131) in (120):

$$\frac{C_0^{(1)}\beta}{\tau^2}\frac{\pi}{2} \to \frac{\log n}{n}\left\{\frac{1-a}{1-r} - \frac{(1-a)^2}{(1-r)(r-a)} + \frac{a(1-a)}{r(r-a)}\right.$$

$$\left. - \frac{1-a}{1-r} + \frac{(1-a)^2}{r(1-r)(r-a)} - \frac{(1-a)}{r(r-a)}\right\}$$

$$\to \frac{\log n}{n}\frac{(1-a)}{(r-a)}\left\{\frac{1-a}{1-r}\left(\frac{1}{r}-1\right) - \frac{1-a}{r}\right\} \tag{134}$$

$$\to 0$$

Thus there is no contribution to the drag coefficient from terms of this order of magnitude. In order to obtain terms of the next order, we must first find terms of that order in G(n, s) and F(n, s), which might be designated $G^{(2)}$ and $F^{(2)}$. From equation (102) we have

$$G^{(2)}(n,s) \to \frac{1-s}{1+s}\left\{\frac{s\log 2}{n} - \frac{1}{ns}\log(1-s)\right\} \tag{135}$$

and from equation (118)

$$F^{(2)}(n,s) \to \frac{1-s}{1+s}\left\{\frac{\log s}{sn} + \frac{1}{n}\log\frac{2sn^2-1}{n^2(1-s)}\right\}$$

$$\to \frac{1-s}{1+s}\left\{\frac{\log s}{sn} + \frac{1}{n}\log\frac{2s}{1-s}\right\} \tag{136}$$

Denoting the contributions to the drag coefficient in this order by $C_D^{(2)}$, we have, from equations (120),

$$C_{D_{IA}}^{(2)} = \frac{2\tau^2}{\beta\pi}\frac{(1-a)}{1-r^2}\left\{\frac{r\log 2}{n} - \frac{1}{nr}\log(1-r)\right\}$$

$$C_{D_{IB}}^{(2)} = -\frac{2\tau^2}{\beta\pi}\frac{r(1-a)^2}{(r-a)(1-r^2)}\left\{\frac{\log r}{rn} + \frac{1}{n}\log\frac{2r}{1-r}\right\}$$

$$C_{D_{IC}}^{(2)} = \frac{2\tau^2}{\beta\pi}\frac{a(1-a)}{(1-r)(r-a)}\left\{\frac{1-a}{1+a}\left(\frac{\log a}{an} + \frac{1}{n}\log\frac{2a}{1-a}\right)\right.$$
$$\left. - \frac{1-a/r}{1+a/r}\left(\frac{\log a/r}{an} + \frac{1}{rn}\log\frac{2a/r}{1-a/r}\right)\right\}$$

$$C_{D_{IIA}}^{(2)} = -\frac{2\tau^2}{\beta\pi}\frac{(1-a)}{(1-r)(r-a)}\left[\frac{1-a}{1+a}\left\{\frac{a\log 2}{n} - \frac{1}{na}\log(1-a)\right\}\right.$$
$$\left. - \frac{1-r}{1+r}\left\{\frac{r\log 2}{n} - \frac{1}{nr}\log(1-r)\right\}\right]$$

$$C_{D_{IIB}}^{(2)} = \frac{2\tau^2}{\beta\pi}\frac{r(1-a)^2}{(1-r)(r^2-a^2)}\left\{\frac{a\log 2}{r^2n} - \frac{1}{an}\log\left(1-\frac{a}{r}\right)\right\}$$

$$C_{D_{IIC}}^{(2)} = -\frac{2\tau^2}{\beta\pi}\frac{a(1-a)}{r^2-a^2}\left\{\frac{\log a/r}{an} + \frac{1}{rn}\log\frac{2a/r}{1-a/r}\right\}$$

Collecting terms, the entire expression can finally be reduced to:

$$\frac{C_D\beta}{\tau^2} \to \frac{2}{\pi}\frac{(1-a)^2}{n}\left\{\frac{1-a}{a(1-r)(r-a)}\log r(1-a) - \frac{1}{r(r-a)}\log a(1-r) - \frac{1}{ar(1-r)}\log(r-a)\right\} \tag{137}$$

Replacing n by k/β, it is seen that the drag coefficient, C_D/τ^2, approaches a finite limit as M approaches 1. This limit is shown for the curves of drag vs. Mach number plotted in Figs. 30 and 31.

If $\underline{a}$ is allowed to approach 0 in this expression, the first and last terms in (137) give essentially a constant, independent of $\underline{a}$, while from the middle term one obtains

$$\frac{C_D\beta}{\tau^2} \to \frac{2}{\pi}\frac{1}{nr^2}\log\frac{1}{a} \tag{138}$$

The entire expression for drag coefficient was, however, valid only for the case that $\underline{an} \geq 1$, otherwise the expressions for $C_{D_{IC}}$ and $C_{D_{IIC}}$ would have been imaginary. Therefore $\underline{a}$ can approach 0 no faster than $1/n$, or:

$$\frac{C_D}{\tau^2} \to \frac{2}{\pi}\frac{1}{kr^2}\log\frac{1}{\beta} \tag{139}$$

which agrees with equation (133), although the method of approach to $a = 0$ is quite different.

The existence of this finite limiting value of C_D for wings with swept trailing edge raises an interesting question concerning its significance and validity. On the one hand, the present linearized

approach to the solution of the compressible flow problem certainly breaks down at a Mach number of exactly 1; in fact, as brought out in the derivation of the basic equations in Part II, the approximation requires smaller and smaller disturbances as M approaches 1. Furthermore in the present case, if one considers only the area of the delta wing ahead of the maximum thickness point, the pressure coefficient approaches infinity everywhere at a rate given by the limiting form of equation (91a),

$$C_p \rightarrow \frac{4}{\pi k} \log \frac{1}{\beta}$$

and the integral of these pressures over this forward surface, which is proportional then essentially to $G(n, o)$, approaches infinity at the rate

$$\int C_p dA \rightarrow \text{Const.} \log \frac{1}{\beta}$$

The finite limit of the drag coefficient is caused by the existence of negative drag on the remainder of the wing, which approaches infinity at essentially the same rate as the positive contribution.

On the other hand, for a sufficiently thin airfoil, the result may be regarded as accurate for Mach numbers which approach extremely close to 1. The practical question therefore seems to be how far from Mach number 1 the non-linear terms in the equations have an important effect. This question can properly be answered only by experiment, including the possibility that viscous effects might also become important.

Experimental results available so far in this range indicate very strongly that the drag curves are predicted with reasonably good accuracy almost down to Mach number 1 by the linearized results; in fact, the drag rise near or through Mach number 1 seems to be predicted very closely by the limits calculated above. The experiments do not, of course, show any infinite drags or even large peaks near M = 1 for the delta wing with zero trailing edge sweepback; to what extent this is a function of acceleration or viscous effects, or to what extent it could be predicted by a more accurate solution to the equations near Mach number 1, is not yet clear.

Another interesting special case of the above calculation is obtained if a is allowed to approach 1 - which should in the limit correspond to a two-dimensional swept wing, or "arrow wing". For convenience the maximum thickness point may be taken at mid root chord, which implies

$$2(1 - r) = (1 - a)$$

$$r = \frac{1 + a}{2} \tag{140}$$

In this case, from equation (137), the drag coefficient is given by:

$$\frac{C_D \beta}{\tau^2} \to \frac{2}{\pi} \frac{(1-a)^2}{n} \left\{ \frac{4}{a(1-a)} \log \frac{(1+a)(1-a)}{2} - \frac{4}{1-a^2} \log \frac{a(1-a)}{2} - \frac{4}{a(1-a^2)} \log \frac{1-a}{2} \right\}$$

$$\to \frac{8}{\pi} \frac{1-a}{n} \left\{ \frac{1}{a} \log (1+a) - \frac{1}{1+a} \log a \right\} \tag{141}$$

This drag coefficient, based upon the actual plan area, S, apparently approaches 0 as a approaches 1 and the span approaches infinity. In order to obtain a physical idea of the forces involved, however, a new drag coefficient, C_D', might be calculated, based on the square of the root chord, ℓ. From Fig. 8,

$$S = \frac{\ell^2}{k(1-a)}$$

and thus

$$C_D' = C_D \frac{S}{\ell^2} \rightarrow \frac{8\tau^2}{\pi k^2}\left\{\frac{1}{a}\log(1+a) - \frac{1}{1+a}\log a\right\} \qquad (142)$$

which, as a approaches 1, gives

$$\lim_{\substack{a\to 1 \\ n\to\infty}} C_D' = \frac{8\tau^2}{\pi k^2}\log 2 \qquad (143)$$

Since the thickness $t = \tau\ell$, this result may also be interpreted as

$$\frac{D}{q} = \frac{8t^2}{\pi k^2}\log 2 \qquad (144)$$

where q is the dynamic pressure. Thus for a sweepback of 45°, the drag is of the order of the force produced by one dynamic pressure acting over an area equal to the square of the airfoil thickness - a surprisingly low result for the limit at Mach number 1.

The result in equation (143) is exactly twice that computed by von Karman (Ref. 22) for the limiting case of a strictly two-dimensional swept wing as Mach number 1 is approached. Presumably the discrepancy is due to the fact that the limit in the present case is approached for a wing with tips which begin and remain as sharp points, so that there is an essential difference in the character of the tips during the limiting process.

Similar results can be obtained for the case of a rectangular wing of finite aspect ratio. The classical result, for infinite aspect ratio, predicts that the drag increases near $M = 1$ as $(M^2 - 1)^{-1/2}$, while for the finite aspect ratio case, it can be shown that the drag increases only as $\log(M^2 - 1)^{-1}$. The finite aspect ratio drag calculation will be outlined briefly below.

Consider first the rectangular wing of Fig. 38, for which the Mach wave from one tip does not reach the other tip, i.e., $\beta b > C$. The pressure at P will have the value calculated for an infinite two-dimensional wing plus a tip correction. The tip correction may be regarded as the influence at P of a source distribution in region A equal and opposite to the source distribution at corresponding chordwise stations on the remainder of the wing. If $\lambda(x)$ is the slope (in the x-direction) of the airfoil surface, then the correction to the two-dimensional potential, $\Delta\phi$, for a point influenced only by one wing tip will be

$$\Delta\phi = \frac{U}{\pi} \int_0^{x-\beta y} \lambda(\xi)\, d\xi \int_{\eta_1}^{0} \frac{d\eta}{\sqrt{(x-\xi)^2 - \beta^2(y-\eta)^2}}$$

where

$$\eta_1 = y + (x-\xi)/\beta$$

Then

$$\Delta\phi = \frac{U}{\pi\beta}\int_0^{x-\beta y} \lambda(\xi)\cos^{-1}\frac{y\beta}{x-\xi}\,d\xi$$

and the incremental u-velocity is

$$\frac{\partial}{\partial x}(\Delta\phi) = \frac{U}{\pi}\int_0^{x-\beta y} \frac{\lambda(\xi)\;y\;d\xi}{(x-\xi)\sqrt{(x-\xi)^2-\beta^2y^2}} \tag{145}$$

The local pressure increment is $\Delta p = -\rho U \phi_x$, and the local drag increment, for both sides of the airfoil is

$$d(\Delta D) = 2\,\lambda(x)\,\Delta p\,dx.$$

The total drag correction, consisting of the integral of this increment over the region OMN, becomes:

$$\Delta D = -\frac{2\rho U^2}{\pi}\int_0^c \lambda(x)dx \int_0^{x/\beta} y\,dy \int_0^{x-\beta y} \frac{\lambda(\xi)\,d\xi}{(x-\xi)\sqrt{(x-\xi)^2-\beta^2y^2}} \tag{146}$$

$$= +\frac{2\rho U^2}{\pi}\int_0^c \lambda(x)dx \int_0^x \frac{\lambda(\xi)d\xi}{(x-\xi)}\left\{\frac{1}{\beta^2}\sqrt{(x-\xi)^2-\beta^2y^2}\right\}\Bigg|_{y=0}^{(x-\xi)/\beta}$$

where the order of integration was reversed in the last step. From this,

$$\Delta D = -\frac{2\rho U^2}{\pi\beta^2}\int_0^c \lambda(x)dx \int_0^x \lambda(\xi)\,d\xi \tag{147}$$

But if t(x) is the thickness of the airfoil, then

$$\lambda(\xi) = \frac{d}{d\xi}\, t(\xi) = t'(\xi)$$

and

$$\Delta D = -\frac{2\rho U^2}{\pi\beta^2}\int_0^c t'\,t\,dx = 0 \tag{148}$$

Thus the drag correction for this case, $\beta b > C$, is zero, and the drag has its two-dimensional value

$$D_o = \frac{2b\rho U^2}{\beta}\int_0^c \lambda^2(\xi)\,d\xi \tag{149}$$

In the case that $\beta b > C$, illustrated in Fig. 39, the calculation proceeds as before, except that the integration of the drag increment is carried out only over NORQ. But since the integral over MNO will be zero, as before, it is necessary only to calculate minus the integral of the drag increment over MQR. Thus

$$\Delta D = \frac{2\rho U^2}{\pi}\int_{\beta b}^{c}\lambda(x)\,dx\int_{b}^{x/\beta} y\,dy\int_{0}^{x-\beta y}\frac{\lambda(\xi)\,d\xi}{(x-\xi)\sqrt{(x-\xi)^2-\beta^2y^2}}$$

for the influence of one wing tip. For both tips, and reversing the order of integration,

$$\Delta D = \frac{4\rho U^2}{\pi}\int_{\beta b}^{c}\lambda(x)\,dx\int_{0}^{x-\beta b}\frac{\lambda(\xi)\,d\xi}{(x-\xi)}\int_{b}^{(x-\xi)/\beta}\frac{y\,dy}{\sqrt{(x-\xi)^2-\beta^2y^2}}$$

or,

$$\Delta D = \frac{4\rho V^2}{\pi\beta^2}\int_{\beta b}^{c}\lambda(x)\,dx\int_{0}^{\xi=x-\beta b}\frac{\lambda(\xi)\sqrt{(x-\xi)^2-\beta^2b^2}}{(x-\xi)}\,d\xi \tag{149}$$

This increment will always be negative, and can be easily calculated in specific cases. Consider, for example, an airfoil with double-wedge profile, and maximum thickness at the 50% chord point. Then for

$$0 < \xi < c/2\ , \qquad \lambda(\xi) = +\lambda_0$$

$$c/2 < \xi < c\ , \qquad \lambda(\xi) = -\lambda_0$$

Inserting these values of λ in equation (149), and carrying out the successive integrations over the necessary intervals, one obtains finally:

$$\Delta D = \frac{4\rho V^2\lambda_0^2}{\pi\beta^2}\left[c\sqrt{\left(\frac{c}{2}\right)^2-\beta^2b^2} + 2\beta^2b^2\cosh^{-1}\frac{c/2}{\beta b}\right.$$

$$- 2\beta bc\,\cos^{-1}\frac{\beta b}{c/2} - \frac{c}{2}\sqrt{c^2-\beta^2b^2}$$

$$\left. - \frac{\beta^2b^2}{2}\cosh^{-1}\frac{c}{\beta b} + \beta bc\,\cos^{-1}\frac{\beta b}{c}\right] \tag{151}$$

The basic two-dimensional drag is, of course,

$$D_0 = \frac{2bc\,\rho V^2\lambda_0^2}{\beta} \tag{152}$$

As the Mach number approaches 1, ($\beta b \to 0$), the dominant terms in equation (151) are:

$$\Delta D \to \frac{4\rho U^2 \lambda_0^2}{\pi \beta^2}\left[-\frac{3}{2}\beta^2 b^2 \log \beta - \beta b c\, \pi/2\right]$$

Combining this with equation (151), and noting that $\lambda_0 = \tau$ for this wing, one finds that

$$\frac{C_D}{\tau^2} \to \frac{12}{\pi}\frac{b}{c}\log\frac{1}{\beta} \qquad (153)$$

Thus the drag coefficient has the same type of logarithmic singularity near M = 1 as was found for the delta wing with no trailing edge sweep-back. The drag reduction from the two-dimensional case, as given by equation (151) will be quite appreciable for low aspect ratios.

PART VIII

CONCLUSIONS

In Part II it was shown that a reasonable approximate solution to the equations of motion for the supersonic flow of a perfect fluid is obtained by assuming the disturbance velocities to be small. One possible method of representing solutions to the linearized equations, in terms of sources and doublets, was developed and discussed. It was shown that this representation was particularly suitable for calculating the flow over thin three-dimensional airfoils at zero angle of attack, and can also be used to represent the flow over airfoils at finite angles of attack.

The equations were applied in Parts IV, V and VI to the calculation of the pressure distributions and drag forces acting on a family of wings of nearly triangular planform, with a simple thickness distribution, called the delta wings. It was found that with the exception of small regions on the airfoil, the disturbances resulting from the solution do fall within the assumptions of the linearized theory, if the airfoil thickness is sufficiently small. It was also found that the drag acting on these airfoils may depend critically upon the details of the planform and thickness distribution, and that optimum choices may be made of these various geometrical parameters for particular design problems. The essential results of the drag calculations for this airfoil family were summarized in Figs. 20 to 32.

In general, the results indicated that (a) the "sweepback" of a wing is characterized not only by its planform, but the geometry of its maximum thickness lines, and (b) the essential effect of increasing

sweepback is to lower the drag coefficient in the low supersonic speed range, with a drag rise or peak at some higher Mach number, near the range where the Mach waves are parallel to the leading edge or maximum thickness lines.

Finally, it was concluded that the possible adjustments to the shape of the drag curve as a function of Mach number could be used to advantage in several ways, with the choice depending on the requirements of a particular engineering problem.

REFERENCES

1. Ackeret, J., "Luftkrafte auf Flugel, die mit grossere als Schallgeschwindigkeit bewegt werden", Z.F.M., Vol. 16, pp. 72-74, 1925.
2. von Karman, Th., and Moore, N. B., "Resistance of Slender Bodies Moving with Supersonic Velocities", Transactions of A.S.M.E., 1932.
3. Glauert, H., "The Effect of Compressibility on the Lift of Airfoils", Proc. Royal Society, (A), Vol. 118, p. 113, 1927.
4. Prandtl, L., "Theory of the Lifting Wing in a Compressible Medium", Luftfahrtforschung, Vol. 13, p. 313, 1936.
5. Busemann, A., "Aerodynamischer Auftrieb bie Uberschallgeschwindigkeit", Proc. Volta Congress, 1935.
6. Busemann, A., "Infinitesimale kegelige Uberschallstromung", Schriften der Dutschen Akademie der Luftfahrtforschung, 7B, p. 105, 1943.
7. Hantzsche, W., and Wendt, M., "Gasstromungen mit Ubergang von Unterschall-zu Uberschallgeschwindigkeiten", Z.A.M.M., Vol. 22, p. 72.
8. Stewart, H. J., "The Lift of a Delta Wing at Supersonic Speeds", Quarterly of Applied Mathematics, Vol. IV, No. 3, October, 1946.
9. Schlichting, H., "Deutsche Luftfahrtforschung" Jahrbuch, 1937.
10. Puckett, A. E., "Supersonic Wave Drag of Thin Airfoils", Journal of the Aeronautical Sciences, Vol. 13, No. 9, 1946.
11. Evvard, John C., "Distribution of Wave Drag and Lift in the Vicinity of Wing Tips at Supersonic Speeds", NACA TN-1382, 1947.

12. Liepmann, H. W., and Puckett, A. E., "Introduction to the Aerodynamics of a Compressible Fluid", Wiley and Sons, New York 1947.

13. Jones, R. T., "Thin Oblique Airfoils at Supersonic Speed", NACA TN-1107, 1946.

14. Jones, R. T., "Estimated Lift-Drag Ratios at Supersonic Speed", NACA TN-1350, 1947.

15. Evvard, John C., "Theoretical Lift Distribution and Upwash Velocities at Supersonic Speeds", NACA TN-1484, 1947.

16. Evvard, John C., "Theoretical Distribution of Lift on Thin Wings at Supersonic Speeds, (An Extension)", NACA TN-1585, 1948.

17. Evvard, John C., "The Effects of Yawing Thin Pointed Wings at Supersonic Speeds", NACA TN-1429, 1947.

18. Heaslet, M. A., and Lomax, H., "The Calculation of Downwash Behind Supersonic Wings", NACA TN-1620, 1948.

19. Margolis, K., "Supersonic Wave Drag of Sweptback Tapered Wings at Zero Lift", NACA TN-1448, 1947.

20. Margolis, K., "Effects of Chordwise Location of Maximum Thickness on the Supersonic Wave Drag of Sweptback Wings", NACA TN-1543, 1948.

21. Margolis, K., "Supersonic Wave Drag of Nonlifting Sweptback Tapered Wings with Maximum Lines Behind the Line of Maximum Thickness", NACA TN-1672, 1948.

22. von Karman, Th., "Supersonic Aerodynamics", Journal of the Aeronautical Sciences, Vol. 14, p. 373, 1947.

23. Puckett, A. E., and Stewart, H. J., "Aerodynamic Performance of Delta Wings", Journal of the Aeronautical Sciences, Vol. 14, p. 567, 1947.

APPENDIX I

SUMMARY OF SYMBOLS

U_o = Undisturbed or free stream velocity (in x-direction).

Note: The subscript is dropped in the linearized solutions.

U, V, W = Total velocities in directions of x, y and z axes respectively.

u, v, w = Perturbation velocities in directions of x, y and z axes.

= Perturbation velocity potential.

M = Mach number

p = pressure

ρ = density

q = dynamic pressure = $\rho U^2/2$.

= ratio of specific heats, C_p/C_v.

C_p = pressure coefficient = $(p - p_o)/q$, where p_o is free stream pressure.

β = $M^2 - 1$ = cotangent of Mach angle.

= angle between airfoil leading edge and normal to stream direction (sweepback angle); see Fig. 6 or 8.

k = tan

n = k/β, = relative sweepback parameter.

= slope of airfoil surface in x-direction.

c = total airfoil chord, apex to tip, (see Fig. 8).

= airfoil root chord

ac = x-distance from trailing edge at root to airfoil tip.

rc = x-distance from maximum thickness point at root chord to airfoil tip.

b = maximum thickness point location, fraction of root chord.

D = airfoil drag, both sides of a symmetrical airfoil.

S = airfoil actual planform area.

C_D = drag coefficient = D/qS.

t = airfoil maximum thickness.

= t/ = thickness ratio.

F, G = functions used in drag calculations, defined by equations.

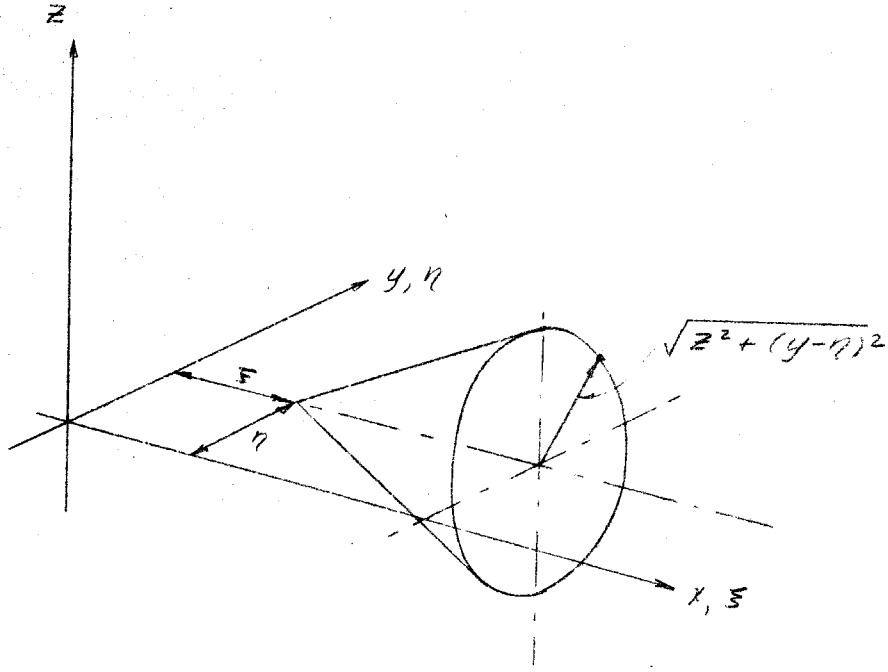

FIG. 1
INFLUENCE CONE FOR SOURCE

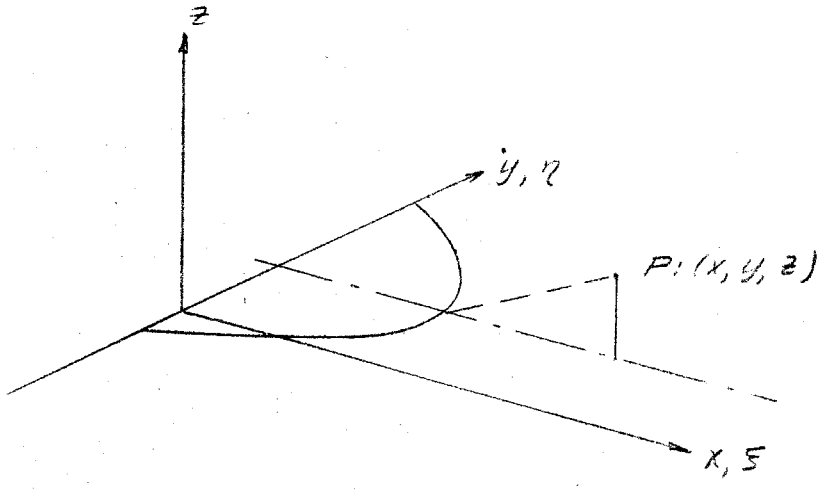

FIG. 2
FORECONE OF P

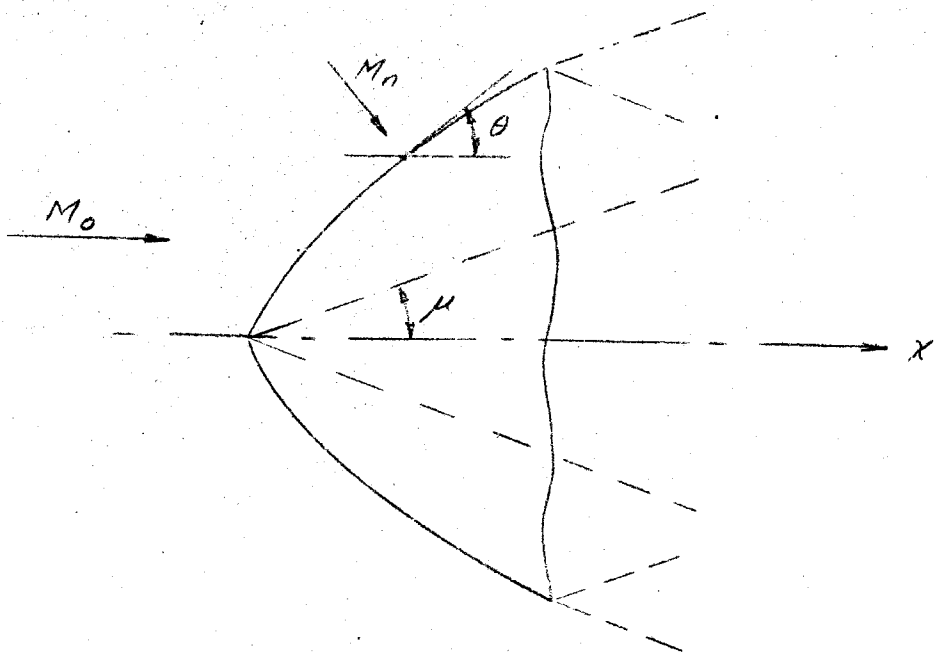

FIG. 3

SUPERSONIC LEADING AND TRAILING EDGES

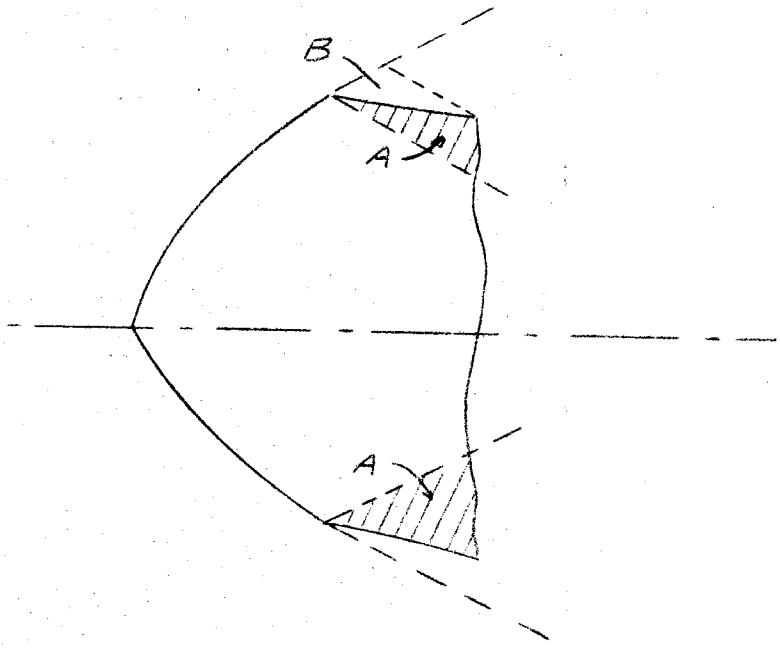

FIG. 4

SUBSONIC TIPS

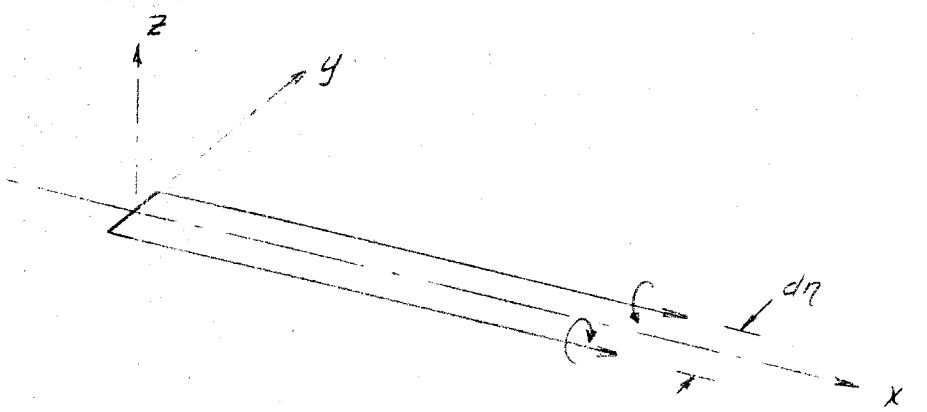

FIG. 5

ELEMENTARY DOUBLET LINE

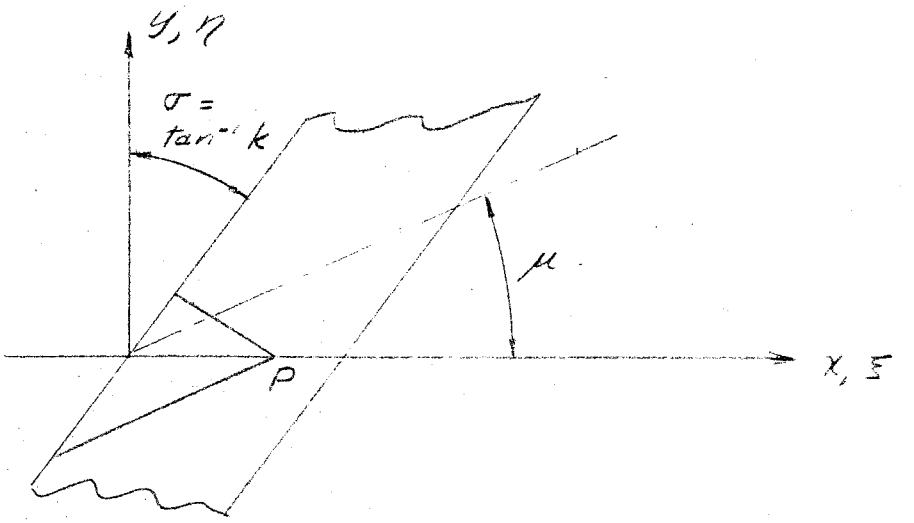

FIG. 6

SWEPT WING, $k < \beta$

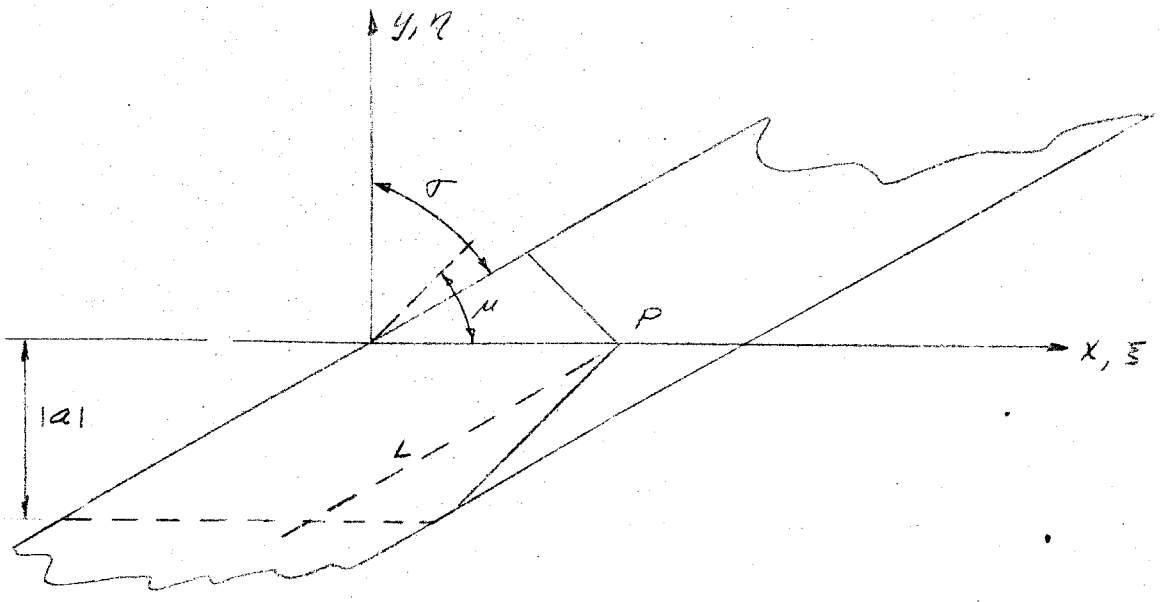

FIG. 7

SWEPT WING, $k > \beta$

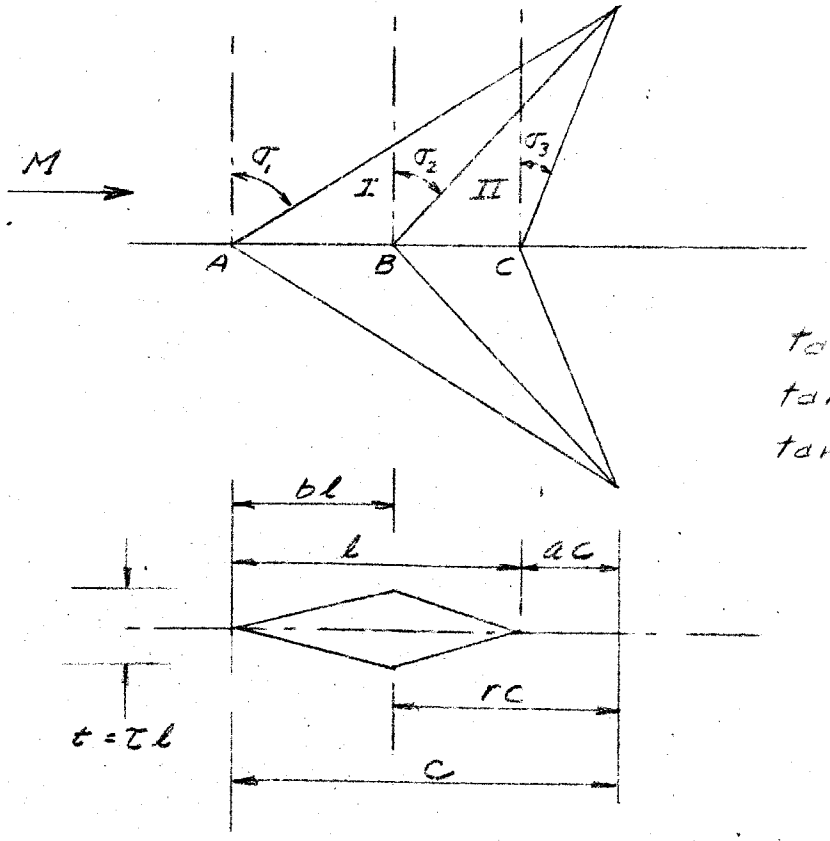

$\tan \sigma_1 = k_1$

$\tan \sigma_2 = k_2 = rk_1$

$\tan \sigma_3 = k_3 = ak_1$

$n = k_1/\beta$

FIG. 8

GEOMETRY OF DELTA WING

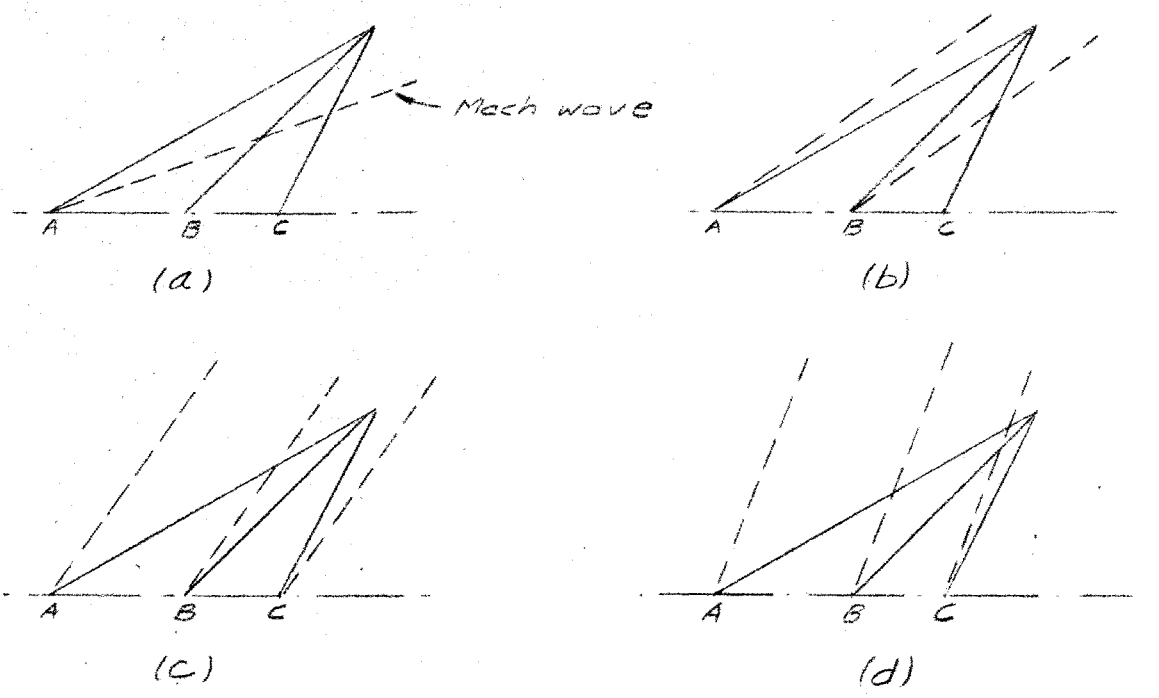

FIG 9

FOUR MACH NUMBER RANGES

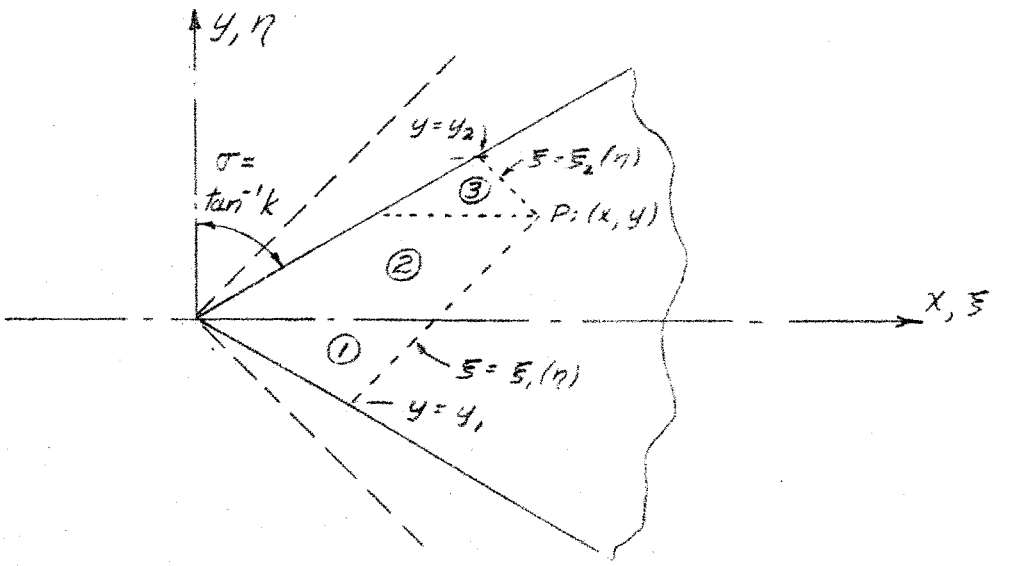

FIG. 10

BASIC TRIANGLE, $n > 1$

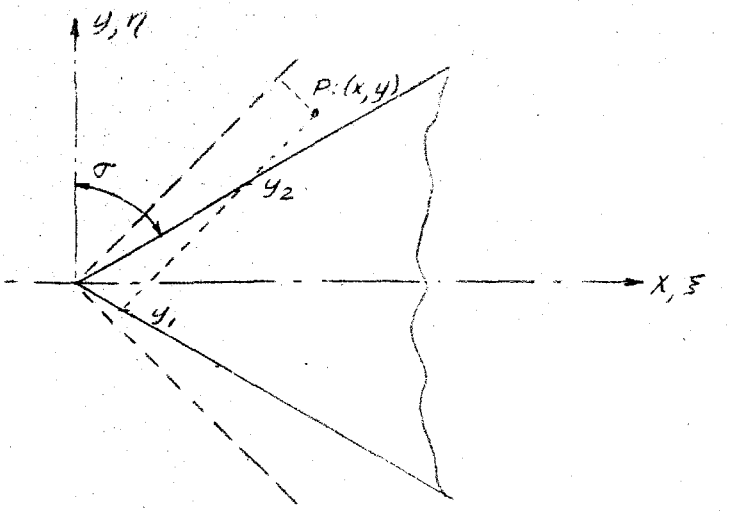

FIG. 11

INFLUENCE ZONE FOR $t > 1$

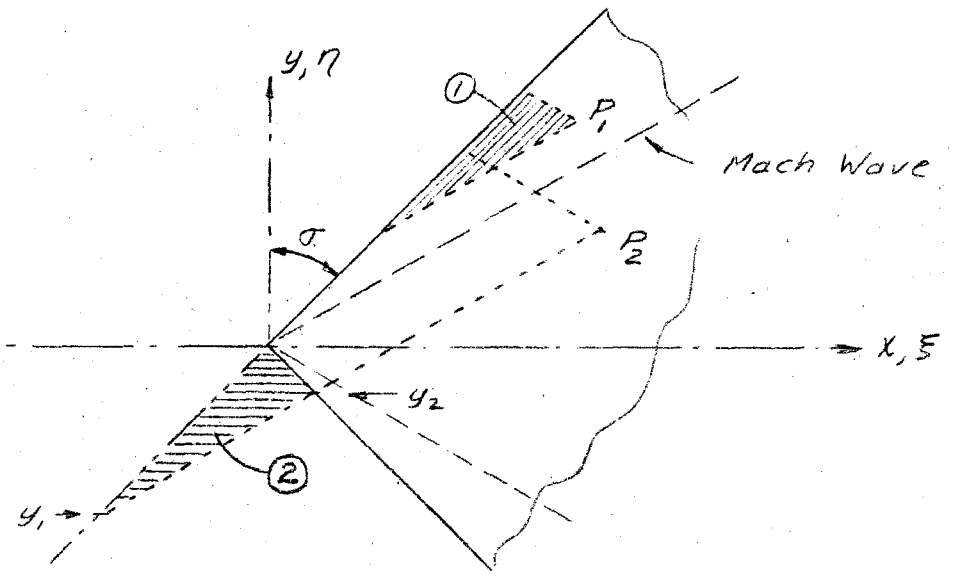

FIG. 12

BASIC TRIANGLE, $n < 1$

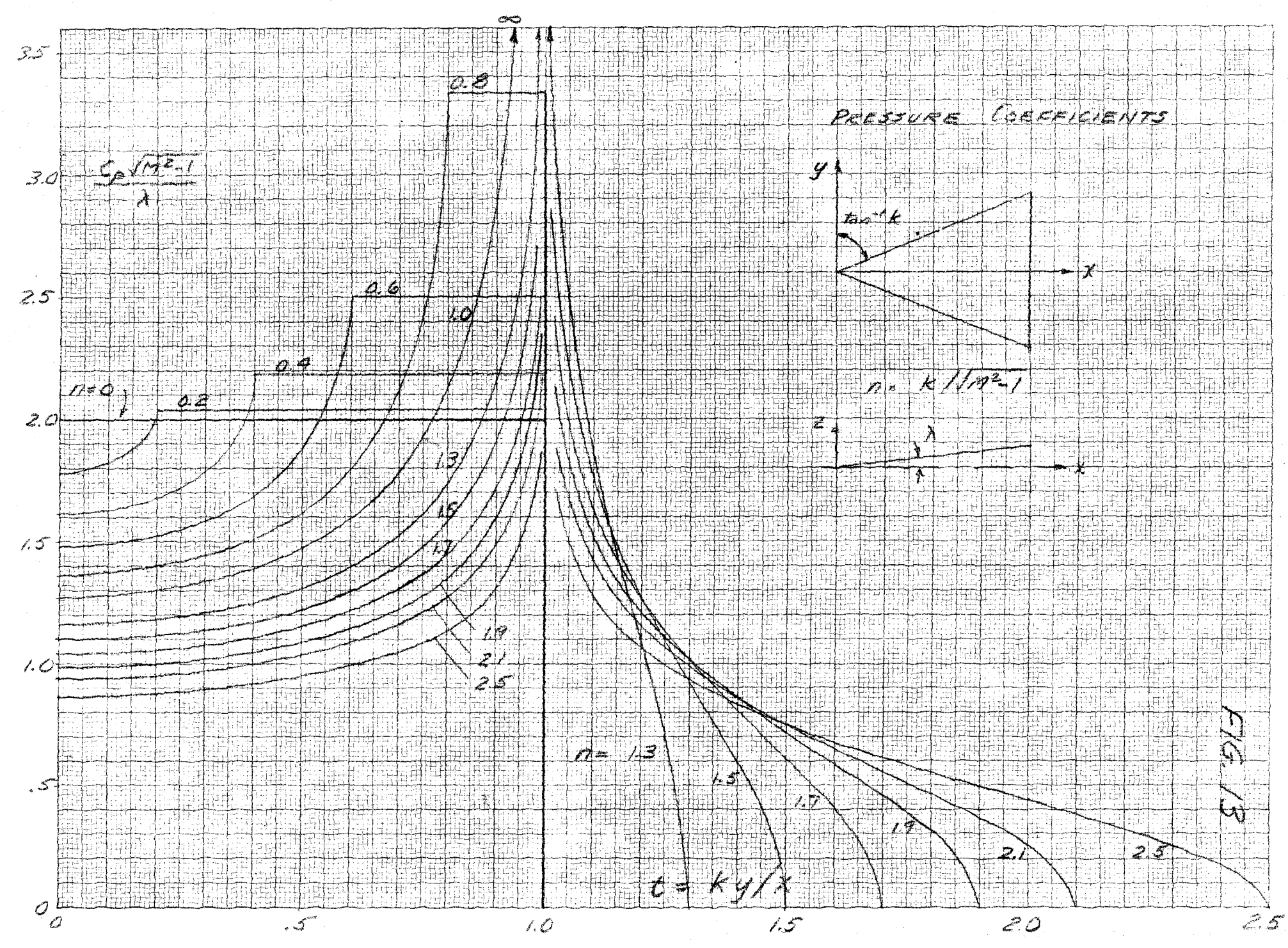
PRESSURE COEFFICIENTS
$\frac{C_p\sqrt{M^2-1}}{\lambda}$
∞
0.8
0.6
0.4
0.2
1.0
n=0
1.3
1.5
1.7
1.9
2.1
2.5
$n = k/\sqrt{M^2-1}$
$\tan^{-1}k$
y
x
z
λ
$\theta = ky/x$
3.5
3.0
2.5
2.0
1.5
1.0
.5
0
.5
1.0
1.5
2.0
2.5

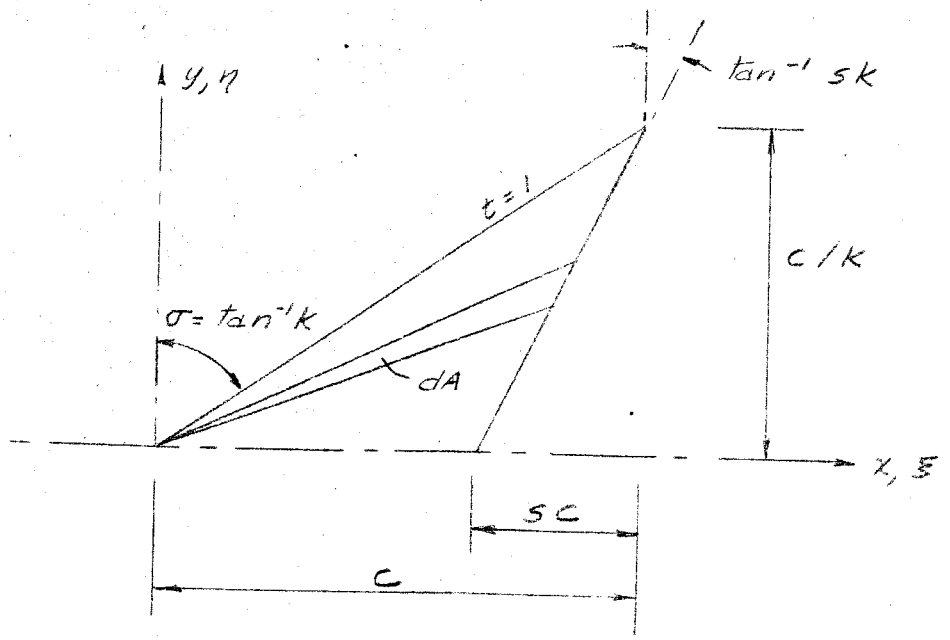

FIG. 14

INTEGRATION REGION FOR S_1

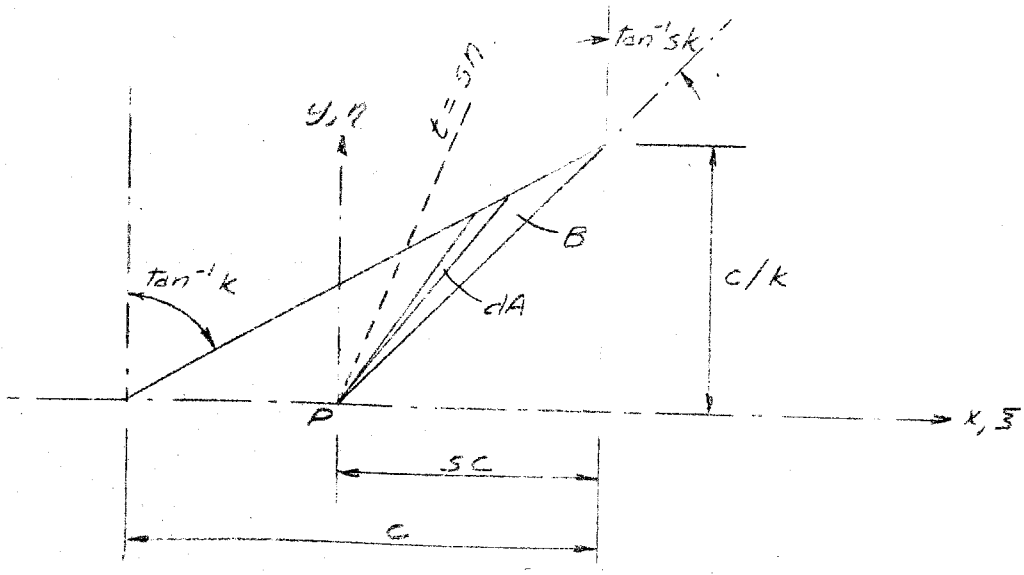

FIG. 15

INTEGRATION REGION FOR S_2

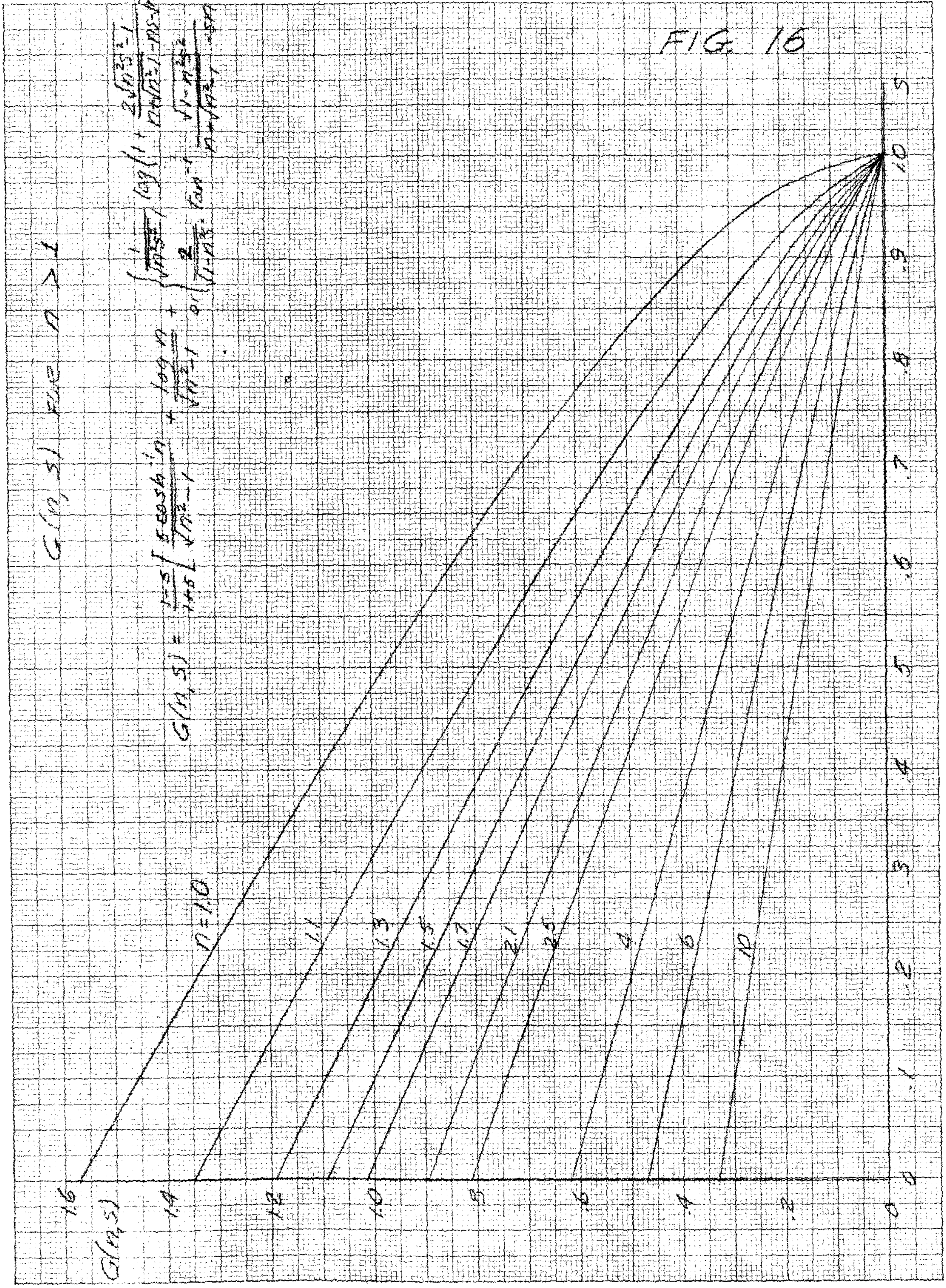
G(n, s) FOR n > 1
n=1.0
1.1
1.3
1.5
1.7
2.1
2.5
4
6
10
G(n,s)
1.6
1.4
1.2
1.0
.8
.6
.4
.2
0
s
.1
.2
.3
.4
.5
.6
.7
.8
.9
1.0

FIG. 16

FIG. 17

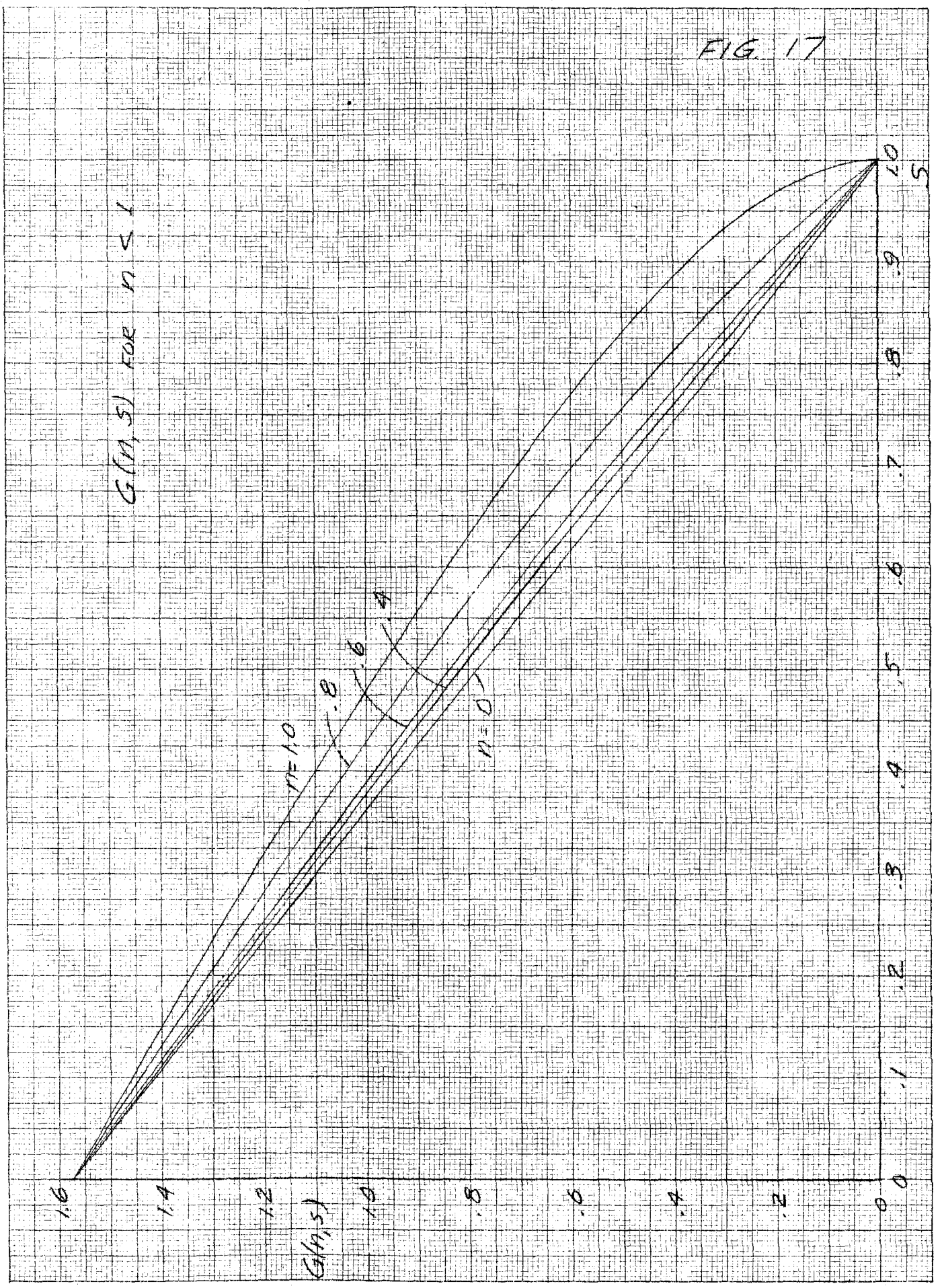

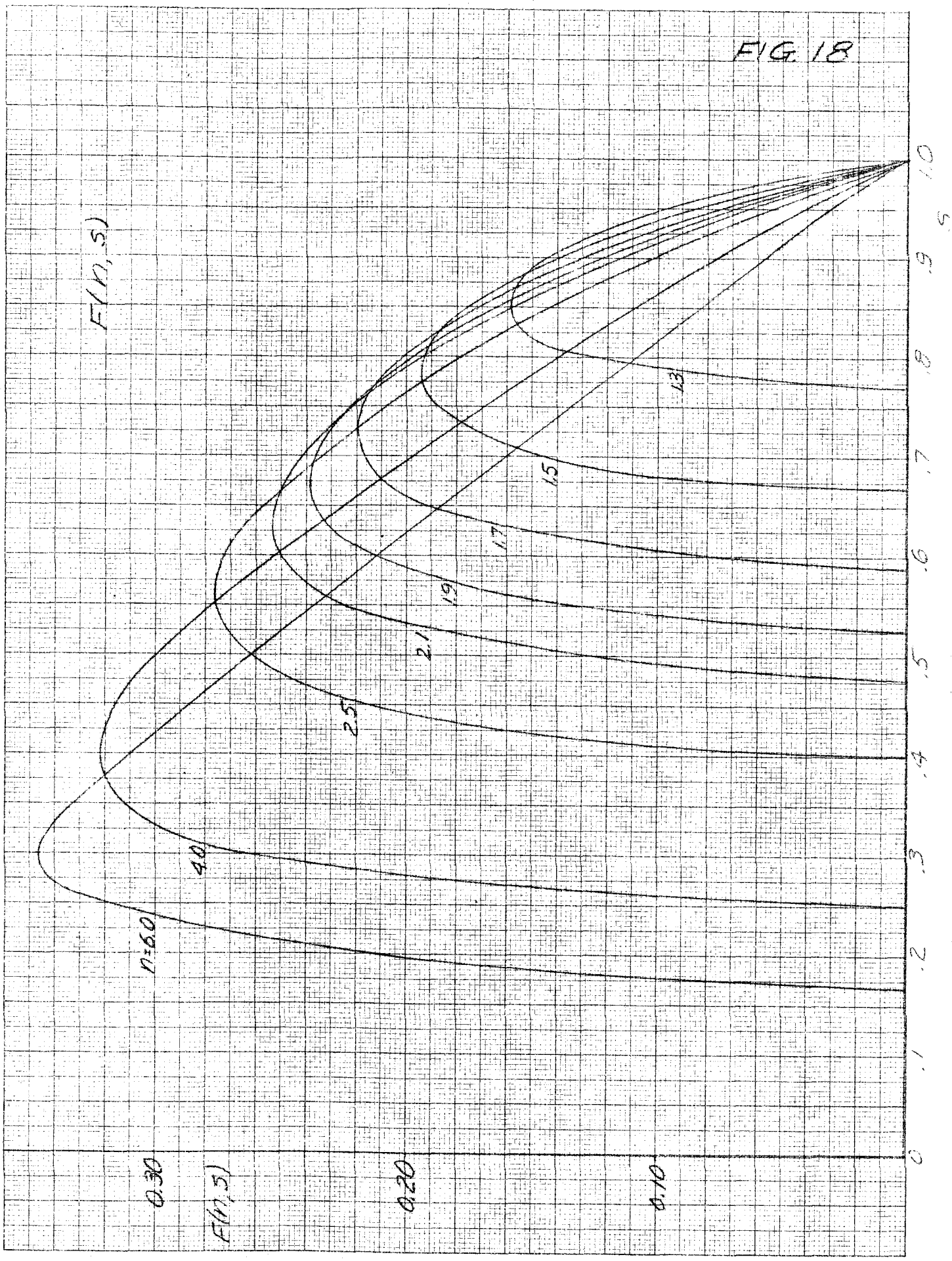
FIG 18
F(η, s)
F(η, s)
0.30
0.20
0.10
η=6.0
4.0
2.5
2.1
1.9
1.7
1.5
1.3
0
.1
.2
.3
.4
.5
.6
.7
.8
.9
1.0
s

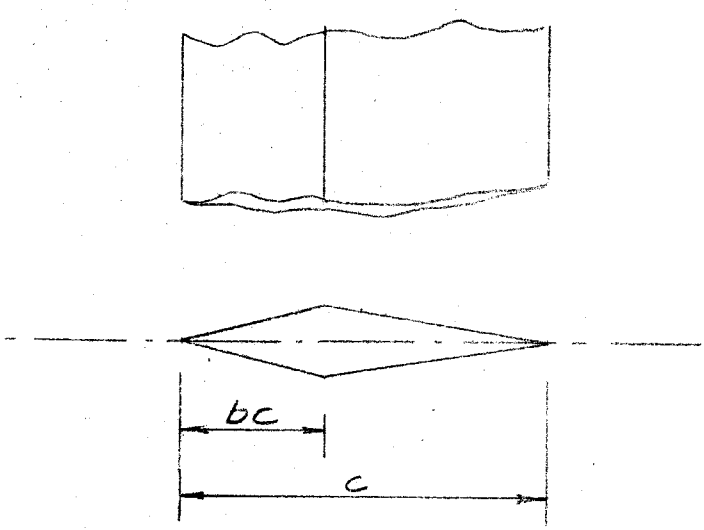

FIG. 19

DOUBLE WEDGE PROFILE

$\frac{C_D \beta}{\tau^2}$

Δ WING DRAG
VS
MAXIMUM THICKNESS POSITION
$a = 0$

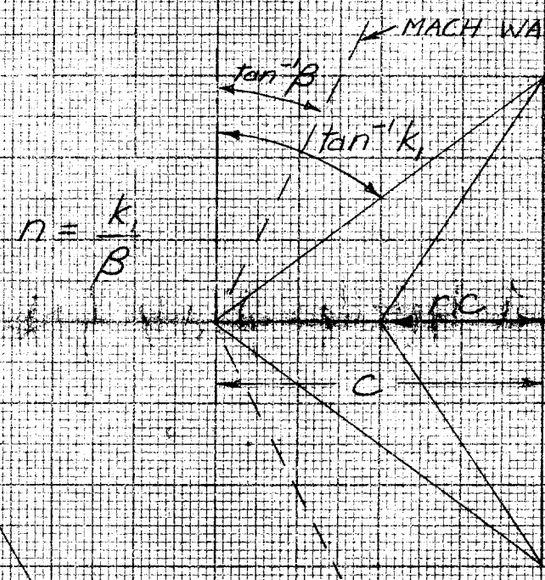

$n = 1.1$ $n = 1.0$

$n = 1.3$

$n = 0$

1.5

1.7

2.1

2.5

4.0

6.0

10.0

FIG 20

$(1-r) = b$

AEP 12-28-45

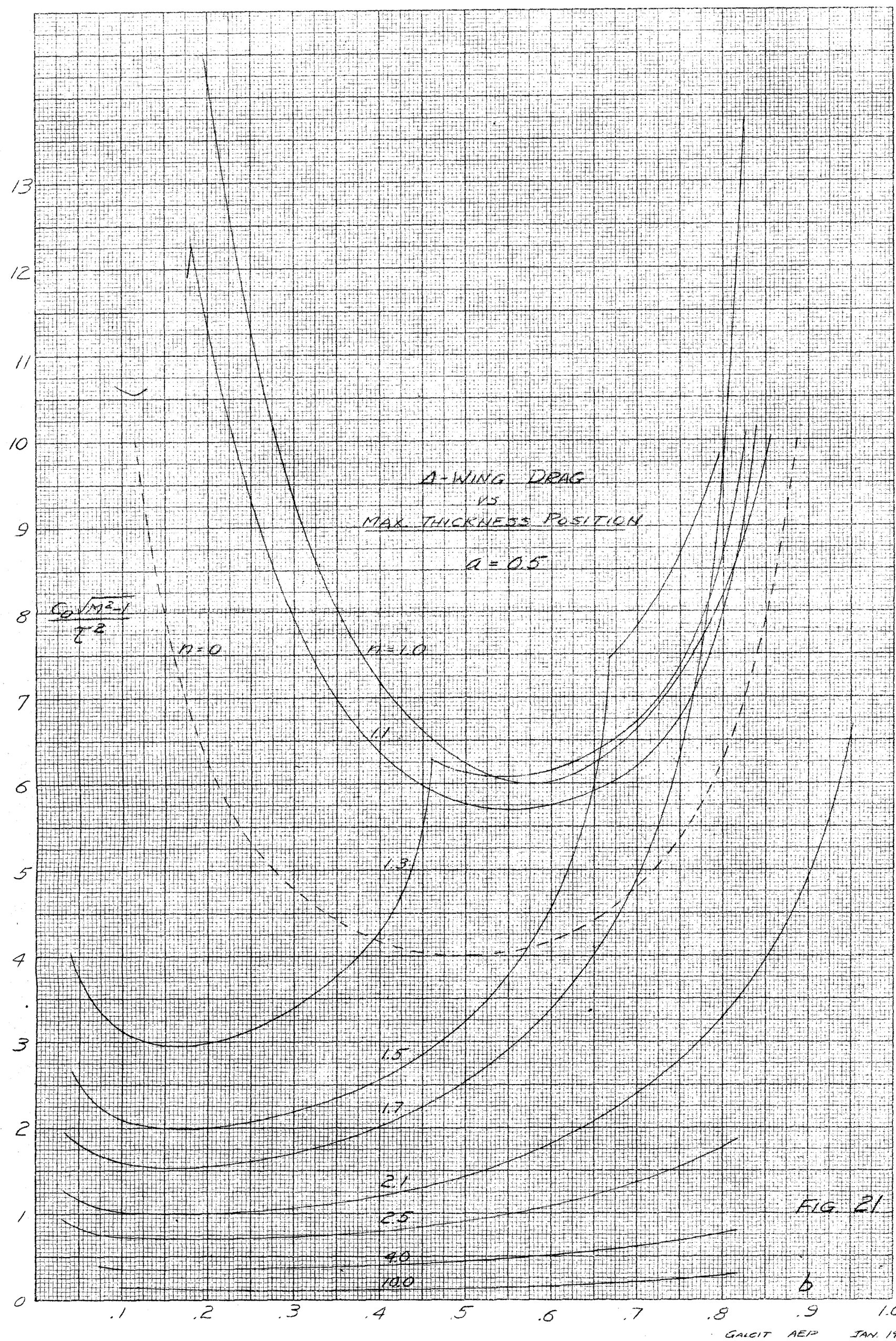

FIG. 21

GALCIT AEP JAN. 1947

Δ-WING DRAG FOR α = 0

FIG 22

$\frac{C_D\sqrt{M^2-1}}{\tau^2}$

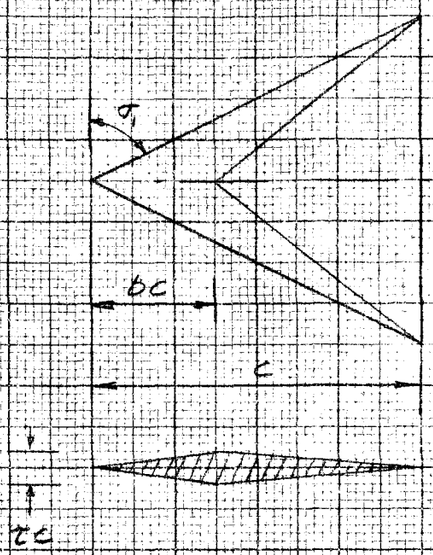

b = 0.2

b = 0.3

b = 0.4

b = 0.5

0 2 4 6 8 10 12 14 16 18 20

0 0.5 1.0 1.5 2.0 2.5 3.0

$1/n = \sqrt{M^2-1} / \tan\sigma$

Δ-WING DRAG FOR $a = 0.25$

FIG. 23

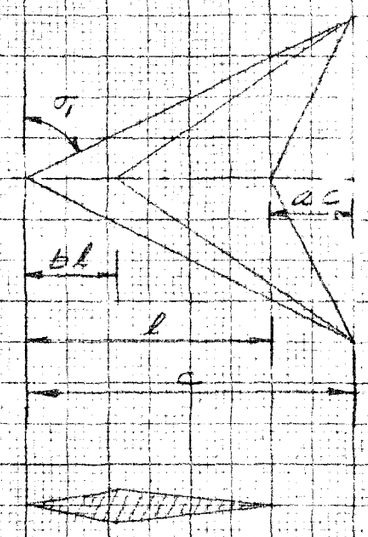

$\frac{C_D\sqrt{M^2-1}}{\tau^2}$

b = 0.2
0.3
0.4
0.5

0 2 4 6 8 10 12 14 16 18 20

0 0.5 1.0 1.5 2.0 2.5 3.0

$1/n = \sqrt{M^2-1}\,/\tan\sigma_i$

A-WING DRAG FOR $a = 0.50$

FIG. 24

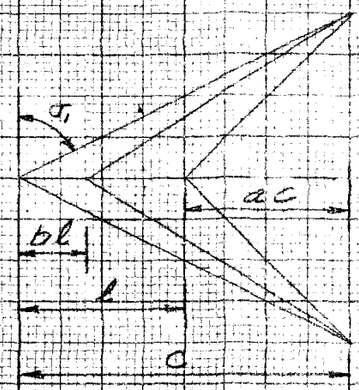

$\frac{C_D\sqrt{M^2-1}}{\tau^2}$

b = 0.2
0.3
0.4
0.5

$1/n = \sqrt{M^2-1}\ /\ \tan\sigma$

0 0.5 1.0 1.5 2.0 2.5 3.0

0 2 4 6 8 10 12 14 16 18 20

Δ - WING DRAG FOR $a = 0.75$ FIG. 25

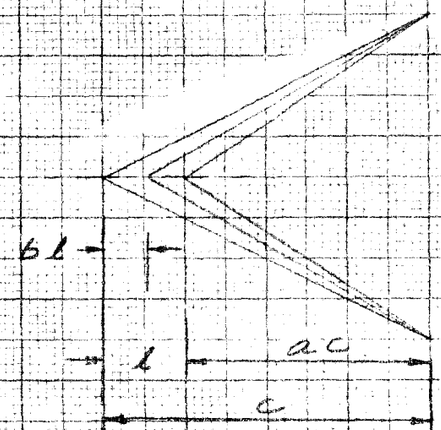

$\frac{C_D\sqrt{M^2-1}}{\tau^2}$

b = 0.2
0.3
0.4
0.5

$1/n = \sqrt{M^2-1} / \tan \sigma$

EFFECT OF TRAILING EDGE SWEEP
ON
Δ-WING DRAG
FOR
$b = 0.2$

FIG. 26

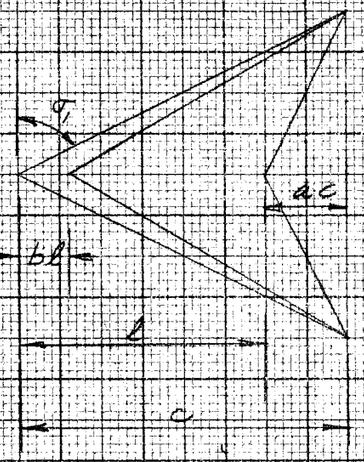

$\frac{C_D\sqrt{M^2-1}}{\tau^2}$

$a = 0$
.25
.50
.75

$1/n = \sqrt{M^2-1} / \tan\sigma$

AER- APR '49

EFFECT OF TRAILING EDGE SWEEP ON
Δ - WING DRAG
FOR
b = 0.5

FIG. 27

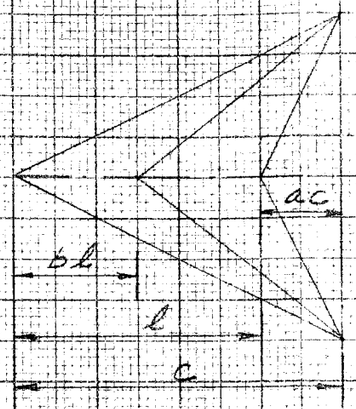

$\frac{C_D\sqrt{M^2-1}}{\tau^2}$

a = 0
.25
.50
.75

0
2
4
6
8
10
12
14
16
18
20

0
0.5
1.0
1.5
2.0
2.5
3.0

$1/\sigma = \sqrt{M^2-1} / \tan \sigma$

FIG. 28

Δ-WING DRAG

EFFECT OF SWEEPBACK ON DRAG

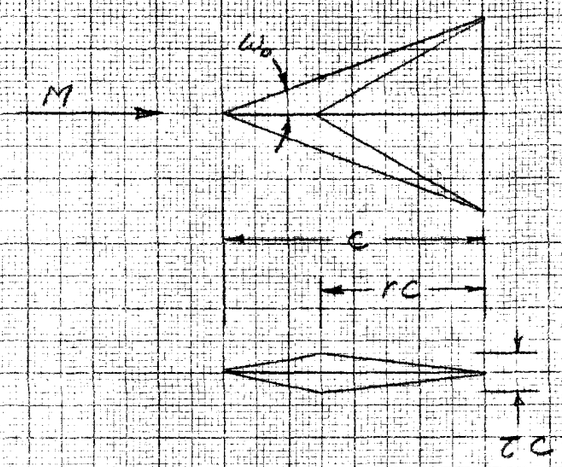

$r = 0.85$

(t_{max} AT 15 % CHORD)

CALIF. INST. OF TECH.
NOV. 1945
A. E. PUCKETT

$\frac{C_D}{\tau^2}$

$\omega_o = 30°$

$\omega_o = 90°$

25°

20°

15°

10°

30°

25°

20°

15°

11
10
9
8
7
6
5
4
3
2
1

1.0 1.5 2.0 2.5 3.0 3.5 4.0 4.5

MACH NUMBER

GALCIT. AEP 8-17-46

FIG 29

Δ WING DRAG

EFFECT OF PEAK LOCATION

$\omega_b = 30°$, $\alpha = 0$

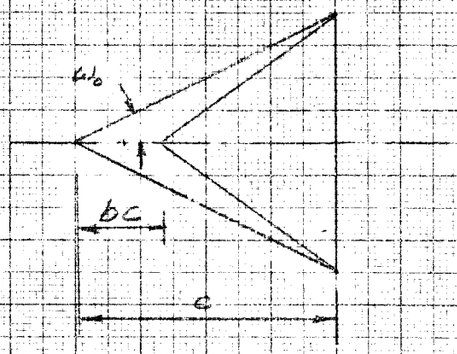

$\frac{C_D}{\tau^2}$

$b = 0.1$

0.2

0.5

0.4

0.3

0.4

0.5

0.3

0.2

0.1

$r = 0.5$, $\omega_b = 90°$

0 1 2 3 4 5 6 7 8 9 10 11 12

1.5 2.0 2.5 3.0 3.5 4.0 4.5

MACH NUMBER

GALCIT AEP 13-9-46

Δ WING DRAG

FIG. 30

FOR
$a = 0.5$, $b = 0.2$

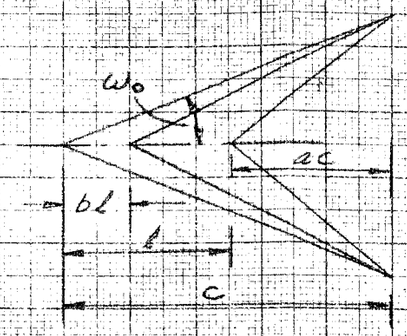

EFFECT OF SWEEP ANGLE

$\frac{C_D}{\tau^2}$

$\omega_0 = 30°$
25°
20°
15°

MACH NUMBER

Δ WING DRAG FIG. 31

FOR

$\omega_0 = 30°$, $A = 0.5$

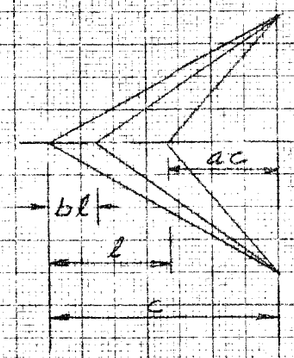

EFFECT OF MAXIMUM THICKNESS LOCATION

$\frac{C_D}{t^2}$

b = 0.2
0.3
0.4
0.5

11
10
9
8
7
6
5
4
3
2
1
0

1.0 1.5 2.0 2.5 3.0 3.5 4.0 4.5

MACH NUMBER

AEP 1949

FIG. 32

Δ-WING DRAG

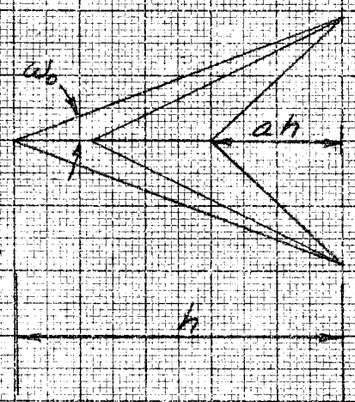

EFFECT OF LEADING AND TRAILING EDGE SWEEP

b = 0.2

$\frac{C_D}{\zeta^2}$

$\omega_0 = 30°$, a = 0

a = 0.5

$\omega_0 = 15°$, a = 0

a = 0.5

0 1 2 3 4 5 6 7 8 9 10 11 12

1.0 1.5 2.0 2.5 3.0 3.5 4.0 4.5

MACH NUMBER

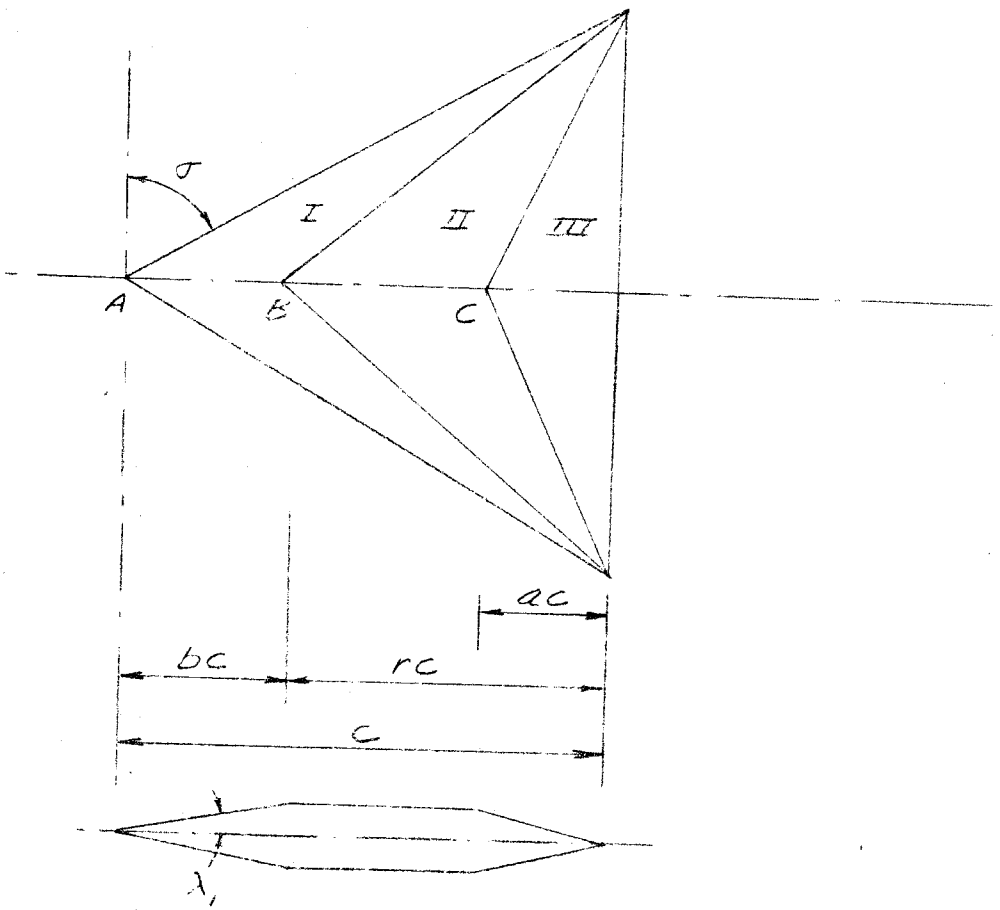

FIG. 33

THREE-SLOPE DELTA WING

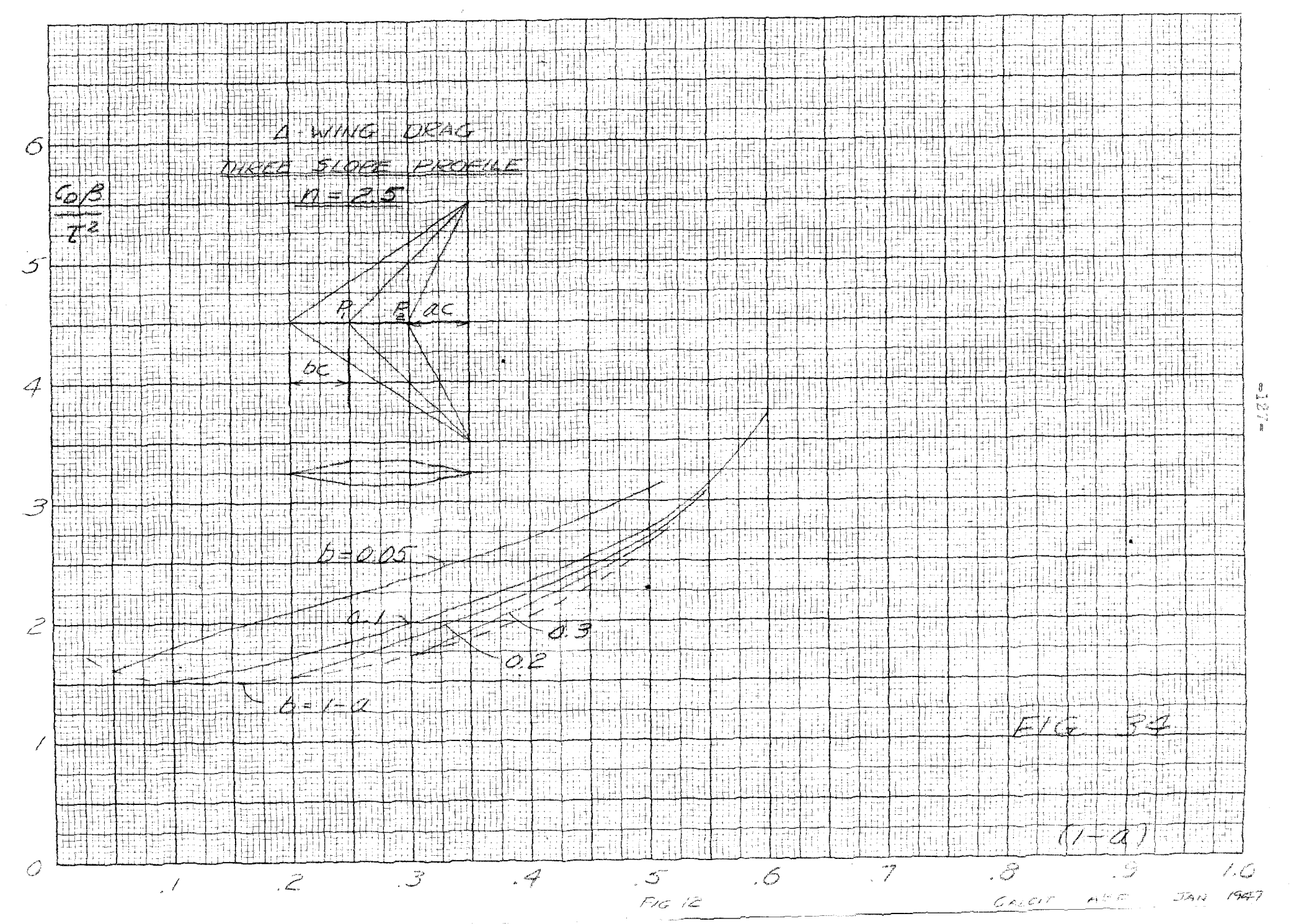

FIG 12

GALCIT AFC JAN 1947

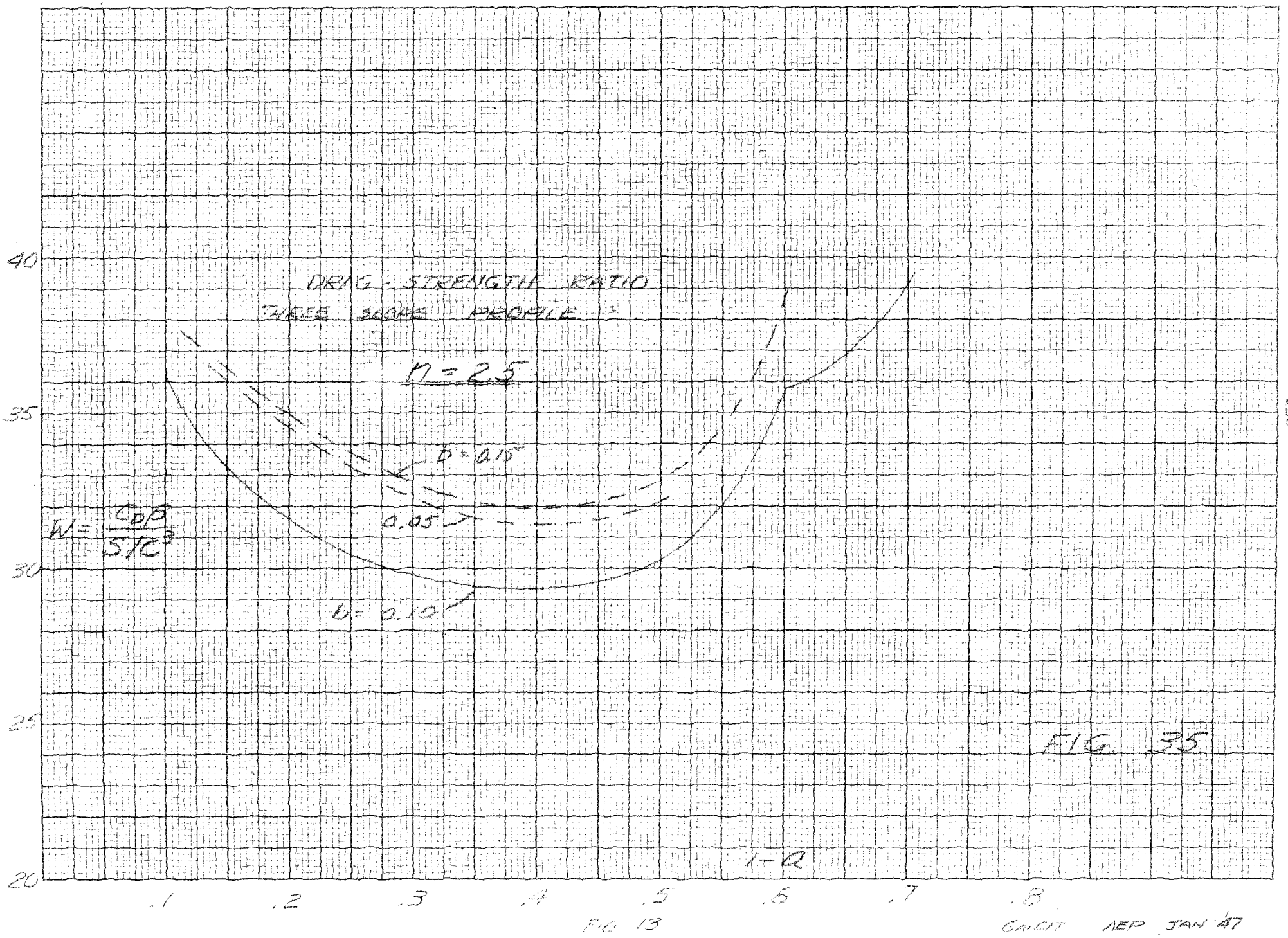
DRAG - STRENGTH RATIO
THESE SLOPES PEORLE
n = 2.5
b = 0.15
0.05
b = 0.10
W = CDρ / 5.1C³
40
35
30
25
20
.1
.2
.3
.4
.5
.6
.7
.8
1-Q
FIG 35
FIG 13
CALCIT NEP JAN 47

$\frac{y}{c/k}$ = .1 .2 .4 .6 .8

3.0 $\frac{C_p \beta}{\tau}$

2.0

2-DIM.

$yk/c = 0$

1.0

0 .1 .2 .3 .4 .5 .6 .7 .8 .9 1.0 C

0

PRESSURE DISTRIBUTION
2- SLOPE, Δ- WING

-1.0

$n = \frac{k_1}{\beta} = 0.8$ $b = 0.5$

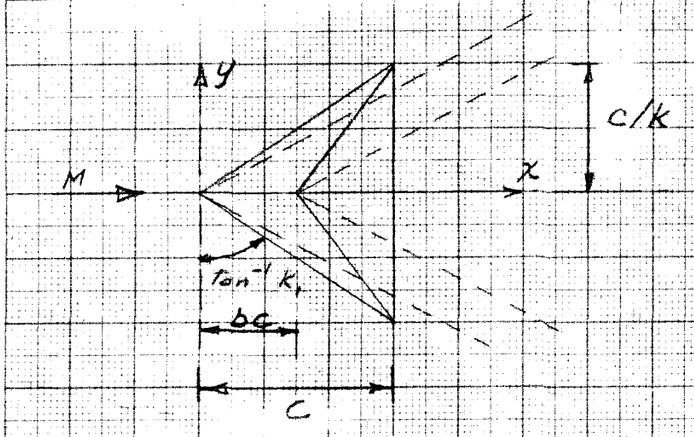

-2.0

$yk/c = 0$

.8

.6

.4

$yk/c = .1$ .2

-3.0

$\beta = \sqrt{M^2 - 1}$

0 .1 .2 .3 .4 .5 .6 .7 .8 .9 1.0 x/c

FIG. 36

PUCKETT 8-10-45

FIG. 37

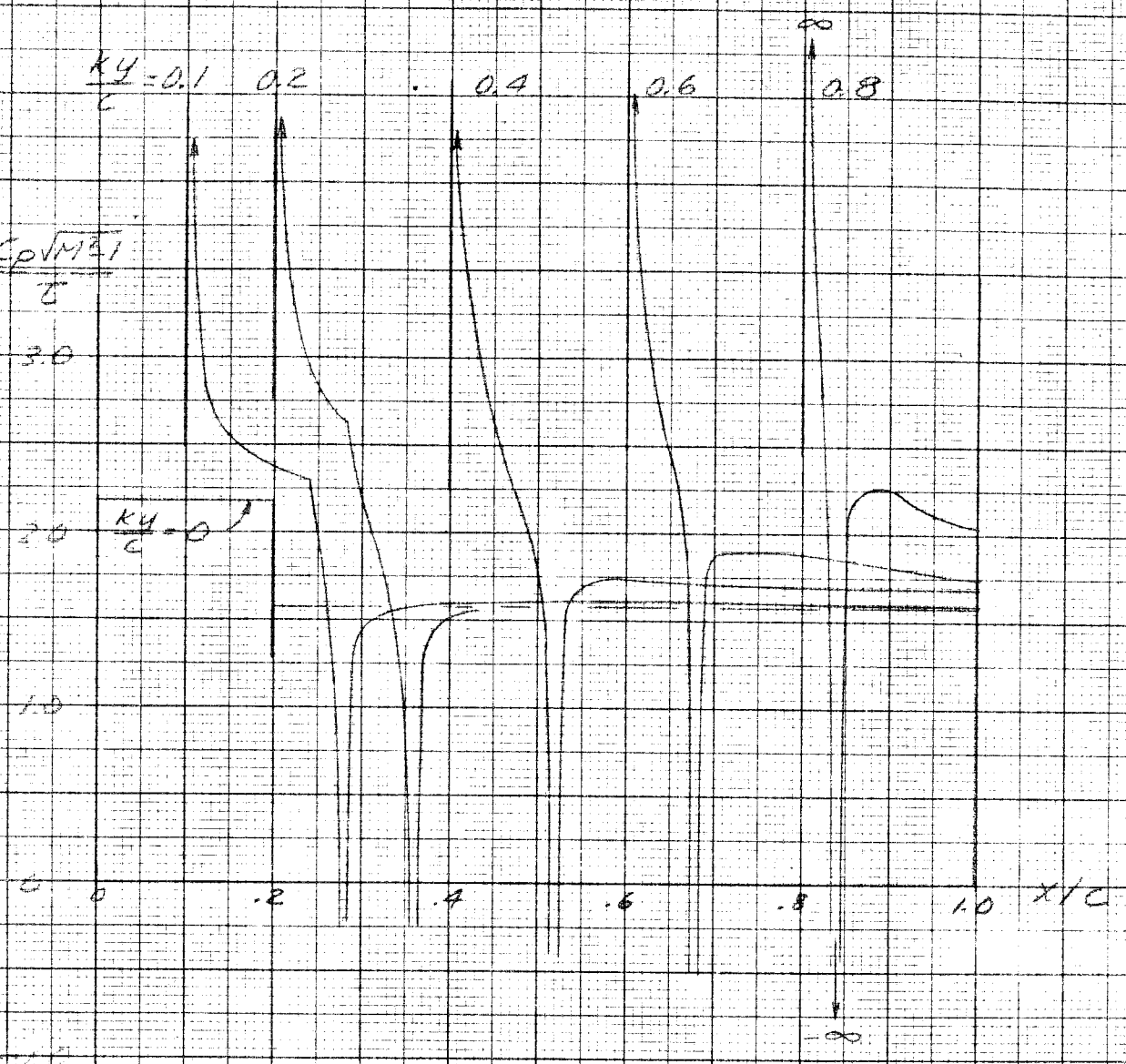

PRESSURE DISTRIBUTION

$M_1 = 2.5$, $b = 0.2$